MMSE Equalizers and Precoders in Turbo Equalization

Mohammed Yusuf Abdul Gaffar

Submitted in fulfillment of the academic requirements
for the degree of MSc Eng
in the School of Electrical, Electronic and Computer Engineering
at the University of Natal, Durban, South Africa

21 November 2003

Abstract

Transmission of digital information through a wireless channel with resolvable multipaths or a bandwidth limited channel results in intersymbol interference (ISI) among a number of adjacent symbols. The design of an equalizer is thus important to combat the ISI problem for these types of channels and hence provides reliable communication. Channel coding is used to provide reliable data transmission by adding controlled redundancy to the data.

Turbo equalization (TE) is the joint design of channel coding and equalization to approach the achievable uniform input information rate of an ISI channel. The main focus of this dissertation is to investigate the different TE techniques used for a static frequency selective additive white Gaussian noise (AWGN) channel. The extrinsic information transfer (EXIT) chart is used to analyse the iterative equalization/decoding process and to determine the minimum signal to noise ratio (SNR) in order to achieve convergence.

The use of the Minimum Mean Square Error (MMSE) Linear Equalizer (LE) using a priori information has been shown to achieve the same performance compared with the optimal trellis based Maximum A Posterior (MAP) equalizer for long block lengths. Motivated by improving the performance of the MMSE LE, two equalization schemes are initially proposed: the MMSE Linear Equalizer with Extrinsic information Feedback (LE-EF (I) and (II)). A general structure for the MMSE LE, MMSE Decision Feedback Equalizer (DFE) and two MMSE LE-EF receivers, using a priori information is also presented. The EXIT chart is used to analyse the two proposed equalizers and their characteristics are compared to the existing MAP equalizer, MMSE LE and MMSE DFE.

It is shown that the proposed MMSE LE-EF (I) does have an improved performance compared with the existing MMSE LE and approaches the MMSE Linear Equalizer with Perfect Extrinsic information Feedback (LE-PEF) only after a large number of iterations. For this reason the MMSE LE-EF is shown to suffer from the error propagation problem during the early iterations. A novel way to reduce the error propagation problem is proposed to further improve the performance of the MMSE LE-EF (I).

The MAP equalizer was shown to offer a much improved performance over the MMSE equalizers, especially during the initial iterations. Motivated by using the good quality of the MAP equalizer during the early iterations and the hybrid MAP/MMSE LE-EF (I) is proposed in order to suppress the error propagation problem inherent in the MMSE LE-EF (I). The EXIT chart analysis reveals that the hybrid MAP/MMSE LE-EF (I) requires fewer iterations in order to achieve convergence relative to the MMSE LE-EF (I). Simulation results demonstrate that the hybrid MAP/MMSE LE-EF (I) has a superior performance compared to the MMSE LE-EF (I) as well as approaches the performance of both the MAP equalizer and MMSE LE-PEF at high SNRs, at the cost of increased complexity relative to the MMSE LE-EF (I) receiver.

The final part of this dissertation considers the use of precoders in a TE system. It was shown in the literature that a precoder drastically improves the system performance. Motivated by this, the EXIT chart is used to analyse the characteristics of four different precoders for long block lengths. It was shown that using a precoder results in a loss in mutual information during the initial equalization stage. However,, we show by analysis and simulations that this phenomenon is not observed in the equalization of all precoded channels. The slope of the transfer function, relating to the MAP equalization of a precoded ISI channel (MEP), during the high input mutual information values is shown to play an important role in determining the convergence of precoded TE systems. Simulation results are presented to show how the precoders' weight affects the convergence of TE systems. The design of the hybrid MAP/MEP equalizer is also proposed. We also show that the EXIT chart can be used to compute the trellis code capacity of a precoded ISI channel.

Preface

The research work presented in this dissertation was performed by Mr Mohammed Yusuf Abdul Gaffar, under the supervision of Dr. H. Xu, at the University of Natal's school of Electrical, Electronic and Computer Engineering, in the Centre of Radio Access Technologies. This work was partially sponsored by Telkom South Africa Ltd and Alcatel Altech Telecoms as part of the Centre of Excellence programme.

Parts of this dissertation have been presented at a SATNAC conference and submitted for publications in SAIEE Transactions and the IEE Proceedings Communications.

The entire dissertation, unless otherwise indicated, is the author's work and has not been submitted in part, or in whole, to any other Universities for degree purposes.

Acknowledgements

I would like to thank my supervisor, Dr. H. Xu, for his excellent supervision and support throughout the course of my research work. His patience, advice and guidance are very much appreciated and have directly contributed to the completion of this dissertation. I would also like to thank Prof. F. Takawira for his guidance and helpful discussions.

I am greatly indebted to my parents for their constant support and encouragement. They are the source of my inspiration and have been instrumental in my pursuit of higher education. Special thanks also go to my twin brother Yunus, my sister Tasneem and Fanny for their perennial love and care. Their presence is without any question one of the best things in my life.

I am also grateful for the financial support received from Telkom SA Ltd and Alcatel S.A. during my M.Sc.

Finally, I would like to thank my postgraduate friends for proof reading parts of my dissertation and for allowing me the use of their computers in order to generate some of the simulation results in my dissertation. My time spent at university has been greatly enriched by their friendship and support.

Contents

List of Figures

List of Tables

List of acronyms

2G	Second Generation
3G	Third Generation
ADSL	Asymmetric Digital Subscriber Line
ASK	Amplitude Shift Keying
AWGN	Additive White Gaussian Noise
BAD	Bidirectional Arbitrated Decision feedback equalizer
BCH	Bose-Chaudhuri-Hocquenghem
BER	Bit Error Rate
BPSK	Binary Phase Shift Keying
CC	Convolutional Code
CDF	Cumulative Distributive Function
CDMA	Code Division Multiple Access
CIR	Channel Impulse Response
CMA	Constant-Modulus Algorithm
DFE	Decision Feedback Equalizer
DSL	Digital Subscriber Lines
ETSI	European Telecommunications Standards Institute
EXIT	Extrinsic Information Transfer
FEC	Forward Error Correction
FIR	Finite Impulse Response
FSK	Frequency Shift Keying
GSM	Global System for Mobile Communication
HM	Histogram Method
i.i.d.	Independent and identically distributed
IC	Interference Canceller
IEEE	Institute of Electrical and Electronic Engineers
ISDN	Integrated Services Digital Network
ISI	Intersymbol Interference
K-S	Kolmogorov-Smirnov
LDPC	Low Density Parity Check
LE	Linear Equalizer

LE-EF	Linear Equalizer with Extrinsic Feedback
LE-PEF	Linear Equalizer with Perfect Extrinsic Feedback
LLR	Log Likelihood Ratio
LMS	Least Mean Square
MEP	MAP equalization of the super-channel when a precoder is used
MAP	Maximum A Posteriori
MF	Matched Filter
ML	Maximum likelihood
MMS	Multimedia Media Service
MLSE	Maximum likelihood Sequence Estimation
MLVA	Maximum likelihood Viterbi Algorithm
MMSE	Minimum Mean Squared Error
OFDM	Orthogonal Frequency Division Multiplexing
PAPR	Peak to Average Power Ratio
PCCC	Parallel Concatenated Convolutional Codes
PDA	Personal Digital Assistant
PDF	Probability Density Function
PSK	Phase Shift Keying
RBF	Radial Basis Functions
RLS	Recursive Least Squares
RS	Reed-Soloman
RSSE	Reduced-State Sequence Estimation
SC	Single Carrier
SCCC	Serially Concatenated Convolutional Codes
SISO	Soft-Input Soft-Output
SNR	Signal to Noise Ratio
SO-DFSE	Soft-Output Decision Feedback Sequence Estimation
SOSA	Soft Output Sequential Algorithm
SOVA	Soft Output Viterbi Algorithm
SOVE	Soft Output Viterbi Equalizer
TAAM	Time Average Approximation Method
TCM	Trellis Coded Modulation
TDMA	Time Division Multiple Access
TE	Turbo Equalization
UMTS	Universal Mobile Telecommunications System

VDSL	Very high-data rate DSL
WCDMA	Wideband Code Division Multiple Access
WLAN	Wireless Local Area Network
WLL	Wireless Local Loop

List of symbols

a_n	AWGN
C	Channel capacity (bits/symbol)
C_T	Trellis code capacity
$C_{T,1}$	Trellis code capacity of super-channel utilizing precoder 1
$C_{T,2}$	Trellis code capacity of super-channel utilizing precoder 2
$C_{T,3}$	Trellis code capacity of super-channel utilizing precoder 3
$C_{T,4}$	Trellis code capacity of super-channel utilizing precoder 4
$C_{i.i.d}$	Independent and identically distributed channel capacity
d_j	Data bits
$\hat{d}_j$	Estimate of the data bits
D	The maximum absolute distance between two CDFs
E_s	Energy of symbol
$\mathbf{F}_n$	A priori covariance matrix of y_n
$g^e_{a,y_n}(l)$	PDF of the extrinsic information of the equalizer given y_n
$g^d_{a,x_n}(l)$	PDF of the extrinsic information of the decoder given x_n
$\psi^e_{a,y_n=+1}(l)$	CDF of $\lambda^e_{a,y_n}(l)$
$\psi^d_{a,x_{n+1}}(l)$	CDF of $\lambda^d_{a,x_n}(l)$
$\mathbf{H}$	Channel convolution matrix
$H(Y)$	Differential entropy of source Y
$H(Y \mid R)$	Differential entropy of source Y after observing R
h_k	Coefficients of the CIR
i.i.d.	Independent and identically distributed
$\mathbf{I}_M$	M x M identity matrix
$\mathbf{1}_{(M+L-1)\times 1}$	$(M+L-1)$ x 1 row vector with all 1's
$I(Y,R)$	Mutual information between Y and R
I_i^E	Input mutual information of the equalizer

I_o^E	Output mutual information from the equalizer
I_i^D	Input mutual information of the decoder
I_o^D	Output mutual information from the decoder
k_c	Number of output bits at the output of a CC
L	Finite impulse response length of ISI channel
$L_a(x_n)$	A priori LLR to the decoder
$L_a(y_n)$	A priori LLR to the equalizer
$L_{app}(y_n)$	A posteriori LLR from the equalizer
$L_{app}(x_n)$	A posteriori LLR from the decoder
$L_e(x_n)$	Extrinsic LLR from the decoder
$L_e(y_n)$	Extrinsic LLR from the equalizer
m_c	Memory order of encoder
M	Number of taps of feedforward FIR filter of MMSE LE
M_1	Length of precursor in feedfoward FIR filter of MMSE equalizer
M_2	Length of postcursor in feedback FIR filter of MMSE equalizer
M_b	Length of FB FIR filter in the MMSE DFE
n_c	Number of information bits at the input of a CC
N_{blocks}	Number of transmitted blocks
N_b	Number of data bits in the uncoded data stream
N_i	Length of interleaver
N_o	Single-sided power spectral density
p_k^i	The k^{th} branch connection for the i^{th} output of a CC
$\mathbf{P}$	Generator set of a CC
$\mathbf{P}_{nrc}$	Generator set of a non-recursive CC
$\mathbf{P}_{src}$	Generator set of a recursive CC
R_c	Code rate of encoder
$R_{inner\ code}$	Rate of inner code
R_p	Code rate of precoder
R_{tot}	Total code rate of inner and outer code
r_k	Output from channel

$\mathbf{r}_k$	Vector of outputs from channel
s	Current state of the trellis
s'	Previous state of the trellis
t_n	Training symbol stream
$v^e_{a,y_n=+1}(\gamma \mid \sigma^2_{ev})$	Conditional PDF generated with Gaussian distribution given variance σ^2_{ev} and mean $\sigma^2_{ev}/2$
$v^d_{a,x_n=+1}(\gamma \mid \sigma^2_{ev})$	Conditional PDF generated with a Gaussian distribution given variance σ^2_{ev} and mean $\sigma^2_{ev}/2$
$V^e_{a,y_n=+1}(\gamma \mid \sigma^2_{ev})$	CDF of $v^e_{a,y_n=+1}(\gamma \mid \sigma^2_{ev})$
$V^d_{a,x_n=+1}(\gamma \mid \sigma^2_{ev})$	CDF of $v^d_{a,x_n=+1}(\gamma \mid \sigma^2_{ev})$
w_n	FIR coefficients of the MMSE equalizers
x_n	Coded symbols
$\tilde{x}_n$	Coded bits
y_n	Interleaved coded symbols
$\tilde{y}_n$	Interleaved coded bits
$\tilde{y}^p_n$	Output bits from the precoder
y^p_n	Output symbols from the precoder
$\hat{y}_n$	Estimate of transmitted symbol
$\overline{y}^{\mathrm{pr}}_n$	Precursor mean estimates
$\overline{y}^{\mathrm{c}}_n$	Cursor mean estimates
$\overline{y}^{\mathrm{po}}_n$	Postcursor mean estimates
$\alpha_n(s)$	Forward probability in the MAP algorithm
$\beta_n(s)$	Backward probability in the MAP algorithm
$\gamma_n(s)$	Branch probability in the MAP algorithm
ρ	Correlation between a priori and extrinsic information
σ^2_a	Variance of the AWGN
σ^2_e	Variance of the generated a priori LLRs
σ^2_{ev}	Expected variance of a priori LLRs
η^{α}_n	Normalization constant of the alpha messages in the MAP

	algorithm
$\lambda^{e}_{a(\cdot,y_n)}(l)$	PDF for the a priori LLRs of the equalizer given y_n
$\lambda^{d}_{a(\cdot,x_n)}(l)$	PDF for the a priori LLRs of the decoder given x_n
$\psi^{e}_{a(\cdot,y_n=+1)}(l)$	CDF of $\lambda^{e}_{a(\cdot,y_n=+1)}(l)$
$\psi^{d}_{a(\cdot,x_{n=+1})}(l)$	CDF of $\lambda^{d}_{a(\cdot,x_n=+1)}(l)$
μ	Weighting term on the extrinsic LLRs for the MMSE LE-EF (I)
$\prod$	Interleaver
$\prod^{-1}$	Deinterleaver

Chapter 1

Introduction

1.1 General

The digital revolution has lead to the introduction of a number of different electronic devices, such as laptops, mobile phones, personal digital assistants (PDAs), etc. Further advances in the telecommunication industry are expected in the twenty-first century in order to bridge the digital divided across various technologies and electronic devices. The ability to transfer information anytime to anyone across the world is envisaged for future communication systems.

The Internet is expected to play an integral role in people's life with the ability to provide features such as web browsing, e-mail, e-commerce, real time voice and video. Communication systems are thus required in order to provide high-speed Internet connections for delay sensitive services such as streaming voice and video. This demand for high data rates and increased bandwidth has lead to the provision of broadband access to business and residential users. A number of different technological approaches have been developed to provide broadband access, such as Digital Subscriber Lines (DSL), cable modems, cellular systems, wireless local area networks (WLANs) and satellite. These competing technologies aim to provide a high quality of service for Internet applications.

The xDSL market has expanded over the years to establish numerous different variants. The most popular is Asymmetric Digital Subscriber Line (ADSL) which is suited for asymmetric Internet traffic. ADSL uses the existing copper line network to provide data over voice as well as independent voice and data transmission. This wireline access technology allows data transfer rates that are about 60 times higher than Integrated Services Digital Network (ISDN) systems in the downlink connection, while data rates up to 640 kbps are possible for the uplink direction. Since xDSL is a loop technology rather than a broadband access

technology, it can be used in different configurations and equipments. The development of standards in the xDSL market is still pending and is rather important to provide spectrum compatibility, interoperability and self-installation of xDSL modems.

Cable modems are a direct competitor with xDSL services which can offer speeds as high as 10 Mbps. The data rates offered by cable modems are much faster than all the xDSL technologies except the very high-data rate DSL (VDSL). Cable modems were initially designed to handle one-way traffic, but are being upgraded to carry two-way traffic.

The need for high data rate services in broadband access has seen the cellular industry migrating from second generation (2G) systems, such as Global System for Mobile communication (GSM), into third generation (3G) systems such as Universal Mobile Telecommunication System (UMTS). The goal of 3G systems is to provide the following variety of multimedia services: streaming video, multimedia message service (MMS), web browsing, etc. These 3G systems are expected to have the following advantages over 2G systems: bit rates up to 2 Mega bits per second (Mbps), variable bit rate to offer bandwidth on demand, high spectrum efficiency and support of asymmetric uplink and downlink traffic, etc. Wideband code division multiple access (WCDMA) offers an increased capacity over time division multiple access (TDMA) systems and is hence the air interface chosen by the European Telecommunications Standards Institute (ETSI) for UMTS.

Cellular systems are designed with a base station in order to provide communication with mobile and fixed line users. However,, in some cases the use of cellular systems can be expensive especially for a wireless link within a small area. WLANs are efficiently employed in such situations in order to eliminate the need for cables and extending the mobility of a fixed network. The two main competing technologies for WLANS are: Bluetooth and the Institute of Electrical and Electronic Engineers (IEEE) 802.11. These technologies aim to provide high data rates while maintaining a high quality of service.

These above emerging technologies are expected to gain increasing attention in communication systems. However, these systems are expected to encounter the problem of intersymbol interference (ISI) due to the need of high data rates. The design of such communication systems is thus critical to combat the problem of ISI and to achieve a high quality of service. Turbo equalization (TE) is one possible design solution to successfully design communication systems with the above requirements.

1.2 Digital communication systems

This section describes the basic components that make up a digital communication system. An introduction to equalization and channel coding techniques is given and the concepts behind the turbo principle are explained.

1.2.1 An overview

The goals of a communication system are to reliably and efficiently transmit data from a source to a destination over a physical channel. Shannon pioneered this field of research in 1948 and his excellent work laid the foundations for information theory [1]. A basic communication system, shown in Fig. 1.1, is essentially composed of the transmitter, the channel and the receiver.

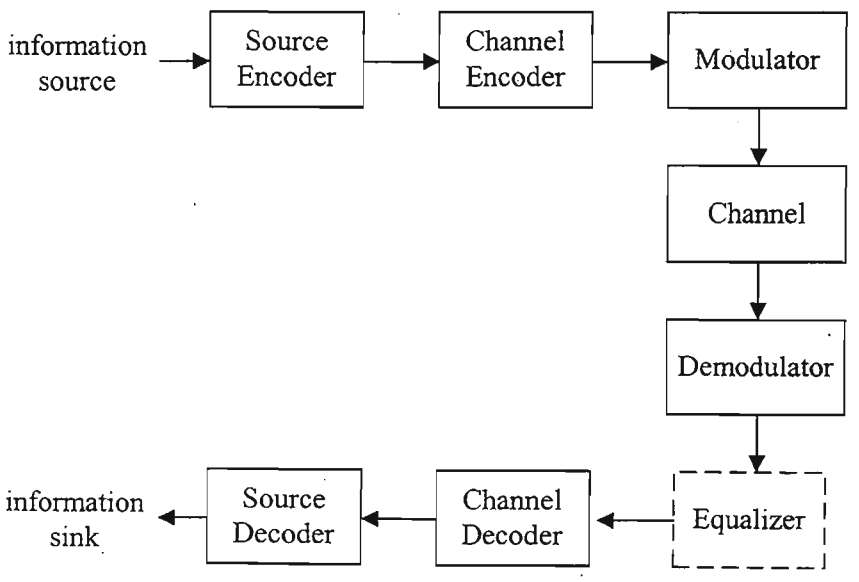

Fig. 1.1: Block diagram of a basic communication system

The information source can either be an analogue or a digital signal. Some types of information sources, like image and speech sources, often exhibit a substantial form of redundancy. A source encoder is beneficial in these circumstances and would eliminate the redundancy present in the information source by using a lossy or lossless compression technique. The channel encoder then adds a controlled amount of redundancy to the

compressed data in order to make the transmission of the compressed data more reliable. Shannon's separation theorem [1] proved that the source and channel coding can be treated separately without any degradation in performance. A digital modulation technique, such as Frequency Shift Keying (FSK), Phase Shift Keying (PSK), Amplitude Shift Keying (ASK), is used to perform the signal constellation mapping and transforms the bandwidth of the data into a desired pass band region. When modulation and coding are combined, this is referred to as trellis coded modulation (TCM).

The channel is the medium that separates the transmitted and received data. Different types of distortions can occur on the channel, such as ISI and additive white Gaussian noise (AWGN). The following are typical examples of physical channels which are used in communication systems: wireless, copper, cable, optical fiber, magnetic disks, etc.

The demodulator receives the channel corrupted output signals, transforms the frequency range of the transmitted signal into its baseband form and estimates the signal constellation mapping that occurred at the transmitter. An equalizer is required after the demodulator only if the channel experiences ISI. The channel and source decoder perform the inverse operation of the channel and source encoder, in order to obtain estimates of the information source.

1.2.2 Discrete-time model for a channel with ISI

A channel experiences frequency selective fading if the time delay between multipaths is much greater than the symbol duration. This phenomenon is experienced in bandwidth limited and wireless channels. The distortion introduced by frequency selective fading is called ISI. We also refer to an ISI channel as a frequency selective channel in this dissertation.

In this dissertation the model for an ISI channel will be represented by the equivalent discrete-time white noise filter model [2]. Fig. 1.2 illustrates the model of an equivalent discrete-time system with AWGN, where D is a delay operator. This model of the ISI channel is essentially a finite impulse response (FIR) filter where the receiver input r_n is given by,

$$r_n = \sum_{k=0}^{L-1} h_k y_{n-k} + a_n \tag{1.1}$$

where h_k are the tap coefficients, L is the length of the FIR filter, y_n are the transmitted symbols and a_n is the AWGN.

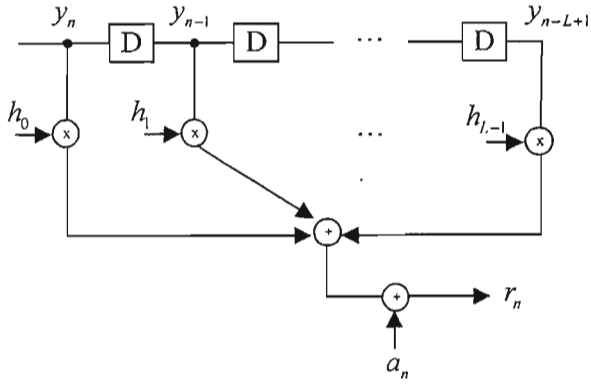

Fig. 1.2: Equivalent discrete-time model of an ISI channel with AWGN noise

The AWGN is due to the noise inherent in the electronics of the communication system and is referred to as thermal noise [2]. The coefficients of the FIR filter are referred to as the channel impulse response (CIR). In wireless channels, the CIR varies in time due to the relative motion of the transmitter, receiver or any objects between the transmitter and receiver. In this dissertation only ISI channels are considered.

1.2.3 Equalization techniques

The equivalent discrete-time white noise filter model indicates that the receiver inputs are distorted by the combined effects of ISI and AWGN. It is thus important to devise techniques to either combat the effects of ISI through efficient equalizer structures or mitigate the effects of ISI through the use of techniques like orthogonal frequency division multiplexing (OFDM). In this dissertation we only focus on the use of equalizers to overcome the effects of ISI and AWGN. This section provides a brief review of the various equalization techniques in the literature.

Equalizers can be generally classified as either blind or supervised. Blind equalizers are defined as equalizers that do not require training bits in order to overcome the detrimental effects of an ISI channel. These methods use higher order statistics, stochastic gradient algorithms such as the constant-modulus algorithm (CMA) and blind equalization algorithms based on the maximum likelihood (ML) criterion. An introduction to these blind equalization algorithms can be found in [2]. In this dissertation we focus on supervised equalizers which can be classified as either: trellis based, non linear or linear equalizers.

Trellis based equalizers in the literature can be classified as either sequence estimators or symbol by symbol estimators. The sequence estimators minimize the sequence error rate while the symbol by symbol estimators minimize the bit error rate (BER). The optimal sequence estimator is the maximum likelihood sequence estimator (MLSE) [3] and can be efficiently implemented using the maximum likelihood Viterbi algorithm (MLVA) [4]. The optimum maximum a posteriori (MAP) symbol by symbol detector (MAPSD) [5] minimizes the BER and hence is the optimal BER equalizer.

The disadvantage of trellis based equalizers is that the complexity increases exponentially with respect to the length of the CIR. For this reason the reduced-state sequence estimation (RSSE) [6] was proposed in order to reduce the complexity of trellis based equalizers.

Breakthroughs in signal processing techniques have lead to the introduction of various nonlinear equalizers. These include neural network equalizers [7] and radial basis functions (RBF) [8].

The linear equalizer (LE) [9] and the decision feedback equalizer (DFE) [10] are suboptimal equalizers that have a computational complexity linear with respect to the length of the CIR. These equalizers are composed of FIR filters and attempt to provide a lower computational complexity compared with trellis based equalizers. The LE is made up of a feedforward FIR filter while the DFE is composed of a feedforward and feedback FIR filter. The feedback filter in the DFE uses the past decisions at the output of the equalizer in order to suppress part of the ISI. The design of these equalizers is based on different optimization criteria, such as the peak distortion and minimum mean square error (MMSE).

The optimal, in the MMSE sense, MMSE LE or MMSE DFE requires exact knowledge of the CIR. A channel estimation algorithm is therefore required before equalization. The most

common algorithms used to estimate the CIR are the least mean square (LMS) and the recursive least squares (RLS) algorithm.

In [2], it was discussed that the LE is not suitable for channels with spectral nulls. In these circumstances the DFE is more appropriate and is the popular choice for the equalization of non minimum phase channels.

The design of a DFE is usually based on the assumption that the past decisions made by the equalizer are correct. However, when the DFE does make an error, the probability of subsequent errors increases even further. This results in the error propagation problem which is common in DFEs. The probability of error for a DFE with error propagation was presented in [11]. The study of error propagation was presented from a dynamical systems perspective in [12]. In [13], techniques for detecting decision errors in a DFE were presented. The use of soft decisions in the feedback path of the DFE was shown to mitigate the error propagation effect [14]. Recently, the bidirectional arbitrated DFE (BAD) [15] was proposed and was shown to offer an improved performance compared with the classical DFE. This improved performance is due to the BAD being composed of a forward and backward running DFE.

The use of a precoder was proposed in [16, 17] to provide a form of pre-equalization at the transmitter. This type of precoder basically acts as an inverse filter with respect to the frequency selective channel and can be interpreted as a form of spectral shaping and pre-filtering. However, the disadvantage of this type of precoder is an adverse increase in the computational complexity of the equalizer and that knowledge of the CIR is required at the transmitter. Other types of precoders do exist in the form of recursive convolutional codes (CCs) [18].

1.2.4 Channel coding

Channel coding comprises the use of a channel encoder and decoder in a communication system and is a power efficient way to combat the impairments caused by the channel. Forward error correction (FEC) codes essentially add a controlled amount of redundancy to the information bits such that they are more robust to the detrimental effects of the channel. Generally FECs are divided in two classes: block codes and CCs.

Block codes were originally invented and include the following types of codes: Low Density Parity Check (LDPC) codes [19], Bose-Chaudhuri-Hocquenghem (BCH) codes [20], Reed-Soloman (RS) codes [21], etc. These codes allow a detection of errors and a limited number of errors to be corrected. Recently, soft decision decoding of block codes have gained increasing attention by the coding research community [22].

CCs [23] are different from block codes in that the data bits are continuously encoded by the use of linear shift registers. The Maximum A Posteriori (MAP) [24] or SISO (Soft-Input Soft-Output) algorithm [25] is used to optimally decode CCs. Furthermore,, it was shown by the use of factor graphs in [26] that the MAP algorithm is actually an instance of the sum-product algorithm. The max log MAP algorithm [27] is a sub-optimal version of the MAP algorithm and is used to decode CCs at a much reduced computational complexity.

The Soft Output Viterbi Algorithm (SOVA) presented in [28] is another decoding algorithm for CCs. This algorithm offers a large saving in computational complexity compared with the MAP or SISO algorithm. However, the performance of the SOVA is inferior to the performance of the MAP algorithm.

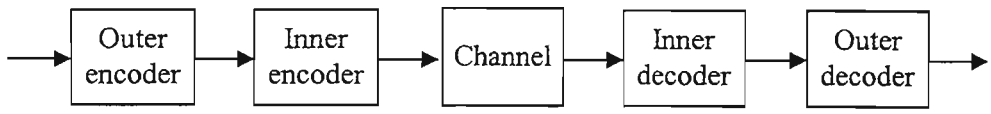

Fig. 1.3: Encoding and decoding structure of serially concatenated codes

In [29], the performance of serially concatenated codes was shown to be much improved compared with the performance of the individual codes. Fig. 1.3 shows the block diagram of the serially concatenated codes proposed in [29]. However, the limitations of this scheme were the hard decision decoding of the constituent codes and the bursts of errors at the output of the inner decoder which affected the decoding capability of the outer decoder. A solution to these problems was proposed in [30] which used soft decision decoders, an interleaver between the concatenation of CCs and a deinterleaver between the outer and inner decoders. The use of the deinterleaver at the receiver proved vital in the separation of bursts errors at the input of the outer decoder. The full decoding potential of concatenated codes was not realised until the remarkable breakthrough of turbo codes [31].

1.2.5 The turbo principle

Since the invention of turbo codes, many researchers have tried to identify their underlying principles in order to explain their amazing performance. The great interest in turbo codes is motivated by the fact that their performance is close to the Shannon limit with a reasonable computational complexity. This section explains the concept of the turbo principle which is constantly referred to in the literature and how these were derived from turbo codes.

Turbo codes are defined as the use of parallel concatenated convolutional codes (PCCC), separated by an interleaver, at the transmitter, and serially concatenated MAP decoders at the receiver. The fundamental difference between turbo codes and other encoding/decoding proposed prior to the introduction of turbo codes is the iterative decoding at the receiver. This innovative idea is critical in order to obtain substantial coding gains.

The type of information that is passed between component decoders is also important during the iteration decoding process. It was shown in [32] that for a systematic code such as a recursive CC, the a posteriori information at the output of the MAP decoder is composed of the: a priori information, channel reliability measure and extrinsic information. A good explanation of the terms: a posteriori information, a priori information, and extrinsic information is given in [33]. The extrinsic information is passed during the iterative decoding process at the receiver. This is due to the extrinsic information not being a function of the MAP decoder's inputs and hence keeping the correlation between the decoders' extrinsic information relatively low during the early iterations.

The interleaver and deinterleaver are also important mechanisms in turbo codes. One main function of the interleaver and deinterleaver is to separate bursts errors at the output of the decoders during the iterative decoding process. A well structured interleaver would also produce high weight codewords at the input of one encoder when low weight codewords are present at the input of the other encoder. The performance of an iterative decoding process is directly affected by the size of the interleaver and deinterleaver used. A large interleaver results in an improved performance with respect to a small interleaver. Various interleavers have been proposed in the literature, such as the random, S-random, block and code matched interleaver [34].

The foundation of turbo codes is therefore built with three important ingredients: interleaving/deinterleaving, soft iterative decoding and exchange of extrinsic information. The use of these three features is generally referred to as the turbo principle.

The turbo principle was applied to a serially concatenated convolutional code (SCCC) scheme in [35]. Simulation results demonstrated that the SCCC scheme offered a much improved performance with respect to the PCCC system at high signal to noise ratios (SNRs). Further applications of the turbo principle have been presented in various communication problems, such as TCM [36], code division multiple access (CDMA) [37], TE [38], etc.

1.3 Motivation for research

The future of the telecommunications industry is predicted to be driven by technologies that support mobility. One such technology is broadband wireless access systems. This technology would provide the resources need of broadband access to everyone, everywhere. For this reason wireless broadband access systems are thus expected to produce highly reliable communication systems while maintaining low costs and power efficiency.

Two major impediments in high performance digital wireless communication systems are ISI and AWGN. Equalization and OFDM are techniques that are often used to overcome the detrimental effects of the wireless channel. It was reported in [39] that the delay spreads in wireless access urban environments are within the order 1- 10us. In this situation a time domain equalizer does provide an adequate solution [40]. Furthermore, OFDM systems have the following disadvantages: excessive peak to average power ratio (PAPR) and sensitivity to frequency offsets and phase noise. This would result in higher hardware costs for OFDM systems compared with single carrier (SC) systems. Motivated by these facts a SC wireless broadband access system was developed by Cambridge Broadband which operates in the 3.4-3.8 GHz Wireless Local Loop (WLL), and delivers data rates up to 60Mbps full duplex to a single subscriber [40]. For these reasons the design of high performance equalizers is essential for SC systems.

Equalization in SC systems is an ongoing field of research. The use of channel coding also plays an important role in the quest for communication systems to reach the channel

capacity. Recently, TE has reached increasing attention since it was shown that the turbo principle could be applied to the field of channel coding and equalization. The use of MMSE equalizers in TE systems has only received limited attention. Furthermore, the performance and analysis of precoders in TE systems has only been considered for short block lengths.

In this dissertation, we focus on MMSE equalizers and precoders in TE systems. A general structure for MMSE equalizers is presented. Two MMSE equalizers and a hybrid MAP/MMSE equalizer are proposed in order to further improve the performance of MMSE equalizers in TE systems. Four precoders are investigated for a TE system in order to further improve the performance of TE systems. The influence of four precoders' weight on the convergence of TE systems is investigated for long block lengths. The extrinsic information transfer (EXIT) chart analysis of nonprecoded and precoded TE systems is presented. The validity of the EXIT chart analysis is also investigated. A comparison of the independent and identically distributed (i.i.d.) channel capacity and the trellis code capacities of four precoded channels are presented.

1.4 Dissertation overview

The outline for the remainder of this dissertation is as follows. In Chapter 2 the system model of a TE system is described. A review on the concept of channel capacity is given and related to a frequency selective channel. The i.i.d. channel capacity of an ISI channel is then presented. A literature survey of the various equalization schemes in TE systems is outlined. A general structure to derive MMSE equalizers is presented. The algorithms for the MAP equalizer, MMSE LE and MMSE DFE are then described in detail. Three equalization schemes are then proposed for TE systems in order to improve the performance of MMSE equalizers in TE systems. A comparison between the computational complexity of the MAP and MMSE equalizers is given. Channel coding techniques used in TE systems are also reviewed. CCs and the MAP decoder are then described. We compare the performance of TE systems employing the MMSE LE, MMSE DFE and two of the proposed equalization schemes.

In Chapter 3, the existing analysis tools in iterative decoding processes are reviewed. The EXIT chart is then explained in detail. The transfer functions of the three proposed equalization schemes are presented and compared with the existing MAP equalizer, MMSE

LE and MMSE DFE on the EXIT chart. We then compare two different methods to obtain the EXIT chart for TE systems utilizing various SISO equalizers. A novel technique to reduce the error propagation of one of the proposed equalizer is proposed. We then investigate whether the PDFs of the a priori information is Gaussian distributed using the Kolmogorov-Smirnov (K-S) test and the correlation between the a priori and extrinsic information, for the TE systems employing the three proposed equalizers and the existing MAP, MMSE LE and MMSE DFE. Finally, the computation of the i.i.d. channel capacity is then presented using the EXIT chart.

The performance and analysis of precoders in TE systems are considered in Chapter 4. We describe the system model of a TE system using a precoder. The concept of trellis code capacity is introduced. We then apply this idea to compute the trellis code capacities of four precoded channels and compare their results with the i.i.d. channel capacity. The performance of four precoded TE systems are investigated to show the effect of the precoders' weight on the convergence of TE systems. We then use the output mutual information measure to determine whether the equalization of precoded channels does incur a loss of information during the initial equalization stage. The EXIT analysis of four precoded TE systems is presented. We assess the validity of the EXIT chart analysis using the K-S test, for the four precoded TE systems. A hybrid nonprecoded/precoded transmitter scheme is proposed such that further improvements in the performance of TE systems can be achieved. Finally, the computation of the trellis code capacities is presented using the EXIT chart.

Lastly, conclusions are drawn and topics for future work are discussed in Chapter 5.

1.5 Original contributions in this dissertation

The original contributions of this dissertation include:

1. In Chapter 2, we present a general structure for MMSE equalizers. Three equalization schemes are proposed for TE systems such that improvements in the performance of MMSE equalizers in TE systems are obtained. We show that two of the proposed equalizers perform better than the existing MMSE LE in a TE system.

2. In Chapter 3, we use the EXIT chart to analyse the three proposed equalizers. A comparison of two methods to compute the output mutual information on the EXIT chart for the existing MAP equalizer, MMSE LE, MMSE DFE and the three proposed equalization schemes is presented. We then investigate the validity of the EXIT chart analysis using the K-S test and the correlation between the a priori and extrinsic information. A novel method to suppress the error propagation in one of the proposed equalizers is proposed. We also compare the computation of the i.i.d. channel capacity using the Arnold-Loeliger and the EXIT chart methods.

3. In Chapter 4, we investigate the influence of the precoders' weight on the performance of TE systems. We analyse the initial equalization stage of a precoded and nonprecoded TE system using the mutual information measure. The EXIT chart analysis of four precoded TE systems is presented for long block lengths. We show by simulations and analysis that a precoded TE system can perform better than a nonprecoded TE system, during the initial iterative phase, at high SNRs. Further, we observe that the gradient of the transfer function relating to the MAP equalizer of a precoded channel, during the high input mutual information values, plays an important role in the convergence of precoded TE systems. We then investigate the validity of the EXIT chart analysis using the K-S test. A hybrid equalization scheme is proposed for a TE system which uses no precoding and precoding at the transmitter. We compare the computation of the trellis code capacities of four precoded channels using the Arnold-Loeliger and the EXIT chart method.

Parts of this work in this dissertation have been presented and submitted for the following conferences and journals.

- M. Y. Abdul Gaffar, H. Xu, F. Takawira, "Improved performance of the MMSE linear equalizer in turbo equalization by the use of extrinsic feedback information", in *Proc. SATNAC 2003, George, South Africa*, Sept 2003.
- M. Y. Abdul Gaffar, H. Xu, F. Takawira, "Reduced error propagation effect by the use of the hybrid MAP/MMSE linear equalizer with extrinsic feedback in turbo equalization", *submitted to the SAIEE Transactions.*
- M. Y. Abdul Gaffar, H. Xu, F. Takawira, "EXIT chart analysis and performance of precoded turbo equalization systems for long block lengths" *submitted to the IEE Proceedings on Communications.*

Chapter 2

Turbo Equalization

2.1 Introduction

The use of channel coding in a frequency selective channel does yield significant improvements in the BER performance compared with an uncoded system. A coded data transmission over an ISI channel separated by an interleaver resembles a SCCC system, where the outer code is the channel encoder and the inner code is the frequency selective channel. The turbo principle can therefore be applied to this system to optimize the decoding performance. TE can thus be described as iterative equalization and decoding at the receiver. This field of study was pioneered by the authors in [41] to show that TE does provide substantial coding gains compared to one time equalization and decoding.

This chapter is an overview of TE and focuses on the different SISO equalization and decoding methods that appear in the literature. The achievable information rate of an ISI channel is also investigated. The MMSE linear equalizer with extrinsic feedback (LE-EF) (I), MMSE LE-EF (II) and the hybrid MAP/MMSE LE-EF (I) equalizers are proposed in this chapter for a TE system. The performances of these equalizers are compared to existing SISO equalization algorithms in a TE system.

In section 2.2 the system model for a TE system is described. A literature survey on the capacity of an ISI channel is outlined in section 2.3, where the uniform input information rate of an ISI channel is also computed. The existing MMSE and MAP equalization algorithms and three proposed equalization methods are outlined in section 2.4. A review of the different channel coding techniques in a TE system is shown in section 2.5, where the encoding and decoding of CCs are explained. Lastly, section 2.6 presents the performance of the MAP equalizer, MMSE LE, MMSE DFE, MMSE LE-EF (I) and the hybrid MAP/MMSE LE-EF (I) in a TE system.

2.2 System model for a TE system

This section presents the system model for a single user TE system. This system is based on that presented in [38] but here training symbols are employed. The basic building blocks that are used for a TE system are shown in Fig. 2.1. In this dissertation the frequency selective channel is assumed to be static and the CIR is assumed to be perfectly known at the receiver.

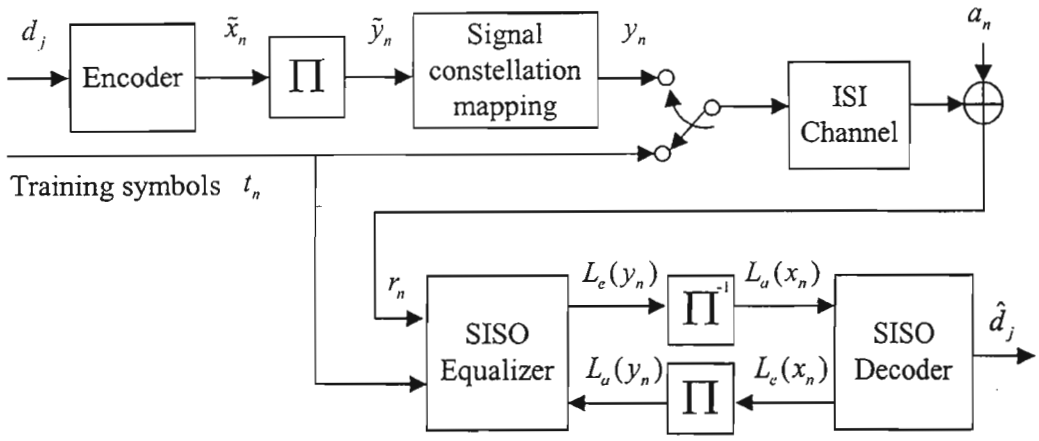

Fig. 2.1: Block diagram for a TE system

A block of N_b data bits, $d_j \in \{0,1\}$, is encoded to $N_i = N_b / R_c$ code bits to form $\tilde{x}_n \in \{0,1\}$, n = 1, 2... N_i, where R_c is defined as the code rate of the encoder. The interleaver ($\prod$), defined by a one to one index mapping function, permutes the encoded bits $\tilde{x}_n$ and outputs N_i interleaved encoded bits $\tilde{y}_n \in \{0,1\}$, n = 1, 2... N_i. Training symbols t_n, which are already mapped to their respective signal constellation, are used to avoid inter-block interference. The interleaved encoded bits $\tilde{y}_n$ are then mapped to their respective signal constellation represented by y_n, together with a block of N_t training symbols t_n, and are then transmitted over an ISI channel with CIR $h_k \in \mathbb{R}$, k = 0, 1, 2... $L-1$. $\mathbb{R}$ is defined as the set of real numbers.

In general higher modulation schemes can be used to reduce the required bandwidth or increase the data throughput. A TE system that uses a higher order modulation format is investigated in [42, 43]. In this dissertation only the Binary Phase Shift Keying (BPSK) modulation scheme is used. For this reason it follows that $y_n \in \{1,-1\}$.

The receiver input $r_n \in \mathbb{R}$ to the equalizer is given by,

$$r_n = \sum_{k=0}^{L-1} h_k y_{n-k} + a_n \tag{2.1}$$

where the noise samples $a_n \in \mathbb{R}$ are i.i.d. Gaussian random variables with zero mean and variance σ_a^2. A coherent symbol-spaced receiving process is assumed at the receiver.

The SISO equalizer receives r_n and computes the extrinsic Log Likelihood Ratios (LLRs) $L_e(y_n)$. The extrinsic LLRs of the equalizer are deinterleaved ($\prod^{-1}$) to provide the correct ordering of the a priori LLRs $L_a(x_n)$ to the input of the SISO decoder. The decoder accepts the a priori LLRs $L_a(x_n)$ and outputs the extrinsic LLRs $L_e(x_n)$. The LLRs $L_e(x_n)$ are then interleaved and used as the a priori LLRs $L_a(y_n)$ to the equalizer for the next iteration.

The transfer of extrinsic information is crucial in the turbo principle in order to prevent premature convergence during the iterative process. A termination criterium [44] or a predetermined number of iterations stops the iterative decoding system.

In a communication system the coded symbols y_n are transmitted on a block by block basis. In this dissertation the CIR is assumed to remain constant for the block duration and between successive blocks.

In wireless channels the CIR is time varying and hence a channel estimation algorithm is required in order to estimate the CIR. Recently, various soft channel estimation algorithms have been presented and compared for a TE system [45]. It was shown in [45] that soft LLRs from the decoder can improve the performance of a channel estimation algorithm.

2.3 Capacity of an ISI channel

In this section we introduce the concept of channel capacity which was presented in the classical paper by Shannon [1]. However, Shannon [1] only considered the case for an AWGN channel. This idea was later extended to consider discrete-time channels with memory [46].

The channel capacity is a measure of the optimal system performance which researchers try to achieve by means of coding. When the inputs to a channel are i.i.d. with a uniform distribution over the input alphabets, the channel capacity is referred to as the i.i.d. channel capacity $C_{i.i.d}$. A method to compute the i.i.d. channel capacity of a frequency selective channel is outlined and this technique is used to compute the $C_{i.i.d}$ of the Proakis C channel [2]. This would later serve as a measure of how closely a TE system approaches the $C_{i.i.d}$ limit.

2.3.1 The concept of channel capacity

Consider the ISI channel shown in Fig. 1.2. Let Y and R be the set of the alphabets for the transmitted symbols y_n and the receiver inputs r_n respectively. The mutual information $I(Y,R)$ describes the information that can be gained about the transmitted bit y_n given r_n. The mutual information depends on the characteristics of the channel and on the statistics of the transmitted symbols y_n. The maximum value of the mutual information over all the distributions of the transmitted symbols y_n is defined as the channel capacity C. We denote C using the expression

$$C = \max_{P(y_n)} I(Y,R). \tag{2.2}$$

Shannon's channel coding theorem [1] relates the channel capacity to the code rate R_c of the channel encoder. The code rate is defined as the ratio of the number of inputs to the number of outputs of the channel encoder. The channel coding theorem states that there exists a channel encoding and decoding algorithm that can provide reliable transmission of data across a channel with an error probability as small as desired, only if $R_c < C$.

2.3.2 Current literature

The capacity of an AWGN channel had been solved by Shannon [1]. However, the computation of the capacity of an ISI channel is still an open problem due to the memory inherent in a frequency selective channel. In [47] a lower bounds on the capacity were

computed. Recently, tight upper bounds [48] and lower bounds [49] of the channel capacity were computed.

The computation of the lower and upper bounds on the $C_{i.i.d}$ of a frequency selective channel was presented in [46]. An exact method to compute the $C_{i.i.d}$ of an ISI channel was presented in [50] and independently in [51] and [52]. The method presented in [50] to compute the $C_{i.i.d}$ of an ISI channel will be referred to as the Arnold-Loeliger method in this dissertation. The next section will detail the algorithm of the Arnold-Loeliger method.

2.3.3 The $C_{i.i.d.}$ of an ISI channel

A summary of the Arnold-Loeliger method is shown below. Fig. 1.2 shown in section 1.2.2 is replicated here for the derivation of the i.i.d. capacity of a frequency selective channel.

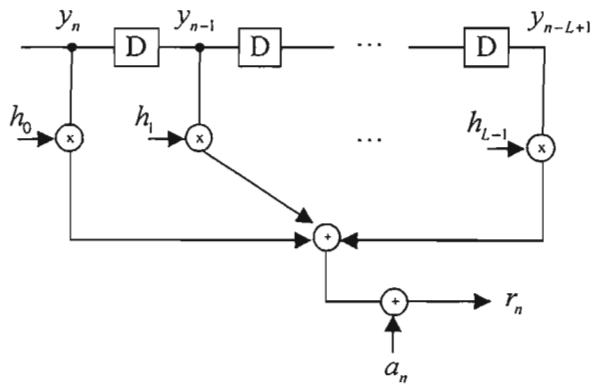

Fig. 2.2: An ISI channel represented by a FIR filter

The $C_{i.i.d}$ of an ISI channel is defined in (2.3) assuming BPSK modulation.

$$C_{i.i.d.} = \max_{P(y_i)=0.5} I(Y,R) \tag{2.3}$$

In [2], it was shown that the mutual information can be represented with respect to the differential entropy. This method of computing the mutual information is given in (2.4).

$$I(Y,R) = H(Y) - H(Y \mid R) \tag{2.4}$$

Let A be the set of alphabets for the AWGN a_n. As the output R is a sum of two independent random variables X and A, the mutual information can be expressed as

$$I(Y,R) = H(Y) - H(A). \tag{2.5}$$

The differential entropy of a random Gaussian variable was shown in [2] to be

$$H(A) = \frac{1}{2}\log_2(2\pi e\sigma_a^2). \tag{2.6}$$

It can be seen that the problem of computing the i.i.d. capacity of an ISI channel reduces to only finding $H(Y)$, when the transmitted symbols are i.i.d. with a uniform distribution. The Shannon-McMillan-Breimann theorem [53], applied to the case when Y is continuous [54], is a method to calculate $H(Y)$. Therefore $H(Y)$ can be computed using the expression shown in (2.7) below.

$$\lim_{n\to\infty} -\frac{1}{n}\log_2(p(y_n)) \to H(Y) \tag{2.7}$$

In the MAP equalization algorithm [44], the normalisation constant of the alpha messages yields the expression for $p(y_n)$ [55]. For this reason the normalisation constant of the alpha messages is used as the expression for $p(y_n)$ in (2.7). Let η_n^α be the normalisation constant of the alpha messages, for the nth stage of the trellis, in the MAP equalizer. Thus the expression for the i.i.d. capacity of an ISI channel can be obtained by computing the expression,

$$C_{i.i.d.} = \lim_{n\to\infty} \frac{1}{n}\log_2(\eta_n^\alpha) - \frac{1}{2}\log_2(2\pi e\sigma_a^2). \tag{2.8}$$

The computation of the capacity of ISI channels given in (2.8) demonstrates that the capacity is dependant on the variance of the noise σ_a^2 and the channel characteristics. We use the Arnold-Loeliger method to obtain the uniform input information rates of the Proakis C channel, as a function of E_s/N_o, where E_s is the symbol energy and N_o is the single-sided noise power spectral density. Fig. 2.3. illustrates the $C_{i.i.d.}$ for the Proakis C channel, defined as $\mathbf{h}_k = [0.227 \quad 0.46 \quad 0.688 \quad 0.46 \quad 0.227]$, as a function of SNR. The SNR is defined as,

$$SNR = 10\log_{10}\frac{E_s}{2\sigma_a^2} \tag{2.9}$$

when the CIR obeys the following condition

$$\sum_{k=0}^{L-1}(h_k)^2 = 1. \tag{2.10}$$

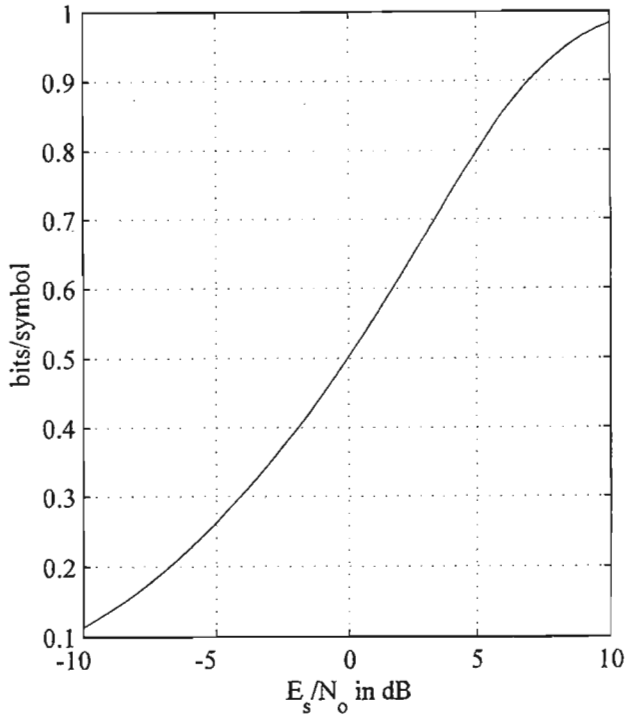

Fig. 2.3: The uniform input information rate of the Proakis C channel

2.4 Equalization techniques in TE

The use of soft decisions, from the decoder, at the input of an equalizer was shown to substantially improve the BER at the receiver [44]. Motivated by this, various SISO equalization algorithms have been developed in the literature to accommodate the interleaved extrinsic LLRs from the decoding stages in an iterative decoding process. A review of existing SISO equalization algorithms in a TE system is given. The details of the MAP equalizer, MMSE LE and the MMSE DFE are then outlined. The proposed MMSE LE-EF (I) and (II) and hybrid MAP/MMSE LE-EF (I) algorithms are also explained. A comparison between the computational complexity of the MAP and MMSE equalizers is given.

2.4.1 Current literature

The use of the Soft Output Viterbi Equalizer (SOVE) [41] was the first proposed SISO equalizer for an iterative decoding process at the receiver. The idea of the SOVE was based

on the trellis structure of the channel which can be efficiently decoded using the Viterbi algorithm. However, the SOVE minimizes the sequence error rate and not the BER.

Improvements in the trellis based SOVE algorithm was made by the introduction of the MAP equalizer in [44] which minimized the BER. The superior performance of the MAP equalizer compared with the SOVE was due to the computational intensive MAP equalization algorithm. The Max Log MAP equalizer, presented in [56], has a reduced computational complexity in comparison to the MAP equalizer but with an inferior BER performance.

Another technique used to reduce the complexity of the MAP equalizer was to decrease the number of states in the trellis. This idea was applied to the scheme presented in [43] for a TE system.

The Soft Output Sequential Algorithm (SOSA) which is another trellis based equalizer, was proposed in [57] to show that sequential estimation algorithms can also be applied in a TE system. A SOVA based Soft-Output Decision Feedback Sequence Estimation (SO-DFSE) equalizer was also presented in [58].

The computational complexity of an equalizer using a priori information was shown in [37] to be reduced by the use of the MMSE LE. However, this is only the case if the taps of the FIR length of the MMSE LE is chosen to be not much greater than the length of the ISI channel. The MMSE LE incorporating a prior information was first introduced in [37] as part of a multi-user detector in a CDMA system. The MMSE LE was then used in a single user TE scheme, extending the FIR length of the MMSE LE to be greater than the length of the ISI channel, to show that the MMSE LE can approach the performance of the MAP equalizer for long block lengths at high SNRs [38]. The complexity of the MMSE LE was further reduced by the use of a frequency domain equalizer in [59, 60].

The use of the matched filter (MF)/Interference canceller (IC) equalizer was initially proposed by the authors in [61] and was later presented in [38, 62]. Furthermore, the MF/IC equalizer was shown in [38] to be an instance of the MMSE LE. However, it was also shown in [38] that the MF/IC equalizer did not provide reliable decisions during the early iterations and is only effectively used during the later iterations. For this reason a hybrid equalization scheme was developed in [38] which uses a low complexity MMSE LE during the early

iterations and then switches to the MF/IC equalizer during the later iterations. The advantage of this hybrid equalizer was that it approached the performance of the MAP equalizer at high SNRs at a much reduced computational complexity compared with the MAP equalizer.

The use of a combined DFE and MF/IC equalization structure, for a TE system, was proposed in [63, 64] which used soft decision feedback from the output of the equalizer and hard decisions from the decoder in order to minimize the error propagation problem of a DFE.

A MMSE DFE, incorporating a prior knowledge in the feedforward and feedback FIR filters, with hard decision feedback was proposed in [38]. In [65] a MMSE DFE with soft decision feedback, not incorporating a priori knowledge in the feedforward and feedback filters was presented.

Lastly, a SISO equalizer based on neural networks and radial basis functions was proposed in [66]. In this dissertation we focus on the MAP equalizer, MMSE LE and the MMSE DFE. A review of these two equalization algorithms is given in the next sections.

2.4.2 The MAP equalizer

The MAP equalizer minimizes the BER and computes the a posteriori information defined in (2.11) using the MAP algorithm. The details of the MAP equalization algorithm given in [44] is outlined in this section.

$$L_{app}(y_n) \triangleq \ln \frac{\Pr\{y_n = +1 \mid r_n\}}{\Pr\{y_n = -1 \mid r_n\}} \tag{2.11}$$

The a posteriori LLR of the MAP equalization algorithm is computed by the expression,

$$L_{app}(y_n) = \ln \frac{\sum_{\substack{(s',s) \\ y_n=+1}} \alpha_{n-1}(s')\gamma_n(s',s)\beta_n(s)}{\sum_{\substack{(s',s) \\ y_n=-1}} \alpha_{n-1}(s')\gamma_n(s',s)\beta_n(s)} \tag{2.12}$$

by considering the states of the channel trellis s_n being associated with the information symbols y_n. The expressions s' and s denote the states during the $(n-1)^{\text{th}}$ and n^{th} stage of

the trellis. Furthermore, $\alpha_n(s)$, $\gamma_n(s)$ and $\beta_n(s)$ are termed the forward, branch and backward probabilities respectively and are defined as,

$$\alpha_{n-1}(s) \triangleq \Pr(s_n = s \mid r_1, r_2 \ldots r_{n-1}) \tag{2.13}$$

$$\gamma_n(s',s) \triangleq \Pr(s \mid s') \cdot \Pr(r_n \mid s',s) \tag{2.14}$$

$$\beta_n(s) = \frac{\Pr(r_{n+1} \ldots r_{N_i} \mid s)}{\Pr(r_{n+1} \ldots r_{N_i} \mid r_1 \ldots r_n)}. \tag{2.15}$$

The computation of these expressions is given by,

$$\alpha_n(s) = \frac{\sum_{s'} \gamma_n(s',s)\alpha_{n-1}(s')}{\sum_{s}\sum_{s'} \gamma_n(s',s)\alpha_{n-1}(s')} \tag{2.16}$$

$$\gamma_n(s',s) = \exp\left(-\frac{1}{2\sigma_u^2} \mid r_n - \sum_{k=0}^{L-1} h_k y_{n-k} \mid^2\right) \cdot \exp\left(\frac{1}{2} y_n L_a(y_n)\right) \tag{2.17}$$

$$\beta_{n-1}(s') = \frac{\sum_{s} \gamma_n(s',s)\beta_n(s)}{\sum_{s}\sum_{s'} \gamma_n(s',s)\alpha_{n-1}(s')}. \tag{2.18}$$

Note that the expression $\gamma_n(s',s)$, in (2.17), is a function of the previous state $s' \in \{y_{n-1}, \cdots, y_{n-L}\}$ and the current state $s \in \{y_n, \cdots, y_{n-L+1}\}$.

The training symbols t_n are used to initialise $\alpha_n(s)$ to the zero state of the trellis before the symbols y_n are transmitted over the channel. However, no trellis termination symbols are used to force the start of the channel to the zero state after the coded symbols y_n are transmitted. Therefore the boundary conditions for $\alpha_n(s)$ and $\beta_n(s)$ are set to,

$$\alpha_0(0) = 1 \quad \text{and} \quad \alpha_0(s) = 0 \quad \forall s = 1,2,\cdots,2^{L-1} \tag{2.19}$$

$$\beta_{N_i}(s) = \frac{1}{2^{L-1}} \qquad \forall s = 0,1,2,\cdots,2^{L-1}. \tag{2.20}$$

The a posteriori information of the MAP equalizer is only composed of the a priori information and the extrinsic information. This is due to the ISI channel having real addition rather than the modular 2 addition in CC and hence the channel reliability measure is included in the extrinsic information. The extrinsic LLRs $L_e(y_n)$ at the output of the equalizer are passed to the decoder for the next iteration and are obtained from the expression given in (2.21).

$$L_e(y_n) = L_{app}(y_n) - L_a(y_n) \tag{2.21}$$

The computational burden of a trellis based equalizer is exponential with respect to the length of the channel L for every receiver input r_n. Furthermore, if the length of the channel L is excessively long, the MAP equalizer would not be a practical equalizer for real communication systems. In this situation, MMSE equalizers are more appropriate since it was shown in [67] that MMSE equalizers have a quadratic computational complexity with respect to the length of the CIR.

2.4.3 MMSE equalizers using a prior information

The difference between the MMSE equalizers and the MAP equalizer is the processing of the receiver inputs to compute the extrinsic LLRs based on different performance criteria. The MMSE equalizers compute the initial extrinsic LLR value after receiving the number of symbols corresponding to the FIR length of the MMSE equalizer and then subsequently only requiring one receiver input to compute the next extrinsic LLR. However, the MAP equalizer computes the extrinsic LLRs after receiving the entire N_t training and N_i data symbols.

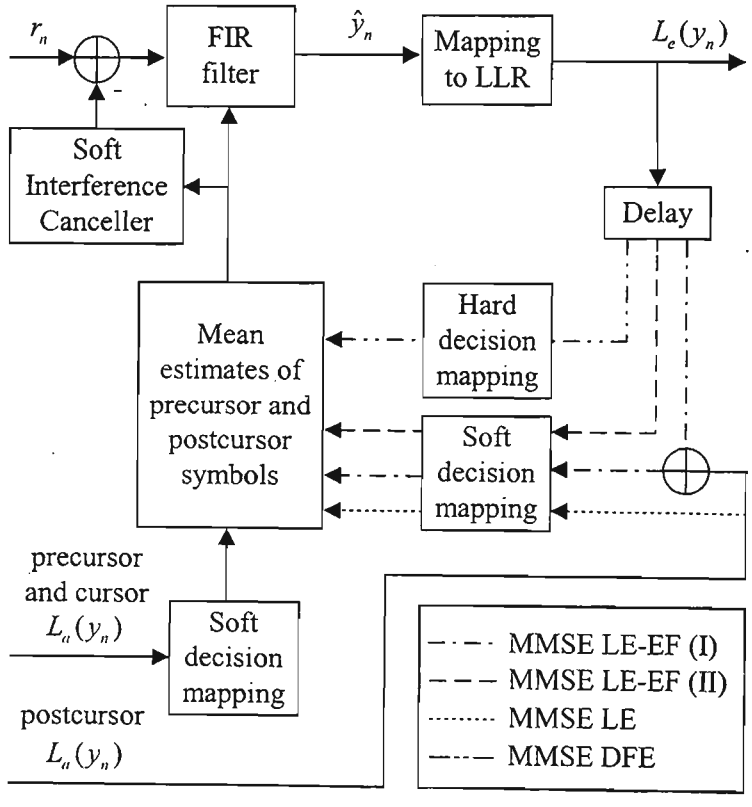

Fig. 2.4: General structure of MMSE equalizers using a priori information

Four MMSE equalizers have been considered in this dissertation: the MMSE LE, MMSE LE-EF (I), MMSE LE-EF (II) and the MMSE DFE. A general structure for MMSE equalizers that use a priori information is presented and can be obtained by following the respective legends in Fig. 2.4.

The diagram of the MMSE DFE, in Fig. 2.4, is only valid if the feedforward and feedback FIR filters are defined as in section 2.4.3.2. Note that the instances that are derived from the general MMSE equalizer structure only differ in the way the postcursor mean estimates are computed. The next sections will detail the algorithm used for the four MMSE equalizers.

2.4.3.1 MMSE LE

The MMSE LE that is used in a TE system is an extension of the MMSE LE in [2] to include a priori information. The algorithm for the MMSE LE with a priori information is outlined below and is a summary of the algorithm shown in [67].

The following notation is introduced before the derivation of the MMSE LE. Vectors are written in bold letters and matrices are expressed in bold capital letters. The expression $E\{\cdot\}$ is the first moment operator. The transpose and Hermitian operators are given by $()^T$ and $()^H$ respectively.

The core aspect of the MMSE LE involves the time varying FIR filter $w_{n,k}$, $k = M_2, M_2 - 1, \cdots, 0, \cdots, -M_1$ of length $M = M_1 + M_2 + 1$. The a priori LLRs are converted to their respective precursor $\bar{y}_n^{\text{pr}}$, cursor $\bar{y}_n^{\text{c}}$ and postcursor $\bar{y}_n^{\text{po}}$ mean estimates using the same soft decision mapping,

$$\bar{y}_n^{\text{pr}} \triangleq \tanh(L_a(y_n)/2) \tag{2.22}$$

$$\bar{y}_n^{\text{c}} \triangleq \tanh(L_a(y_n)/2) \tag{2.23}$$

$$\bar{y}_n^{\text{po}} \triangleq \tanh(L_a(y_n)/2). \tag{2.24}$$

We define the following vectors,

$$\mathbf{w}_n \triangleq [w_{n,M_2} \; w_{n,M_2-1} \cdots \; w_{n,0} \cdots w_{n,-M_1}]^T \tag{2.25}$$

$$\bar{\mathbf{y}}_n \triangleq [\bar{y}_{n-L-M_2+1}^{po} \cdots \bar{y}_{n-1}^{po} \; \bar{y}_n^{c} \; \bar{y}_{n+1}^{pr} \cdots \bar{y}_{n+M_1}^{pr}]^T \tag{2.26}$$

2.4.3.2 MMSE DFE

The MMSE DFE differs from the MMSE LE only in the computation of the postcursor mean estimates. We assume the length of the feedforward and feedback FIR filter to be of length $M = M_1 + M_2 + 1$ and $M_h = L + M_2 - 1$ respectively.

The postcursor mean estimates for the MMSE DFE are obtained by a hard decision mapping on the estimated transmitted symbol $\hat{y}_n$,

$$\overline{y}_n^{\text{po}} \triangleq \begin{cases} +1, & \hat{y}_n \geq 0 \\ -1, & \hat{y}_n < 0 \end{cases}. \tag{2.34}$$

In summary, the MMSE DFE can be obtained from the MMSE LE by replacing (2.24) in section 2.4.3.1 by (2.34). A more detailed derivation of the MMSE DFE can be found in [67].

2.4.3.3 MMSE LE-EF (I) and (II)

It can be seen from (2.32) that the MMSE LE and the MMSE DFE only require processing of M receiver inputs to compute the extrinsic LLR of the cursor symbol. However, for the computation of consecutive extrinsic LLRs, the current cursor symbol becomes the postcursor symbol. Since the extrinsic information is independent of the a priori information, the extrinsic LLRs can therefore also be used to compute the postcursor mean estimates. Motivated by improving the performance of the MMSE LE, the MMSE LE-EF (I) and (II) are proposed which compute the postcursor mean estimates using different expressions rather than what was used for the MMSE LE or the MMSE DFE.

The postcursor mean estimates for the MMSE LE-EF (I) are computed by using a soft decision mapping on the sum of the a priori and extrinsic LLRs,

$$\overline{y}_n^{\text{po}} \triangleq \tanh((L_a(y_n) + L_e(y_n))/2) \tag{2.35}$$

while for the MMSE LE-EF (II), the postcursor mean estimates are derived using only a soft decision mapping on the extrinsic LLRs

$$\overline{y}_n^{\text{po}} \triangleq \tanh(L_e(y_n)/2). \tag{2.36}$$

The extrinsic information at the output of the MMSE LE-EF (I) and (II) can be obtained by computing the expressions (2.22)-(2.33) given in section 2.4.3.1 and replacing (2.24) by (2.35) and (2.36) respectively.

2.4.4 Hybrid MAP/MMSE LE-EF (I)

The MMSE LE-EF (I) is shown in section 2.6 to suffer from the error propagation problem after the initial equalization stage which inhibits its performance. Motivated by suppressing the error propagation problem inherent in the MMSE LE-EF (I) a hybrid equalization scheme is proposed.

The MAP equalizer is shown in [38] to offer a much improved performance over the MMSE equalizers, especially during the initial iterations. The hybrid MAP/MMSE LE-EF (I) is hence proposed which uses the MAP equalizer during the initial equalization stage and then switches to the MMSE LE-EF(I) for further iterations. Therefore the hybrid MAP/MMSE LE-EF (I) can be realised by using the expressions for the MAP equalizer, given in section 2.4.2, for the initial equalization stage and the expressions for the MMSE LE-EF (I), given in section 2.4.3.1 and section 2.4.3.3, for subsequent iterations.

2.4.5 Complexity comparison - MMSE and MAP equalizers

The computational complexity of the MAP and MMSE LE and MMSE DFE equalizers was outlined in [38]. It was shown that the MAP equalizer has an exponential increase in complexity, while the complexity of the MMSE equalizers increases with a quadratic order, with respect to the length of the ISI.

The MMSE LE-EF (I) and (II) have the same complexity as that of the MMSE LE if the computation of the precursor, cursor and postcursor mean estimate mappings $L_a(y_n) \rightarrow \overline{y}_n^{pr}, \overline{y}_n^{c}, \overline{y}_n^{po}$ and the extrinsic information mapping $\hat{y}_n \rightarrow L_e(y_n)$ is neglected. Table 2.1 compares required number of real additions and multiplications for the MAP equalizer and the MMSE equalizers, neglecting the mean estimate mapping and the extrinsic information mapping per receiver input r_n per iteration.

Table 2.1: Computational complexity comparison between the MAP equalizer and the MMSE equalizers

Equalization type	Real multiplications	Real additions
MAP equalizer	$3 \cdot 2^M + 2^M$	$3 \cdot 2^M$
MMSE LE	$16M^2 + 4L^2 + 10L - 4M - 4$	$8M^2 + 2L^2 - 10M + 2L + 4$
MMSE LE-EF (I)	$16M^2 + 4L^2 + 10L - 4M - 4$	$8M^2 + 2L^2 - 10M + 2L + 4$
MMSE LE-EF (II)	$16M^2 + 4L^2 + 10L - 4M - 4$	$8M^2 + 2L^2 - 10M + 2L + 4$
MMSE DFE	$16M^2 + 4L^2 + 10L - 4M - 4$	$8M^2 + 2L^2 - 10M + 2L + 4$

The computational complexity of the hybrid MAP/MMSE LE-EF (I) can be obtained from the MAP equalizer, for the initial equalization stage, and the MMSE LE-EF (I) for subsequent iterations. Note that the MMSE LE-EF (I) would require one more addition, for every receiver input r_n per iteration, compared to the MMSE LE or the MMSE LE-EF (II) if the computation of the postcursor mean estimate mapping $L_u(y_n) \rightarrow \bar{y}_n^{po}$ was considered. This difference can be noted from observing the expressions given in (2.24), (2.35) and (2.36) for the MMSE LE, MMSE LE-EF (I) and (II) respectively.

2.5 Channel coding in TE

The use of encoding schemes that can be decoded with a SISO algorithm is suitable to be used in a TE system. In this section a review of the existing encoding and decoding schemes in a TE system is given. An overview of CCs and the MAP decoding algorithm is then presented.

2.5.1 Literature review

The first encoding/decoding scheme proposed in [41] for a TE system was the use of a CC and the SOVA for the encoder and decoder respectively. A TE system employing a CC was decoded using the MAP decoder in [44] and the Soft-Output DFSE (SO-DFSE) in [58]. Double concatenated CCs in the form of PCCC was presented in [68]. This scheme was

shown to offer substantial performance gains during the iterations. A SCCC encoding scheme was proposed in [69] and was shown, by the EXIT chart, to closely approach the i.i.d. channel capacity.

Block codes is another class of codes which have been invesitaged for a TE system. In [70], BCH codes were proposed and compared to CCs and convolutional turbo codes. It was shown, using the MAP algorithm to decode the respective codes, that convolutional turbo codes performed the best amongst the considered codes.

Regular LDPC codes were proposed in [71] and were shown to be an attractive alternative to CCs. The design of irregular LDPC codes, using linear programming techniques and density evolution, was proposed in [72] and was shown to closely approach the $C_{i.i.d.}$ of an ISI channel. Regular and irregular LDPC codes were presented in [73], for a TE system utilizing the MMSE LE, where the irregular LDPC code was designed using a non-linear optimization procedure called differential evolution and density evolution. The sum-product algorithm was used to decode the LDPC codes in the [71, 72, 73].

TCM was also considered, as the outer encoding scheme, to efficiently improve the bandwidth of a TE system. A TCM encoding scheme was presented in [74] and the performance of this TE system was shown to approach the MF bound.

In this dissertation, CCs are only considered. A brief summary of CCs are given in the next section.

2.5.2 Convolutional Codes

A CC is specified by the memory order m_c, number of input (or information) bits n_c at the input of the encoder, the number of output (or coded) bits k_c at the output of the encoder and the generator set $\mathbf{P}$. A CC can also be represented in the form of a state transition or trellis diagram. Another important parameter is the rate of the code which is defined as

$$R_c = \frac{n_c}{k_c}. \tag{2.37}$$

Puncturing is a technique used to increase the rate of a CC. The puncturing pattern is also required at the receiver and is used by the respective decoder. However, increasing the rate decreases the decoding performance of a CC.

CCs can be classified as either non-recursive CCs or recursive CCs. The next section will discuss these two different types of CCs.

2.5.2.1 Nonrecursive and recursive CCs

The fundamental difference between a nonrecursive CC and a recursive CC is that a nonrecursive CC has a FIR while a recursive CC has a IIR. In this dissertation we only consider the case where $n_c = 1$. The generator set for non-recursive CCs $\mathbf{P}_{nrc}$ and recursive CCs $\mathbf{P}_{src}$ are defined as,

$$\mathbf{P}_{nrc} = \{\mathbf{p}^i, 1 \le i \le k_c\}, \quad \mathbf{p}^i = \sum_{k=0}^{m_c} p_k^i D^k \tag{2.38}$$

$$\mathbf{P}_{src} = \{1, \frac{\mathbf{p}^i}{\mathbf{p}^1}, 2 \le i \le k_c\}, \quad \mathbf{p}^i = \sum_{k=0}^{m_c} p_k^i D^k, \quad \mathbf{p}^1 = \sum_{k=1}^{m_c} p_k^1 D^k, \quad p_0^1 = 1 \tag{2.39}$$

where $p_k^i \in \{0,1\}$. It can be seen from (2.38) and (2.39) that the realization of $\mathbf{P}_{src}$ is exactly the same as $\mathbf{P}_{nrc}$ when $\mathbf{p}^1 = 1$. Octal notation [2] is a simplified way to express the generator sets of CCs. Fig. 2.5 and Fig. 2.6 show the diagrams of a nonrecursive CC and recursive CC, respectively, when $n_c = 1$ and $k_c = 2$.

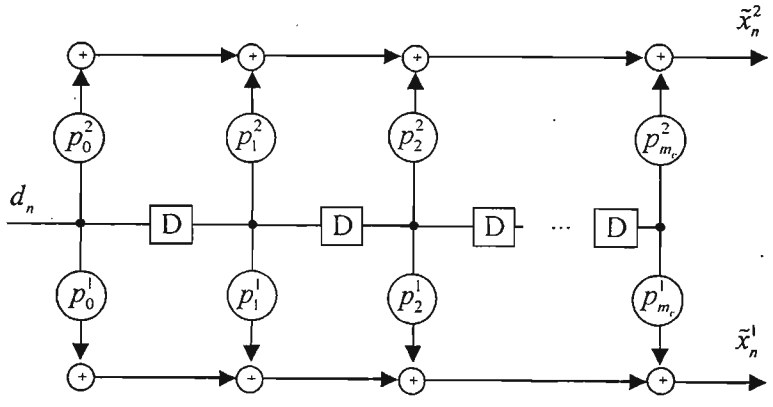

Fig. 2.5: Diagram of a nonrecursive CC

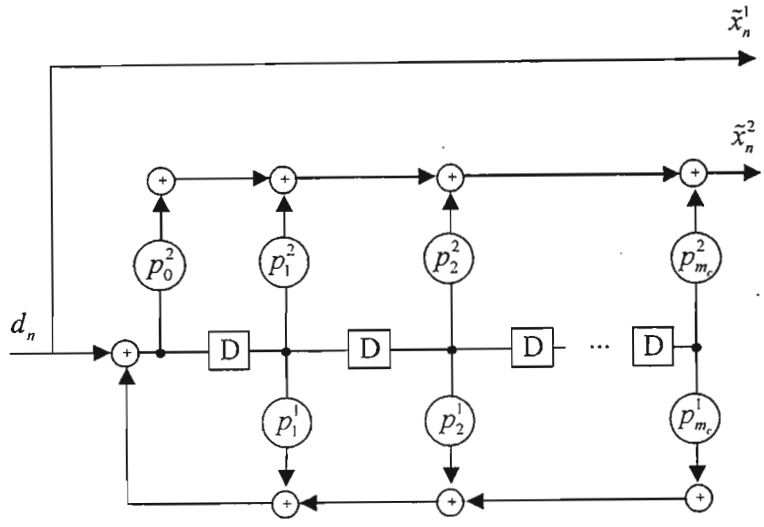

Fig. 2.6: Diagram of a recursive CC

It can be noted from Fig. 2.5 that the non recursive CC only has feedforward connections and hence corresponds to a FIR. However, a recursive CC has feedforward and feedback connections, as can be seen in Fig. 2.6, and thus possesses an IIR.

The MAP decoding characteristics of recursive CCs and nonrecursive CCs were compared in [75] using the EXIT chart. It was shown that the MAP decoding of nonrecursive CCs, which are limited by the constraint length, have inferior performance compared with the MAP decoder relating to recursive CCs. For this reason recursive CCs are chosen to be used in a TE system.

2.5.2.2 Trellis termination

The decoding capability of a CC is improved if the start and end states are set accordingly. Two common approaches are used to achieve this function: trellis termination and tail biting. Trellis termination is a method that uses additional bits to force the state of the encoder to the all zero encoder state. This method requires redundancy bits, at the end of a data block, equal to the memory order m_c of an encoder. Tail biting is a technique that ensures that the start and end states are the same. However, tail biting does increase the decoding complexity at the receiver.

In this dissertation we only consider trellis termination, at the cost of reduced decoding complexity with respect to tail biting, to ensure that the start and end states are set to the all zero encoder state.

2.5.3 MAP Decoder

The MAP decoder, used in a TE system, is derived from the general SISO decoding algorithm presented in [25]. This MAP decoder accepts a priori LLRs of the information and coded symbols from the equalizer and computes the extrinsic information of the *coded symbols* during the iterative process. For this reason it is termed the COD-MAP decoder in [44]. We denote the COD-MAP decoder briefly as the MAP decoder, since the COD-MAP decoder is just an instance of the general SISO decoding algorithm. A summary of the MAP decoder is given below.

Consider the recursive CC in Fig. 2.6 and the TE system in Fig. 2.1. The output of the encoder in Fig. 2.1, is made up of the information bits $\tilde{x}_n^1$ and the coded bits $\tilde{x}_n^2$. We denote x_n^1 and x_n^2 as the signal constellation mapping of $\tilde{x}_n^1$ and $\tilde{x}_n^2$ respectively. The a posteriori LLRs of the MAP decoder is computed by substituting y_n for x_n in (2.12). The forward $\alpha_n(s)$, branch $\gamma_n(s)$ and backward $\beta_n(s)$ probabilities are similarly defined by replacing r_n with x_n in (2.13), (2.14) and (2.15). The forward $\alpha_n(s)$ and backward $\beta_n(s)$ probabilities are computed using (2.16) and (2.18) respectively. However, the branch probability is obtained by computing the expression given in (2.40) below.

$$\gamma_n(s',s) = \exp(\frac{1}{2} x_n L_a(x_n)) \tag{2.40}$$

The encoder is initially set to the all zero state before the data bits are processed and forced to the all zero state, by trellis termination, after $N_d - m_c$ data bits. Therefore the boundary conditions for $\alpha_k(s)$ and $\beta_n(s)$ are set to

$$\alpha_0(0) = 1 \quad \text{and} \quad \alpha_0(s) = 0 \quad \forall s = 1,2...2^{L-1} \tag{2.41}$$

$$\beta_{N_i}(0) = 1 \quad \text{and} \quad \beta_{N_i}(s) = 0 \quad \forall s = 1,2...2^{L-1}. \tag{2.42}$$

The extrinsic LLRs at the output of the MAP decoder are the difference between the a posteriori LLRs and the a priori LLRs. This is due to the absence of the channel reliability

measure at the input of the MAP decoder. The computation of the extrinsic information $L_e(x_n)$ is obtained by substituting y_n for x_n in (2.21).

These extrinsic LLRs are then deinterleaved and passed to the SISO equalizer during the iterative decoding process. However, at the final iteration a hard decision is taken on the a posteriori LLRs of the *information symbols*. The a posteriori information is computed using the expression given by,

$$L_{app}(x_n^l) = \ln \frac{\sum_{\substack{(s',s) \\ x_n^l=1}} \alpha_{n-1}(s')\gamma_n(s',s)\beta_n(s)}{\sum_{\substack{(s',s) \\ x_n^l=-1}} \alpha_{n-1}(s')\gamma_n(s',s)\beta_n(s)}. \tag{2.43}$$

Since the a posteriori LLRs of the information symbols are only needed, the coded symbols can also be used to compute the branch probablity. Therefore the branch probability, during the final iteration, is defined as

$$\gamma_n(s',s) = \exp\left(\frac{1}{2}x_n^l L_a(x_n^l) + \frac{1}{2}x_n^2 L_a(x_n^2)\right). \tag{2.44}$$

A hard decision mapping is then performed on the a posteriori LLRs to estimate the data bits. This hard decision mapping is defined as,

$$\hat{d}_j = \begin{cases} 1, & L_{app}(x_n^l) \geq 0 \\ 0, & L_{app}(x_n^l) < 0 \end{cases}. \tag{2.45}$$

2.6 Simulation results

In this section the BER of various equalizers described in sections (2.4.2)-(2.4.4) are investigated in a TE system. We briefly refer to the performance of a TE system by the name of the respective SISO equalizer.

The following parameters are set in order to obtain the simulation results. The Proakis C channel of length $L = 5$ is chosen as the frequency selective channel. This particular channel causes severe ISI due to the spectral null present in its frequency response. It would therefore

be interesting to investigate whether a TE system can overcome the spectral null of the channel in order to reach the i.i.d. channel capacity.

The length of the data bits is set to $N_b = 32768$. The data bits are encoded using a rate $R_c = 0.5$ recursive CC given by $\mathbf{P}_{rsc} = [1, 5/7]$ in octal form. The coded bits $\tilde{x}_n$ include trellis termination. A random interleaver of length $N_i = 65536$ is used. The FIR length of the MMSE LE, MMSE LE-EF (I) and (II) is set to $M_1 = 9$ and $M_2 = 5$. These same parameters are used for the MMSE DFE, resulting in the length of the feedforward and feedback FIR filter to be $M = 15$ and $M_b = 5$ respectively.

A block of transmitted symbols consists of $N_t = L - 1$ training symbols followed by $N_i = 65536$ encoded data symbols for the MAP equalizer. However, the training symbols are set to $N_t = M_2 + L - 1$ for the MMSE equalizers and the hybrid MAP/MMSE LE-EF (I). These training bits are also used to ensure correct initialization of the alpha messages for the MAP equalizer as well as the postcursor mean estimates for the MMSE equalizers. The SNR defined in (2.9) is used for the simulation results.

The computation of the BER is given by the expression,

$$BER = \frac{1}{N_b \cdot N_{blocks}} \sum_{k=1}^{N_{blocks}} \sum_{j=1}^{N_b} \begin{cases} 0, & \hat{d}_{j,k} = d_{j,k} \\ 1, & \hat{d}_{j,k} \neq d_{j,k} \end{cases} \tag{2.46}$$

where N_{blocks} represents the total number of blocks transmitted, $d_{j,k}$ is the j^{th} bit for the k^{th} block transmitted and $\hat{d}_{j,k}$ is the estimated j^{th} bit for the k^{th} block transmitted. The BER is obtained by transmitting a number of N_{blocks}, such that at least 100 bit errors are observed. Furthermore, at low SNRs N_{blocks} is set to 20. Fig. 2.7 and Fig. 2.8 show the BER of the MAP and MMSE equalizers during the respective iterations. The MMSE LE-EF (II) is not considered in the simulation results due to its slow rate of convergence shown in section 3.3.2.

We note from Fig. 2.3 in section 2.3.3 that the $C_{i.i.d.}$ is -0.0043 dB for the Proakis C channel corresponding to a rate of 0.5. The no ISI legend is the performance of a system using a CC and the MAP decoder over an AWGN channel. This is also referred to as the MF bound in

the literature [38]. The MMSE linear equalizer with perfect extrinsic feedback (LE-PEF) is an ideal equalizer where the extrinsic feedback, given in (2.34), is perfect and similar to the idea of MMSE DFE where the feedback decisions are perfect. The MMSE LE-PEF serves as a measure of how unreliable extrinsic LLRs affect the performance of the MMSE LE-EF (I).

It can be observed from Fig. 2.7 and Fig. 2.8 that the MAP equalizer has the best BER performance compared to all the equalizers considered, especially in the early iterations. Simulation results show that the MAP equalizer achieves convergence after just 2 iterations.

The best BER performance, amongst the MMSE equalizers, is achieved by the MMSE LE-EF (I). The MMSE LE is also shown to be superior to the MMSE DFE, but only after the initial equalization and decoding stage. Fig. 2.8 shows that the convergence of the MMSE LE-EF (I) and the MMSE LE are at a SNR of 4 dB after 4 iterations. Another interesting observation is that the MMSE LE-PEF has substantial performance gains compared with the MMSE LE-EF (I) during the early iterations. This reveals that the MMSE LE-EF (I) does suffer from the error propagation effect during the first few iterations. However, the MMSE LE-EF (I) does mitigate the effects of error propagation to approach the MMSE LE-PEF for SNRs $\geq$ 2dB at 14 iterations.

The MMSE DFE is shown, for one time equalization and decoding, to perform better than the MMSE LE at SNRs $>$ 7.5dB. However, for subsequent iterations the MMSE DFE does not perform well. It was explained in [38] that the poor performance of the MMSE DFE is due to the early use of hard decisions.

Simulation results for the hybrid MAP/MMSE LE-EF (I) reveal an improved performance gain compared with the MMSE LE-EF (I) during all the iterations. This is due to more reliable decisions being passed from the MAP equalizer in the initial equalization stages. For this reason there is a much reduced error propagation effect in the MMSE LE-EF (I) during subsequent iterations compared to the situation if the MMSE LE-EF (I) was used during the initial equalization stage. Fig. 2.7 shows that the hybrid MAP/MMSE LE-EF (I) converges after only 3 iterations at a SNR of 4 dB for a BER of $2.5 \cdot 10^{-6}$. Furthermore, in Fig. 2.8 it can be observed that the hybrid MAP/MMSE LE-EF (I) approaches the MMSE LE-PEF after 14 iterations at SNRs $\geq$ 2dB. This suggests that the hybrid MAP/MMSE LE-EF (I) does overcome the error propagation effect during the later iterations to converge to the performance of the MMSE LE-PEF at high SNRs.

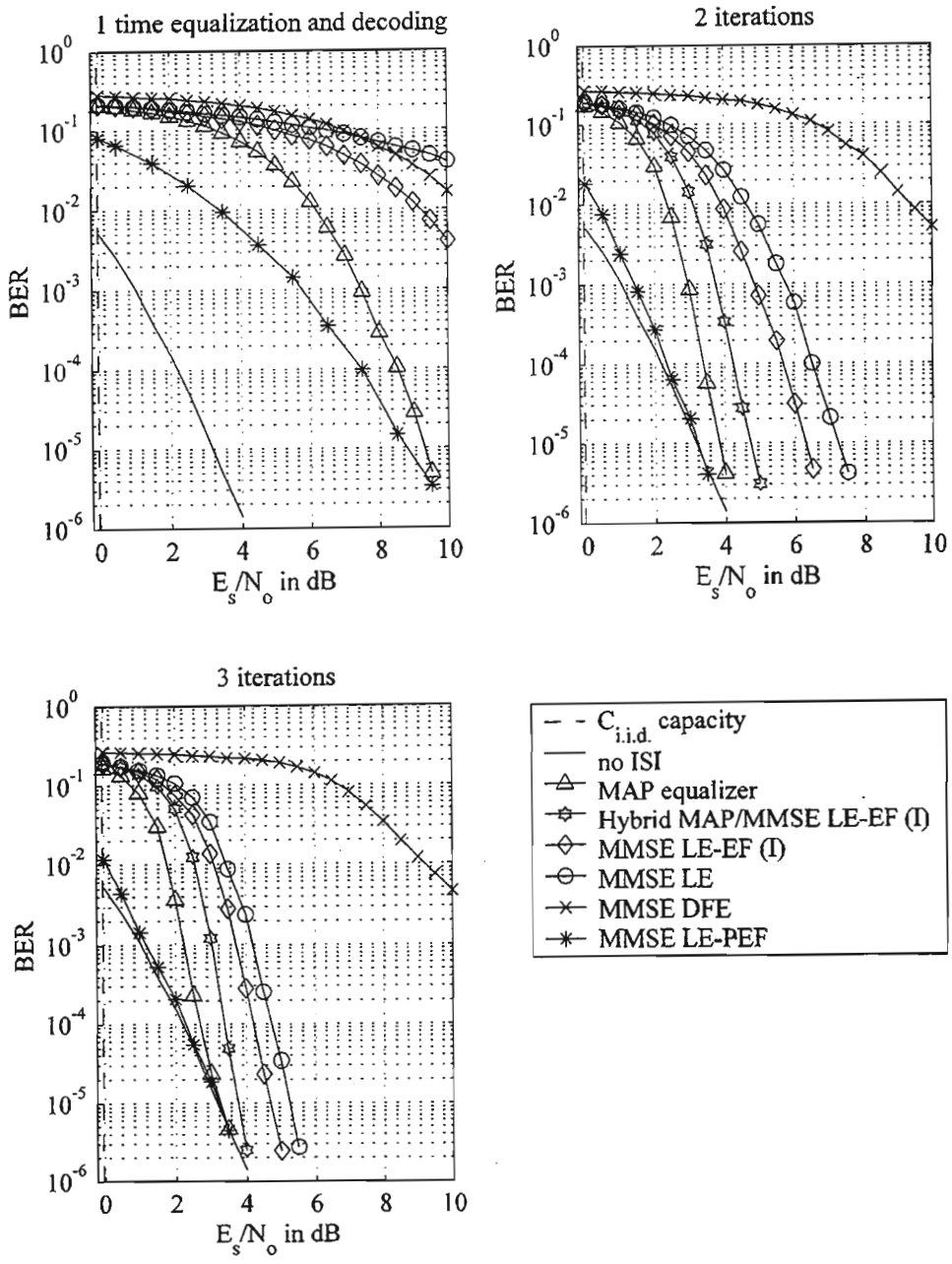

Fig. 2.7: BER performance comparison of one time equalization and decoding, 2 iterations and 3 iterations

It was shown in [35] that the inner code of a SCCC system is required to be recursive in order to achieve an interleaving gain. For this reason a non-precoded TE system is limited by the MF bound [38]. This can be verified by observing the simulation results given in Fig. 2.7 which shows that all the SISO equalizers do approach the MF bound at SNRs $\geq$ 2dB . For

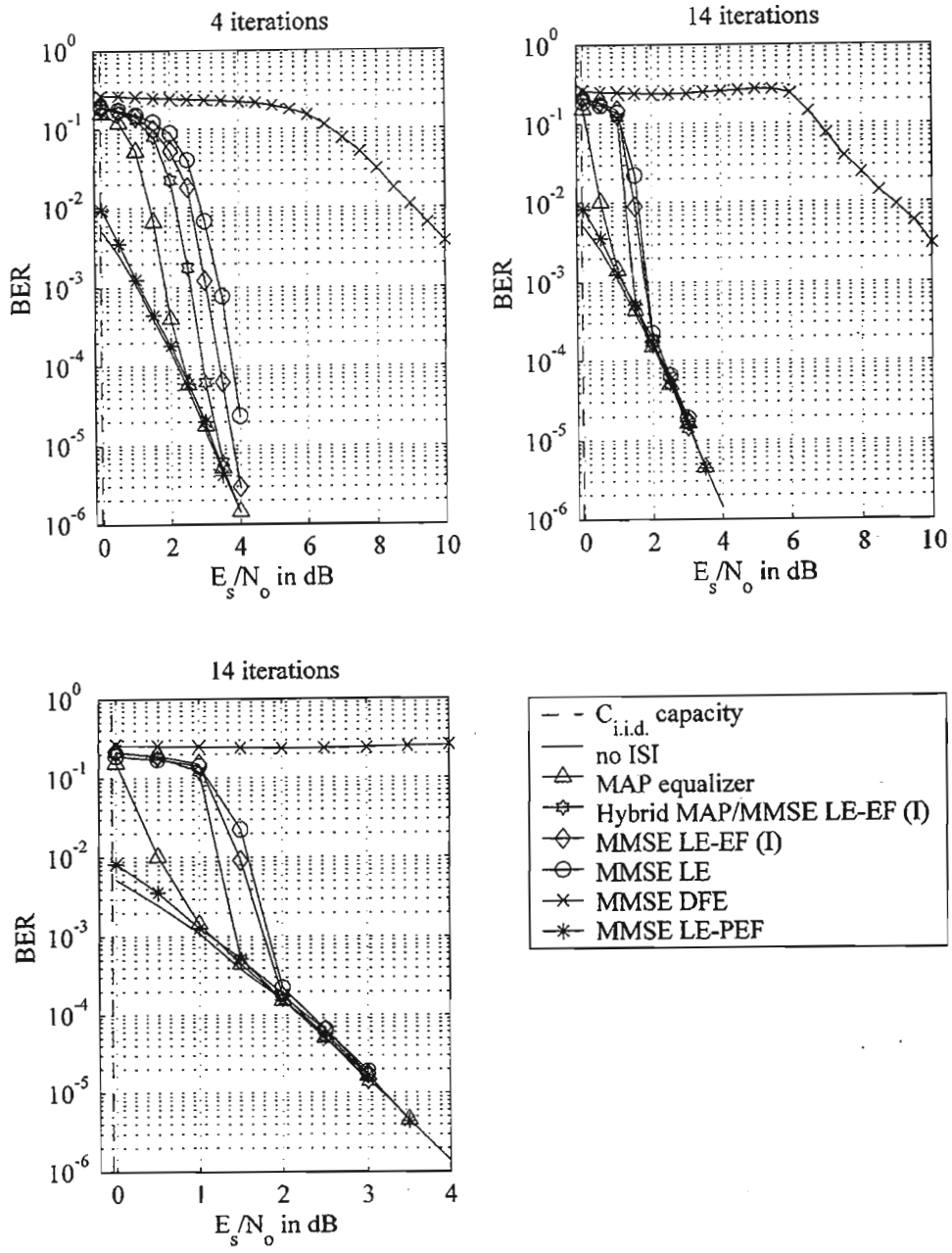

Fig. 2.8: BER performance comparison of 4 and 14 iterations

this reason the MAP equalizer, hybrid MAP/MMSE LE-EF (I) and the MMSE equalizers, for a non-precoded TE system, only approaches the MF bound and not the i.i.d. channel capacity limit. The MAP equalizer, hybrid MAP/MMSE LE-EF (I) and the MMSE LE-EF (I) are shown in Fig. 2.8, for 14 iterations, to be 3.0043 dB away from the $C_{i.i.d.}$ for a BER of $1.5 \cdot 10^{-5}$.

It was shown in [76] that irregular LDPC codes did approach the channel capacity for an AWGN channel. Motivated by this, an irregular LDPC code was designed for a TE system in [72] which was shown to approach the i.i.d. channel capacity. Therefore it is appropriate to use powerful coding schemes in a TE system, such that the MF bound is closer to the $C_{i.i.d.}$ limit.

2.7 Summary

In this chapter the system model for a TE system was presented. The concept of channel capacity was introduced and the i.i.d. channel capacity of an ISI channel was discussed and presented. Existing SISO equalization schemes for TE systems were outlined. The algorithms for the MAP equalizer, MMSE LE and MMSE DFE were then summarised. Three new equalizers were proposed in order to improve the performance of the MMSE LE in a TE system: MMSE LE-EF (I), MMSE LE-EF (II) and the hybrid MAP/MMSE LE-EF (I). We then compared the computational complexity of the MAP equalizer, MMSE LE, MMSE DFE, MMSE LE-EF (I) and (II). A brief review of various channel coding techniques was given. An overview of CCs was given and the MAP decoding algorithm was explained.

We compared the performance of the TE systems using the proposed MMSE LE-EF (I) and hybrid MAP/MMSE LE-EF (I) to TE systems employing the existing MAP equalizer, MMSE LE and MMSE DFE. Simulation results demonstrated that the MMSE LE-EF (I) and the hybrid MAP/MMSE LE-EF (I) performed better than the MMSE LE in a TE system. It was noted that the MMSE LE-EF (I) and the hybrid MAP/MMSE LE-EF (I) suffered from the error propagation problem during the early iteration. However, we found that these equalizers did overcome the error propagation problem during the later iterations. Furthermore, the MMSE LE-EF (I) and the hybrid MAP/MMSE LE-EF (I) was shown to approach the performance of the MF bound (or no ISI), MAP equalizer and the MMSE LE-PEF after 14 iterations at high SNRs. The MMSE LE-EF (I) and the hybrid MAP/MMSE LE-EF (I) were shown to be 3.0043 dB away from the $C_{i.i.d.}$ limit at a BER of $1.5 \cdot 10^{-5}$. This relatively large difference was attributed to the use of a simple CC as the outer code and not to the performance of the respective SISO equalization algorithms.

Chapter 3

Analysis of Turbo Equalization Systems

3.1 Introduction

At the present moment there are no known closed form mathematical expressions to determine the performance of an iterative decoding process. Since the advent of turbo codes, many researchers have undertook the problem of predicting the performance of communication systems that use the turbo principle. Two main areas of analysis techniques are considered: union bound analysis and convergence prediction. A review of the two approaches is given below.

The union bound analysis technique was initially proposed for PCCCs and SCCCs in [77] and [35] respectively. The union bound primarily focuses on the error events and states that the probability of the union of error events is less than or equal to the sum of individual probabilities of each error event. For this reason the union bound is only applicable if the code does possess the uniform error property [78]. However, the union bound is tight only for the performance of ML decoding. The union bound analysis was applied to a TE system in [18] and it was shown that this analysis technique was limited to high SNRs.

Convergence prediction is another approach to predict the performance of iterative decoding systems. The main idea behind convergence prediction methods is to estimate the SNR that an iterative decoding process would converge by estimating the probability density function (PDF) of the extrinsic information using a single parameter. An instant of a convergence prediction method called density evolution was initially presented in [79] to obtain thresholds on the convergence of LDPC codes. In [80], density evolution was proposed to analyse a SCCC and a PCCC system. This particular type of analysis has mainly been used for long block lengths. However, recently in [81] this method has been extended to study iterative decoding of short block lengths.

A good summary of six measures for predicting the convergence of a TE system, turbo decoding and turbo bit-interleaved coded modulation iterative decoding was presented in [82]. It was shown in [82] that the fidelity and the mutual information measures were the most accurate for these different decoding algorithms due to these measures being more robust regarding clipping of LLRs in fixed point arithmetic. The EXIT chart proposed in [83] is the convergence prediction method which uses the mutual information measure to visualise the exchange of extrinsic information during the iterative decoding process. It was also outlined in [83] that the PDFs of the extrinsic information, during the iterations, can be asymmetric and non-continuous with sharp edges thus making the mutual information measure more robust in comparison with the mean or SNR measure. An additional benefit of using the EXIT chart with respect to other measures is that the EXIT chart allows for the computation of the achievable information rate of a particular system [75]. For these reasons the EXIT chart is used in this dissertation to analyse a TE system.

The main focus of this chapter is the EXIT chart analysis applied to the MAP equalizer, hybrid MAP/MMSE LE-EF (I) and (II), MMSE LE, MMSE DFE and the MAP decoder. The validity of the EXIT chart analysis is also investigated. Furthermore, the achievable information rate of an ISI channel is presented using the EXIT chart.

The contents of the remainder of this chapter are as follows. Firstly, an overview of existing analysis techniques in an iterative decoding system is given. In section 3.2 the EXIT chart is reviewed. The EXIT chart analysis of TE systems is presented in section 3.3. The K-S test is performed on the Cumulative Distribution Functions (CDFs) of the a priori equalizer and decoder LLRs in section 3.4. The correlation between the LLRs of the a priori equalizer and decoder information is investigated in sections 3.5. A novel way to reduce the effects of error propagation in the MMSE LE-EF (I) is proposed in section 3.6. Lastly, the EXIT chart is used to compute the uniform input information rate of the Proakis C channel.

3.2 The EXIT chart

Since the invention of the EXIT chart, by the pioneering work of S. ten Brink in [84] to analyse PCCCs, this technique has been used to design a SCCC system [85] and a hybrid equalization scheme for a TE system [38]. In this section a summary of the EXIT chart is given.

We define I_o^E and I_o^D as the output mutual information from the equalizer and decoder respectively given a specific input mutual information. The EXIT chart predicts the exchange of extrinsic information, using the mutual information measure, during the iterative process by independently computing the transfer functions $I_o^E = \Upsilon_e(I_i^E, \text{SNR})$ and $I_o^D = \Upsilon_d(I_i^D)$.

Consider Fig. 2.1 in section 2.2. We define $x_n \in \{-1,1\}$ as the constellation mapping of $\tilde{x}_n$. The output mutual information for the equalizer I_o^E and decoder I_o^D is computed by the following expressions [84],

$$I_o^E = \frac{1}{2} \sum_{y_n \in \{-1,1\}} \int_{-\infty}^{\infty} g_{a,y_n}^e(l).\log_2 \frac{2g_{a,y_n}^e(l)dl}{g_{a,y_{n=+1}}^e(l) + g_{a,y_{n=-1}}^e(l)} \tag{3.1}$$

$$I_o^D = \frac{1}{2} \sum_{x_n \in \{-1,1\}} \int_{-\infty}^{\infty} g_{a,x_n}^d(l).\log_2 \frac{2g_{a,x_n}^d(l)dl}{g_{a,x_{n=+1}}^d(l) + g_{a,x_{n=-1}}^d(l)} \tag{3.2}$$

where $g_{a,y_n}^e(l)$ and $g_{a,x_n}^d(l)$ are the PDFs of the extrinsic information of the equalizer and the decoder respectively, given y_n and x_n.

The computation of the PDFs of the a priori LLRs during the iterations is However, intractable. The EXIT chart makes two assumptions on the PDFs of the a priori LLRs in order to compute the transfer functions of the equalizer and decoder. These assumptions are that the PDFs of the a priori LLRs obey the consistency hypothesis [79] and that they are Gaussian distributed. If these conditions are valid then the PDFs of the a priori LLRs can be represented by a single parameter where the variance is twice the mean σ_e^2. However, in an iterative decoding process these assumptions are only applicable for large interleaver block lengths and a fixed number of iterations [84]. The $J(\cdot)$ function, given in (3.3), was shown in [84] to compute the input mutual information given a specific variance σ_e^2.

$$J(\sigma_e^2) = 1 - \int_{-\infty}^{\infty} \frac{e^{-((\varepsilon-\sigma_e^2/2)^2/2\cdot\sigma_e^2)}}{\sqrt{2\pi}\sigma_e} \cdot \log_2(1+e^{-\varepsilon})d\varepsilon \,. \tag{3.3}$$

The output mutual information I_o^E is obtained as follows. A set of $N_i \cdot N_{blocks}$ i.i.d. LLRs, using a normal distribution with a mean of $x_n \cdot \sigma_e^2/2$ and variance σ_e^2, is generated for the a priori LLRs of the equalizer. Furthermore, a set of $N_i \cdot N_{blocks}$ i.i.d. transmitted symbols and

$N_t \cdot N_{blocks}$ training symbols is transmitted over an ISI channel to generate the receiver inputs r_n. The a priori LLRs and the receiver inputs r_n are then passed to the equalizer to compute the corresponding extrinsic information. The extrinsic LLRs obtained are then used to obtain $g^e_{n,y_n}(l)$ in order to calculate the output mutual information in (3.1). This method to compute the output mutual information is called the histogram method (HM). Similarly, the transfer function for the decoder $I_o^D = \Upsilon_d(I_i^D)$ is correspondingly obtained by the above procedure. However, the decoder only requires a set of a priori LLRs at its input due to the absence of the channel reliability measure.

Note that the PDF of the extrinsic information, at the output of the equalizer or the decoder, is not assumed to be Gaussian distributed when computing the output mutual information and that interleaving does not change the mutual information. The convergence threshold is defined as the lowest SNR at which the two transfer functions $I_o^E = \Upsilon_e(I_i^E, \text{SNR})$ and $I_i^D = \Upsilon_d^{-1}(I_o^D)$ do not intersect each other.

It was shown in [86] that the mutual information can be approximated by a time average approximation if $g^e_{n,y_n}(l)$ and $g^d_{n,x_n}(l)$ are both symmetric and consistent. We call this method to compute the mutual information the time average approximation method (TAAM). The output mutual information for the equalizer I_o^E and decoder I_o^D, using the TAAM, is obtained by the expressions,

$$I_o^E \approx 1 - \frac{1}{N_{blocks} N_i} \sum_{k=1}^{N_{blocks}} \sum_{n=1}^{N_i} \log_2(1 + e^{-y_{k,n} \cdot L_e(y_{k,n})}) \tag{3.4}$$

$$I_o^D \approx 1 - \frac{1}{N_{blocks} N_i} \sum_{k=1}^{N_{blocks}} \sum_{n=1}^{N_i} \log_2(1 + e^{-x_{k,n} \cdot L_e(x_{k,n})}) . \tag{3.5}$$

In (3.4), $y_{k,n}$ is the n^{th} transmitted symbol for the k^{th} block and $L_e(y_{k,n})$ is the corresponding extrinsic information. Similarly $x_{k,n}$ and $L_e(x_{k,n})$ are defined in (3.5). The TAAM significantly reduces the computational complexity of computing the transfer functions $I_o^E = \Upsilon_e(I_i^E, \text{SNR})$ and $I_i^D = \Upsilon_d^{-1}(I_o^D)$ compared with the HM.

The exchange of extrinsic information during the actual iterative decoding process is referred to as the system trajectory in the EXIT chart. The system trajectory is computed using the

actual expressions for $g^{e}_{a,y_n}(l)$ and $g^{d}_{a,x_n}(l)$ during the iterative process. A particular system is successfully analyzed using the EXIT chart when the system trajectory is close to the bounds of the transfer functions in the EXIT chart.

It was shown in [84] that the BER performance can be obtained from the EXIT chart. However, the predicted BER performance is only accurate if the system trajectory does approach the bounds of the transfer functions for the equalizer and decoder.

Although the EXIT chart has been shown to predict the iterative decoding for large interleaver block lengths, this method can only be computed if knowledge of the transmitted symbols y_n and x_n are known at the receiver. For this reason the EXIT chart can only be performed offline rather than in a real communication system and is referred to as a semi-analytical technique in the literature.

The EXIT chart will be used in the next section to analyse the different SISO equalizers given in sections 2.4.2 – 2.4.4 and the MAP decoder. The system trajectories of the TE systems are computed using the HM and the TAAM and compared with the bounds of the transfer functions on the EXIT chart.

3.3 EXIT Chart analysis of TE systems

In [38] the EXIT chart analysis was applied to the MAP equalizer, MMSE LE and the MMSE DFE to determine their respective characteristics. We propose to also use the EXIT chart to analyse the MMSE LE-EF (I) and (II) in this section.

The simulation parameters given in section 2.6 are used for the EXIT chart. The parameter $N_{blocks} = 153$ is set such that at least 10^7 equiprobable symbols for y_n and their corresponding LLRs are used to obtain the transfer function $I_o^E = \Upsilon_e(I_i^E, \text{SNR})$. Similarly, the transfer function for the decoder is also obtained.

It can be noted from Fig. 2.8 that the MF bound converges to a BER of $1.5 \cdot 10^{-6}$ at a SNR of 4 dB after 14 iterations. The TE systems are shown in Fig. 2.8, after 14 iterations, to

approach the MF bound at high SNRs. Therefore we seek to analyse these different TE systems at this particular SNR.

3.3.1 Transfer function of the SISO equalizer and the MAP decoder

In this section the transfer function of the SISO equalizer and the MAP decoder are shown. Fig. 3.1 shows the transfer function characteristics of the MAP equalizer, MMSE equalizers and the MAP decoder using the HM. A comparison between the HM and the TAAM in computing the transfer functions $I_o^E = \Upsilon_e(I_i^E, \text{SNR})$ and $I_i^D = \Upsilon_d^{-1}(I_o^D)$ will be investigated in section 3.3.2.

In Fig. 3.1, the output mutual information of the MAP equalizer is higher than the output mutual information of the MMSE equalizers when $I_i^E \leq 0.55$. Another interesting observation from Fig. 3.1 is that the upper bound on the output mutual information is $I_o^E = 0.95$ for all the SISO equalizers. It was outlined in [69] that the limiting aspect of I_o^E, even with perfect a priori information, is due to the ISI channel or inner code being non-recursive in nature. Therefore as the number of iterations increases the MAP decoder receives a maximum input mutual information of $I_o^D = 0.95$ which is the MF bound for this TE system at a SNR of 4 dB.

Fig. 3.1 also reveals that the MMSE LE-EF (I) and (II) have a higher output mutual information, given the same input mutual information, when compared with the MMSE LE. Furthermore, for $I_i^E \geq 0.55$ the MMSE LE-EF (I) surprisingly performs better than the MAP equalizer. This is thought to be due to the feedback of extrinsic information, inherent in the MMSE LE-EF (I), being beneficial in a SISO equalizer. However, the transfer functions of the equalizer and decoder are obtained under the assumption that the PDFs of the a priori LLRs are Gaussian distributed. If this assumption is valid, the MMSE LE-EF (I) would have a better performance compared with the MAP equalizer during the later iterations.

The characteristics of the MMSE LE, in Fig. 3.1, are observed to be superior in comparison with the MMSE DFE at low input mutual information values. The MMSE DFE performs slightly better in comparison with the MMSE LE when $I_i^E \geq 0.60$. Although it may not be

clear from Fig. 3.1, the MMSE DFE also performs better than the MAP equalizer when $I_i^E \geq 0.95$. It was explained in [38] that this is likely due to the hard decision element in the MMSE DFE algorithm.

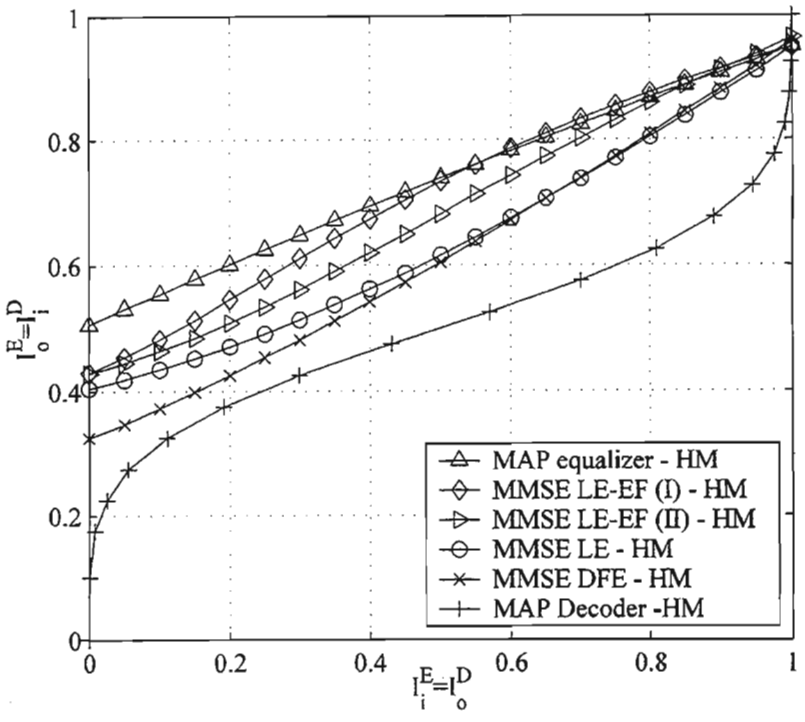

Fig. 3.1: Transfer functions of the MAP equalizer, MMSE equalizers and the MAP decoder

The predicted trajectories of the respective TE systems can also be drawn on the EXIT chart by vertical (for equalization) and horizontal lines (for decoding) starting with the transfer function of the decoder $I_i^D = \Upsilon_{il}^{-1}(I_o^D)$ to predict the number of iterations in order to achieve convergence. However, for clarity they are not shown in Fig. 3.1.

3.3.2. System trajectories and comparison between the HM and the TAAM

The system trajectory is the actual trajectory during the iterative equalization and decoding process. Furthermore, the system trajectory gives a visual interpretation of the rate of convergence for the particular TE system. This section investigates the HM and TAAM to compute the system trajectories and transfer functions of a TE system that uses the SISO

equalizer given in sections 2.4.2- 2.4.4. Figs. 3.2 - 3.7 show the EXIT chart analysis of various TE systems. The method used to compute the mutual information on the EXIT chart are denoted in the respective legend.

Figs. 3.2 - 3.3 show the transfer functions and the system trajectories of a TE system when the MAP equalizer and MMSE LE are used respectively. The computation of the transfer functions and the system trajectories using the HM and the TAAM, in Fig. 3.2 and Fig. 3.3, are very similar. These system trajectories approach the bounds of the transfer functions of the equalizer and decoder respectively. It can also be seen that the MAP equalizer and the MMSE LE achieves convergence after 2 iterations and 4 iterations respectively. This result is consistent with the simulation results given in Figs. 2.7 - 2.8 which showed that the MAP equalizer and the MMSE LE converge to BERs of $4 \cdot 10^{-6}$ and $2 \cdot 10^{-5}$, at a SNR of 4 dB, after 2 and 4 iterations respectively.

The system trajectories of the MMSE DFE, in Fig. 3.4, do not follow the bounds of the transfer functions in the EXIT chart. It is also observed that the system trajectory of the TAAM yields a negative mutual information value after the initial decoding stage and hence

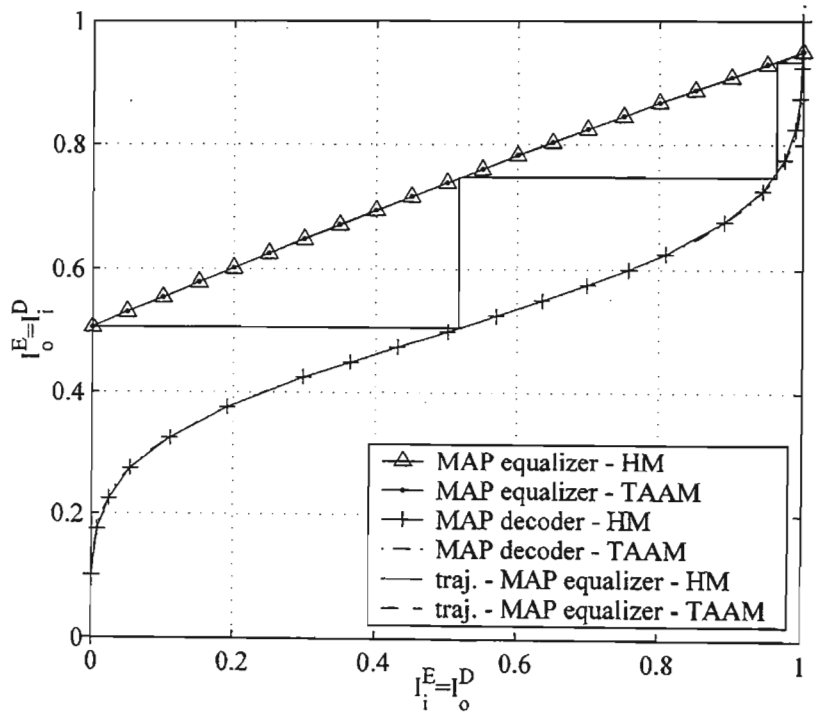

Fig. 3.2: EXIT Chart of the MAP equalizer

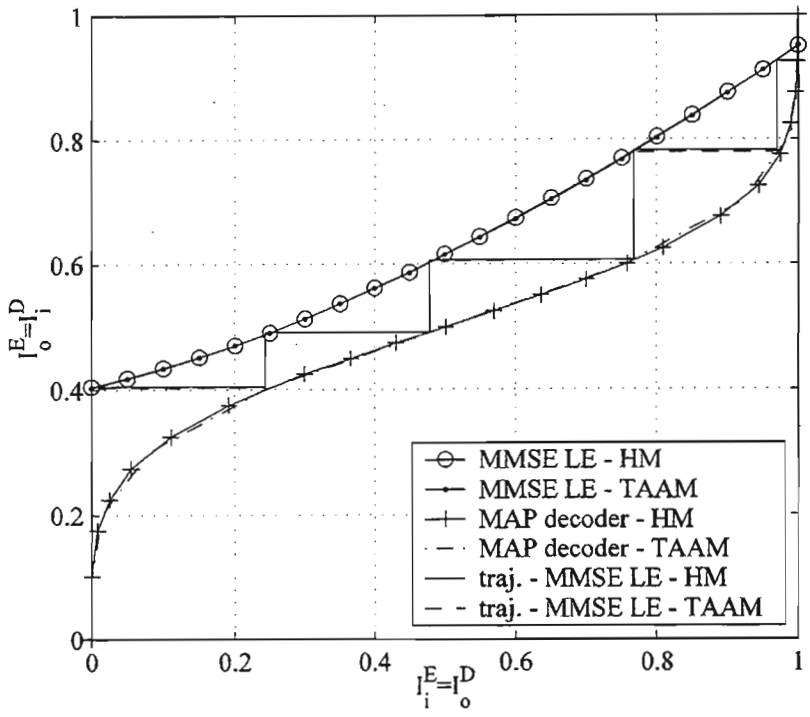

Fig. 3.3: EXIT Chart of the MMSE LE

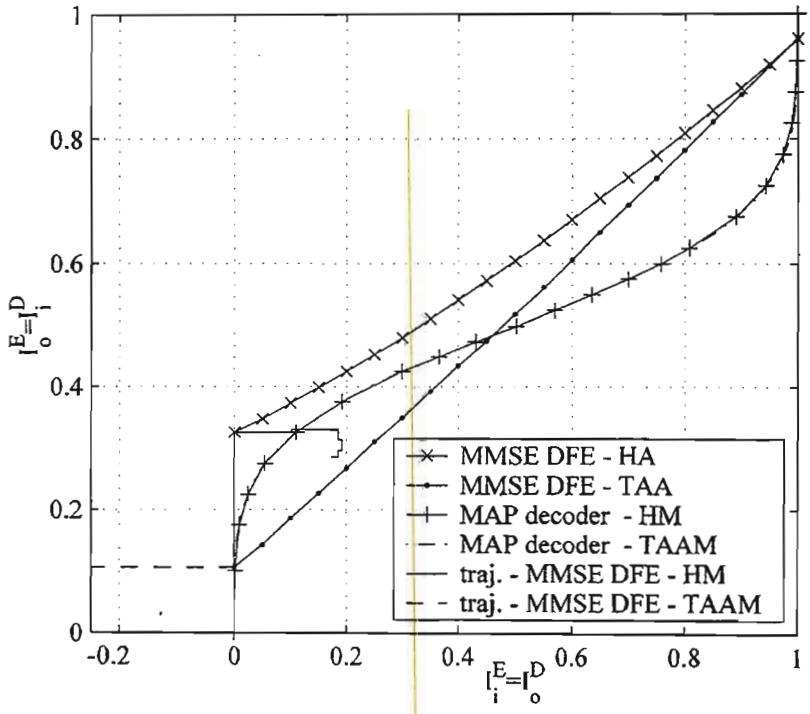

Fig. 3.4: EXIT Chart of the MMSE DFE

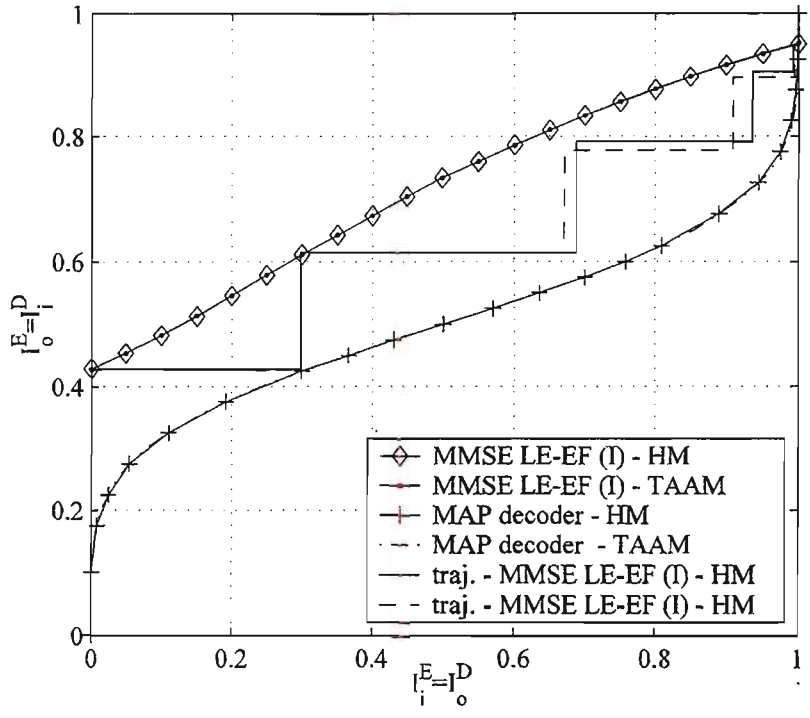

Fig. 3.5: EXIT Chart of the MMSE LE-EF (I)

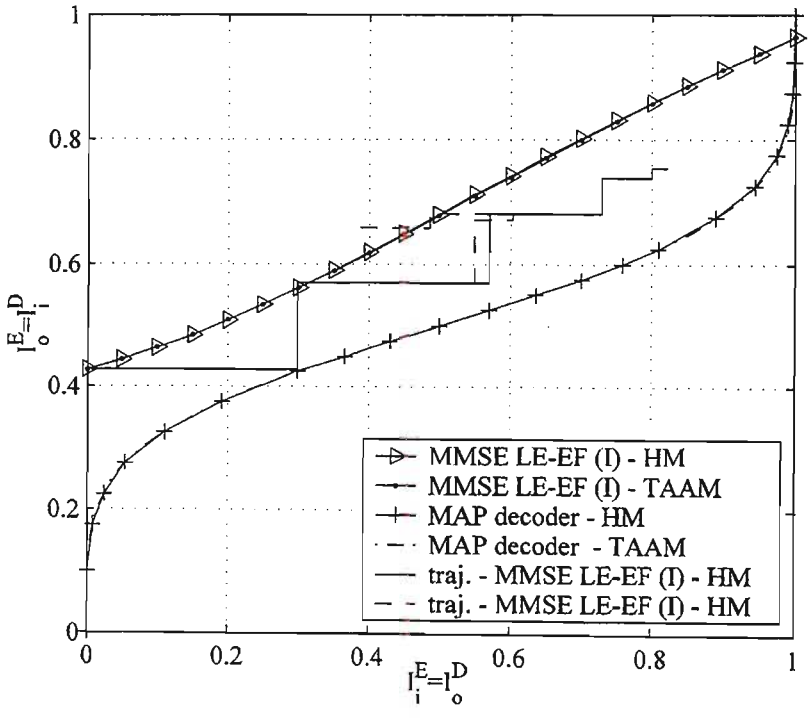

Fig. 3.6: EXIT Chart of the MMSE LE-EF (II)

does not yield meaningful results. This is due to the hard decision mapping in computing the postcursor mean estimates which causes a tremendous error propagation problem. For this reason the EXIT chart cannot be applied to the MMSE DFE.

The transfer functions for the MMSE LE-EF (I) and (II), shown in Fig. 3.5 and Fig. 3.6, are indeed very close when either the HM or the TAAM is used. However, the system trajectories do not approach the bounds of the transfer functions in the EXIT chart after the first iteration. The Gaussian assumption made on the PDFs of the a priori LLRs, during the iterations, is thought to be where the inaccuracies occur in obtaining the transfer functions for the EXIT chart. Therefore the EXIT chart analysis is not accurate for the MMSE LE-EF (I) and (II) after the first iteration.

Although the EXIT chart analysis is not accurate after the first iteration, the system trajectory is a visual representation of the rate of the convergence of a TE system. It is observed that the system trajectories, using the HM and the TAAM, differ for the MMSE LE-EF (I) and (II) after the first iteration. The difference between the system trajectories, using the HM and the TAAM in Fig. 3.5 and Fig. 3.6, is thought to be due to either the consistency or symmetric condition or both on $g^{e}_{a,y_n}(l)$ and $g^{d}_{a,x_n}(l)$ being violated during the iterative decoding process. We therefore only consider the system trajectory relating to the HM. The MMSE LE-EF (I) is shown in Fig. 3.5 to converge after 4 iterations. Simulation results, given in Fig. 2.8, validate that the MMSE LE-EF (I) converges to a BER of $3 \cdot 10^{-6}$ after 4 iterations at a SNR of 4 dB. In Fig. 3.6 the system trajectory, relating to the HM, reveals that the MMSE LE-EF (II) has a significantly slower convergence rate in comparison with the MMSE LE or the MMSE LE-EF (I), in Fig. 3.3 and Fig. 3.5 respectively. This suggests that the MMSE LE-EF (II) is not an appropriate equalizer for a TE system.

The EXIT chart analysis of the hybrid MAP/MMSE LE-EF (I) is shown in Fig. 3.7. Similar to the MMSE LE-EF (I) and (II), in Fig. 3.5 and Fig. 3.6, the EXIT chart analysis of the hybrid MAP/MMSE LE-EF (I) is only valid until the first iteration. It is also observed that the system trajectories, relating to the HM and the TAAM, are very similar in Fig. 3.7. Furthermore, the rate of convergence of the hybrid MAP/MMSE LE-EF (I) is faster that that of the MMSE equalizers shown in Fig. 3.3 – Fig. 3.6. This is due to the fact that the hybrid MAP/MMSE LE-EF (I) uses the MAP equalizer during the initial equalization stage, which results in more reliable LLRs at the output of hybrid MAP/MMSE LE-EF (I) compared with the MMSE LE-EF (I). For this reason the error propagation is somewhat suppressed in the

hybrid MAP/MMSE LE-EF (I). Fig. 3.7 shows that the hybrid MAP/MMSE LE-EF (I) converges after only 3 iterations. This is validated by the simulation results given Fig. 2.7 which show that the hybrid MAP/MMSE LE-EF (I) converges to a BER of $2.5 \cdot 10^{-6}$ after 3 iterations for a SNR of 4 dB.

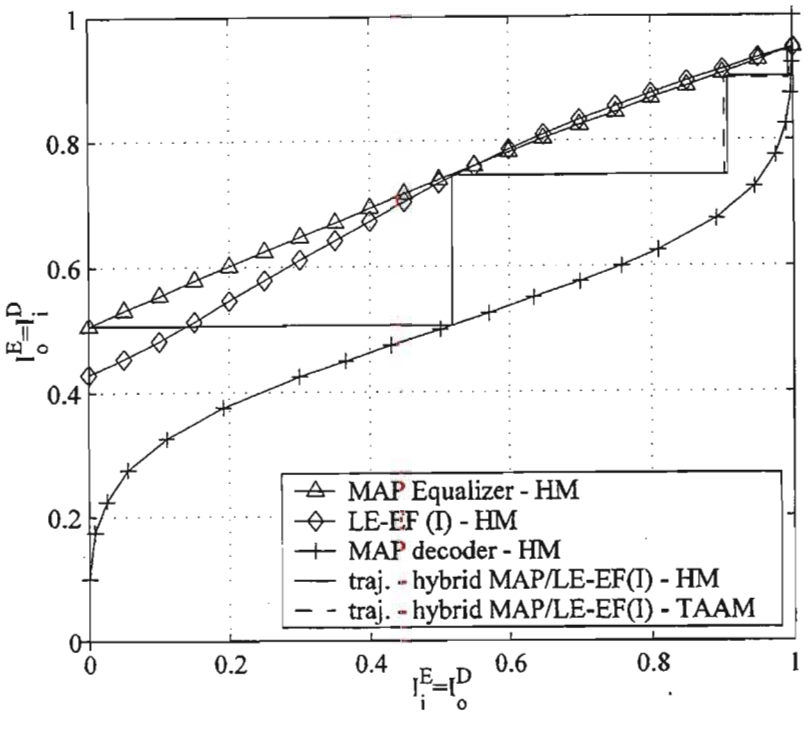

Fig. 3.7: EXIT Chart of the hybrid MAP/MMSE LE-EF (I)

3.4 The K-S test

The EXIT chart assumes that the PDFs of the a priori information are Gaussian distributed during the iterations. The system trajectories, shown in Fig. 3.5 – Fig. 3.7, for the MMSE LE-EF (I), MMSE LE-EF (II) and hybrid MAP/MMSE LE-EF (I) do not approach the transfer function in the EXIT chart. For this reason the PDFs of the a priori equalizer and decoder information need to be investigated in order to validate whether the Gaussian assumption is valid during the iterative equalization and decoding process. In this section the K-S test is presented in order to compare the predicted CDFs to the real CDFs during the iterative equalization and decoding process.

We denote the PDFs for the a priori LLRs of the equalizer and decoder, during the iterations, as $\lambda^{e}_{a,y_n}(l)$ and $\lambda^{d}_{a,x_n}(l)$ respectively. However, we only consider $\lambda^{e}_{a,y_n=+1}(l)$ and $\lambda^{d}_{a,x_{n=+1}}(l)$ for the K-S test. Using the system trajectory, we can predict the expected variance σ^2_{ev} and mean $\sigma^2_{ev}/2$ using the inverse of the $J(\cdot)$ function. Note that the expected variance σ^2_{ev} and mean $\sigma^2_{ev}/2$ are obtained under that assumption that $\lambda^{e}_{a,y_n=+1}(l)$ and $\lambda^{d}_{a,x_{n=+1}}(l)$ are Gaussian distributed and obey the consistency condition. We can then artificially generate two conditional PDFs, with an ideal Gaussian distribution, i.e. $v^{e}_{a,y_n=+1}(\gamma\,|\,\sigma^2_{ev})$ and $v^{d}_{a,x_n=+1}(\gamma\,|\,\sigma^2_{ev})$ to compare with $\lambda^{e}_{a,y_n=+1}(l)$ and $\lambda^{d}_{a,x_{n=+1}}(l)$. A goodness of fit measure can therefore be performed on $\lambda^{e}_{a,y_n=+1}(l)$ and $\lambda^{d}_{a,x_{n=+1}}(l)$ using $v^{e}_{a,y_n=+1}(\gamma\,|\,\sigma^2_{ev})$ and $v^{d}_{a,x_n=+1}(\gamma\,|\,\sigma^2_{ev})$, or their corresponding CDFs, in order to test the validity of the Gaussian assumption for a number of iterations until convergence.

There are obviously a number of different ways to measure the overall difference between two PDFs or CDFs, i.e. the absolute value of the area between the curves, the mean square difference, etc. In this dissertation, the K-S test [87] is chosen as the goodness of fit measure due to its simplicity and ease of use. The K-S test is a simple non-parametric method to test for goodness of fit which requires determining the maximum absolute distance (for the two sided test) between the two CDFs in question. We denote the CDFs of the $\lambda^{e}_{a,y_n=+1}(l)$, $\lambda^{d}_{a,x_{n=+1}}(l)$, $v^{e}_{a,y_n=+1}(\gamma\,|\,\sigma^2_{ev})$ and $v^{d}_{a,x_n=+1}(\gamma\,|\,\sigma^2_{ev})$ as $\psi^{e}_{a,y_n=+1}(l)$, $\psi^{d}_{a,x_{n=+1}}(l)$, $V^{e}_{a,y_n=+1}(\gamma\,|\,\sigma^2_{ev})$ and $V^{d}_{a,x_n=+1}(\gamma\,|\,\sigma^2_{ev})$ respectively. The maximum absolute distance D obtained from the K-S test, before equalization, is computed by the expression,

$$D \triangleq \arg\max(|V^{e}_{a,y_n=+1}(\gamma\,|\,\sigma^2_{ev}) - \psi^{e}_{a,y_n=+1}(l)|). \tag{3.6}$$

Similarly, the D value before decoding is also calculated by replacing $V^{e}_{a,y_n=+1}(\gamma\,|\,\sigma^2_{ev})$ and $\psi^{e}_{a,y_n=+1}(l)$ by $V^{d}_{a,x_n=+1}(\gamma\,|\,\sigma^2_{ev})$ and $\psi^{d}_{a,x_n=+1}(l)$ in (3.6).

Fig. 3.8 shows the results from the K-S test for different TE systems. The integer and half number of iterations correspond to the K-S test performed on $\psi^{d}_{a,x_{n=+1}}(l)$ and $\psi^{e}_{a,y_n=+1}(l)$ respectively. The results of the K-S test are obtained by using 10^7 LLRs for $L_a(y_n)$ and $L_a(x_n)$ over several blocks of transmitted data. The K-S test was also averaged over 100 artificially generated CDFs for $V^{e}_{a,y_n=+1}(\gamma\,|\,\sigma^2_{ev})$ and $V^{d}_{a,x_n=+1}(\gamma\,|\,\sigma^2_{ev})$. The K-S test is not

performed on the MMSE DFE as it was outlined, in section 3.3.2, that the EXIT chart is not applicable for this algorithm.

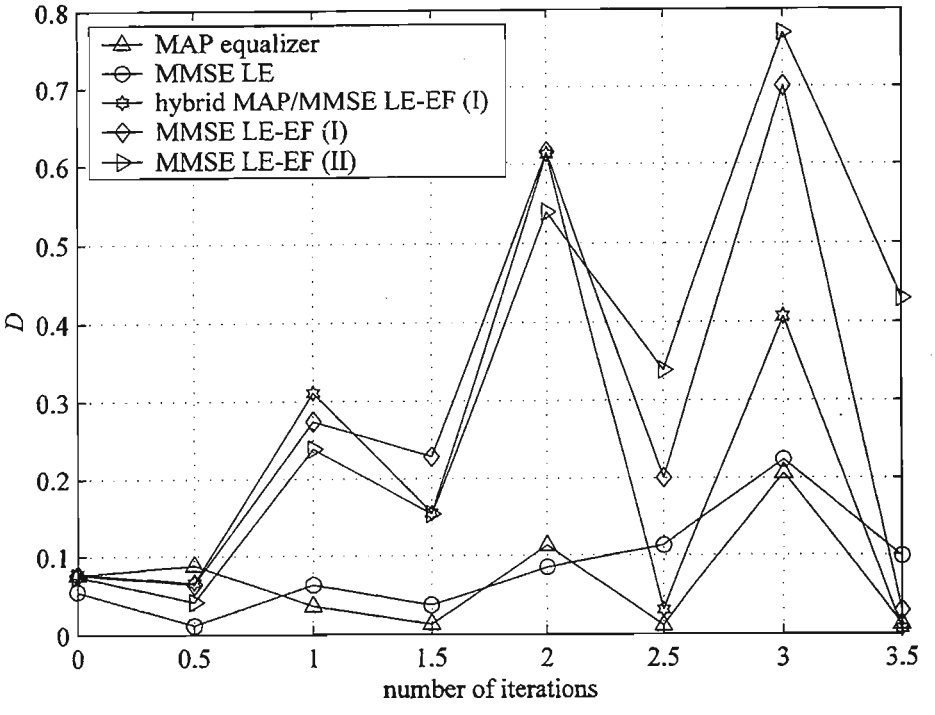

Fig. 3.8: Comparison of the K-S tests performed on various TE systems

It is interesting to observe from Fig. 3.8 that the D value is lower after equalization than after decoding. Therefore the Gaussian assumption is more valid after equalization than after decoding. The D value obtained in the K-S test for the MAP equalizer and the MMSE LE remains almost constant during the early iterations and only increases in the third iteration after decoding. The relative high D value for the MAP equalizer, during the first iteration, can be attributed to the initial skewness of the conditional PDFs [80]. However, the hybrid MAP/MMSE LE-EF (I), MMSE LE-EF (I) and (II) exhibit an increase in the D value after the decoding stage during the first iteration. Therefore the PDFs of the a priori information are not Gaussian distributed after the first iteration when these equalizers are used. This explains why the system trajectories of the hybrid MAP/MMSE LE-EF (I), MMSE LE-EF (I) and (II) do not reach the bounds of the transfer functions in Figs. 3.5 - 3.7.

3.5 Correlation between a priori and extrinsic LLRs

It was discussed in [84] that the EXIT chart is only valid when the correlation between the extrinsic information of the decoders is relatively low. For this reason, we seek to investigate whether the EXIT chart analysis of the hybrid MAP/MMSE LE-EF (I), MMSE LE-EF (I) and (II) is invalid due to the correlation being relatively high. The correlation value ρ between the a priori and extrinsic information after equalization is defined in (3.7) below. Similarly the correlation value ρ after decoding is obtained by substituting $L_a(x_{n,k})$ and $L_e(x_{n,k})$ for $L_a(y_{n,k})$ and $L_e(y_{n,k})$ in (3.7).

$$\rho = \frac{1}{N_i \cdot N_{blocks}} \sum_{k=1}^{N_{blocks}} \sum_{n=1}^{N_i} \frac{L_a(y_{n,k}) \cdot L_e(y_{n,k})}{|L_a(y_{n,k}) \cdot L_e(y_{n,k})|} \tag{3.7}$$

Fig. 3.9 shows the plot of the correlation value using 10^7 LLRs corresponding to data symbols only over several blocks. The integer and half number of iterations are defined as after decoding and equalization respectively. The MMSE DFE is not considered here due to the reason given in section 3.3.2.

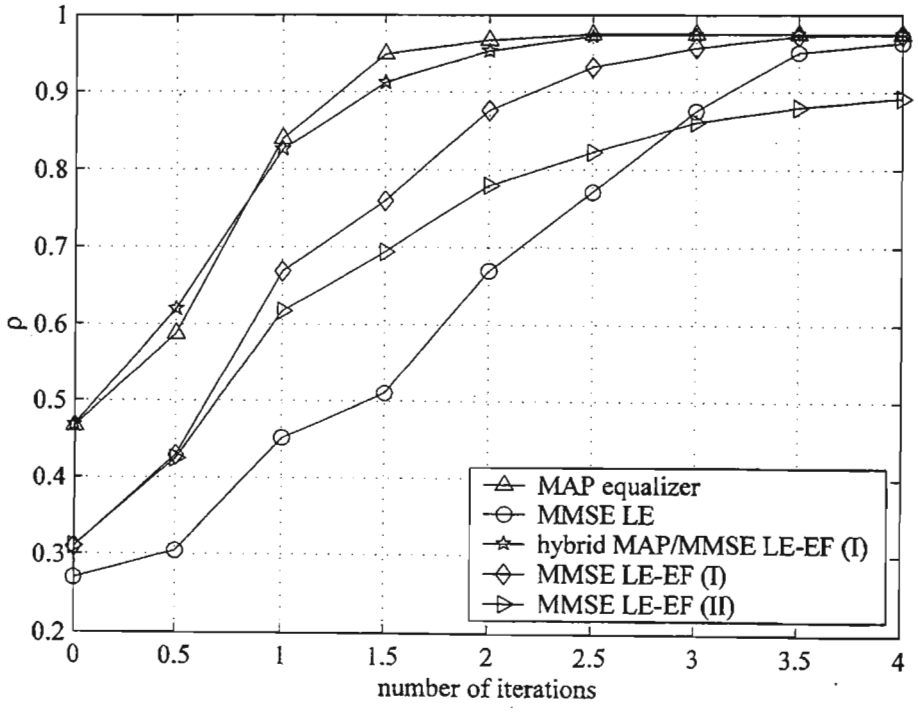

Fig. 3.9: Comparison of ρ values for various TE systems

In Fig. 3.9, we observe a high correlation value ρ for the MAP equalizer and the MMSE LE after decoding during the fourth iteration. It can be noted that ρ corresponding to the hybrid MAP/MMSE LE-EF (I), MMSE LE-EF (I) and (II) after decoding in the first iteration is relatively low in comparison with ρ for the MAP equalizer and the MMSE LE after decoding during the fourth iteration. This suggests that ρ is not the reason why $\lambda^{e}_{a,y_{n-1}}(l)$ is non Gaussian distributed after the first iteration for TE systems using the hybrid MAP/MMSE LE-EF, MMSE LE-EF (I) and (II). Therefore the error propagation effect is the basis for the PDFs of the a priori LLRs being non Gaussian distributed and is the reason why the system trajectories of the TE systems employing the hybrid MAP/MMSE LE-EF (I), MMSE LE-EF (I) and (II) do not follow the bounds of the transfer function on the EXIT chart in section 3.3.2.

Another interesting observation that can be made from Fig. 3.9 is that the curves for the MMSE LE and the MMSE LE (II) intersect just after the equalization stage during the third iteration. The reason for this intersection is due to the MMSE LE-EF (II) having a faster rate of convergence relative to the MMSE LE during the early iterations while the MMSE LE-EF (II) has a slower rate of convergence compared with the MMSE LE during the later iterations. This is verified by the system trajectories, shown in Fig. 3.6 and Fig. 3.3, for a TE system utilizing the MMSE LE-EF (II) and the MMSE LE receivers respectively.

3.6 Reduced error propagation effect in the MMSE LE-EF (I)

It was explained in section 2.7 that the MMSE LE-EF suffers from the error propagation problem during the early iterations. A novel method to reduce the error propagation effect in the MMSE LE-EF (I) is presented in this section.

The error propagation problem inherent in the MMSE LE-EF (I) is due to the feedback of extrinsic information. Consider (2.35) given in section 2.4.3.3. We propose to introduce a weighting term $\mu \in [0 \quad 1], \mu \in \mathbb{R}$ to the extrinsic LLRs in order to reduce the error propagation effect in the MMSE LE-EF (I). Therefore (2.35) in the MMSE LE-EF (I) is replaced with (3.8).

$$\bar{y}_n^{\text{po}} \triangleq \tanh((L_a(y_n) + \mu L_e(y_n))/2) \tag{3.8}$$

We refer to the MMSE LE-EF (I) using the expression in (3.8), during the first iteration only, as the modified MMSE LE-EF (I). The system trajectory for the MMSE LE-EF (I) and the modified MMSE LE-EF (I), using the HM, is shown in Fig. 3.10.

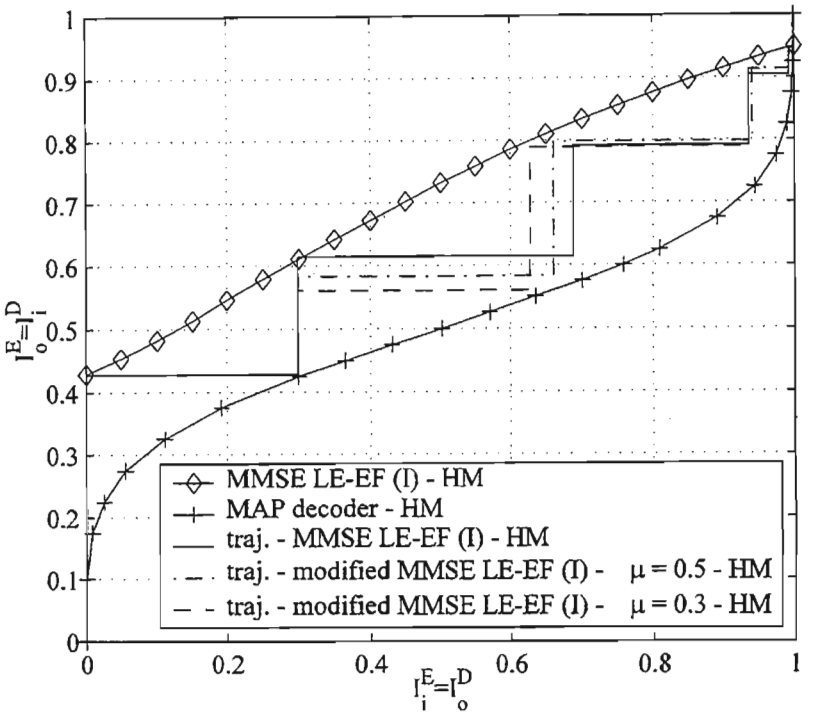

Fig. 3.10: EXIT chart of the MMSE LE-EF (I) and the modified MMSE LE-EF (I)

Fig. 3.10 shows the system trajectory of the modified MMSE LE-EF (I), when $\mu = 0.5$, has an improved performance in comparison with the system trajectory of the MMSE LE-EF (I) after equalization during the second iteration. Furthermore, the system trajectory of the modified MMSE LE-EF (I), when $\mu = 0.3$, has the same performance as the system trajectory of the MMSE LE-EF (I) after decoding in the second iteration but then performs better than the system trajectory of the MMSE LE-EF (I) during the next iteration. This suggests that the modified MMSE LE-EF (I) does yield a slightly reduced error propagation effect after the first few iterations compared with the MMSE LE-EF (I). The results obtained in this section are only empirical and an exact mathematical expression to compute the optimal weighting term μ for all the iterations is an open problem.

3.7 $C_{i.i.d.}$ computation using the EXIT chart

It was observed in [86] that the transfer functions of the EXIT chart can be used to approximate the rate of the outer code R_c and the i.i.d. channel capacity of a frequency selective channel. This section summarises the above observations made in [86] and an estimate of the $C_{i.i.d.}$ of the Proakis C channel is investigated using the EXIT chart.

The transfer function $I_i^D = \Upsilon_d^{-1}(I_o^D)$ of a MAP decoder was observed to exhibit the property given in (3.9).

$$\int_0^1 \Upsilon_d(l)dl = 1 - R_c \tag{3.9}$$

It was discussed in section 3.2 that the convergence threshold is determined by the lowest SNR at which the two functions $I_o^E = \Upsilon_e(I_i^E, \text{SNR})$ and $I_i^D = \Upsilon_d^{-1}(I_o^D)$ do not intersect each other. Using the area underneath the transfer function of the equalizer and the decoder we can reformulate the condition for convergence,

$$\int_0^1 \Upsilon_e(l)dl > \int_0^1 \Upsilon_d^{-1}(l)dl \tag{3.10}$$

Since the EXIT chart is confined by an area of 1 unit squared, the transfer function $I_o^D = \Upsilon_d(I_i^D)$ and the inverse transfer function $I_i^D = \Upsilon_d^{-1}(I_o^D)$ is related by the following expression,

$$\int_0^1 \Upsilon_d(l)dl = 1 - \int_0^1 \Upsilon_d^{-1}(l)dl\,. \tag{3.11}$$

Using (3.9), (3.10) and (3.11) we obtain,

$$R_c < \int_0^1 \Upsilon_e(l)dl\,. \tag{3.12}$$

Furthermore, the total rate of a concatenated system is given by,

$$R_{tot} = R_c \cdot R_{inner\ code} \tag{3.13}$$

where R_c is the rate of the outer code. But for a TE system $R_{inner\ code} = 1$. Substituting (3.12) into (3.13) yields the following expression,

$$R_{tot} < \int_0^1 \Upsilon_e(l)dl\,. \tag{3.14}$$

It was observed that the integral given in (3.14), evaluates to the $C_{i.i.d.}$ of an ISI channel. However, a comparison between the actual $C_{i.i.d.}$ using the Arnold-Loeliger method and the EXIT chart method has not been done. We use the integral given in (3.14) to determine an estimate of $C_{i.i.d.}$ for the Proakis C channel. Fig. 3.11 compares the computation of the $C_{i.i.d.}$ using the Arnold-Loeliger and the EXIT chart methods.

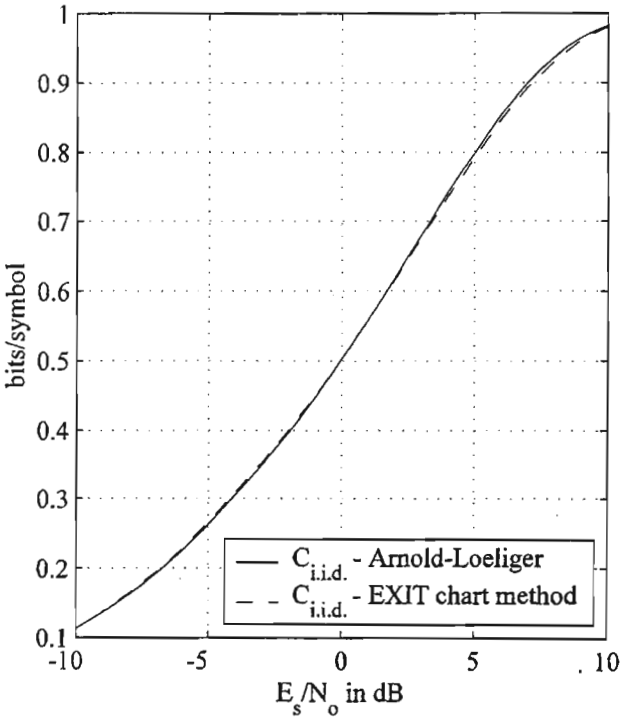

Fig. 3.11: Comparison of the Arnold-Loeliger and EXIT chart methods to compute $C_{i.i.d.}$

Fig. 3.11 reveals that the two methods that are used to compute the i.i.d. capacity of the Proakis C channel are very close to each other. The EXIT chart method slightly underestimates and overestimates the uniform input information rate of the channel for SNRs $\geq$ 0 dB and SNRs $<$ 0 dB respectively. Therefore the EXIT chart method to compute the $C_{i.i.d.}$ of a frequency selective channel is very accurate.

3.8 Summary

In this chapter, current analysis methods were reviewed and the motivation for choosing the EXIT chart to analyse TE systems was given. The basic principles of the EXIT chart were

also reviewed. We then used the EXIT chart to analyse the proposed MMSE LE-EF (I) and (II) and compared their characteristics with the existing MAP equalizer, MMSE LE and MMSE DFE. The transfer functions of the MMSE LE-EF (I) suggested that this equalizer performs better than the MAP equalizer.

A comparison between the HM and the TAAM, to compute the output mutual information on the EXIT chart, was presented for TE systems employing the MAP equalizer, hybrid MAP/MMSE LE-EF (I) and the MMSE equalizers. It was discovered that TAAM method was only accurate for the MAP equalizer and the MMSE LE. This was thought to be due to the symmetric and consistency conditions, underlying in the TAAM, being violated when the other SISO equalizers were used in a TE system.

It was shown that the MMSE LE-EF (I) converges faster than the MMSE LE while the MMSE LE-EF (II) had a slower rate of convergence with respect to the MMSE LE. Furthermore, it was observed that the system trajectories of the MMSE LE-EF (I) and (II) did not follow the bounds of the transfer functions on the EXIT chart. This was due to the error propagation problem inherent in the MMSE LE-EF (I) and (II). It was also noted that the error propagation problem was more severe in the MMSE LE-EF (II). A novel technique to reduce the error propagation problem in the MMSE LE-EF (I) was presented.

We also showed that the hybrid MAP/MMSE LE-EF (I) has a faster rate of convergence with respect to the MMSE LE-EF (I). This was due to the hybrid MAP/MMSE LE-EF (I) using the MAP equalizer during the initial equalization stage and hence providing more reliable decisions in comparison with the MMSE LE-EF (I). It was shown that the hybrid MAP/MMSE LE-EF (I) also suffered from the error propagation problem but the error propagation problem was less severe in the hybrid MAP/MMSE LE-EF (I) in comparison with the MMSE LE-EF (I).

We then tested the Gaussian assumption made on the PDFs of the a priori information, during the iterations, by the use of the K-S test. It was found that Gaussian assumption holds relatively well for the MAP equalizer and the MMSE LE but fails for the MMSE LE-EF (I), MMSE LE-EF (II) and the hybrid MAP/MMSE LE-EF (I) after decoding in the first iteration. This was due to the error propagation problem, inherent in the MMSE LE-EF (I), MMSE LE-EF (II) and the hybrid MAP/MMSE LE-EF (I), consequentially causing incorrect MAP decoding during the first iteration.

Finally, we showed that the EXIT chart could be used to obtain $C_{i.i.d.}$. A comparison between the computation of $C_{i.i.d.}$ using the Arnold-Loeliger and the EXIT chart method was then presented. It was observed that the EXIT chart method provided an accurate measure of the i.i.d. channel capacity. Therefore the EXIT chart has additional benefits compared with other measures used for convergence prediction.

Chapter 4

Precoders in Turbo Equalization

4.1 Introduction

The TE system shown in Fig. 2.1 was observed to be limited by the performance of the outer code. The reason for this is that the inner code, or the ISI channel in this case, is non-recursive in nature. It was shown in [35] that an interleaving gain is observed if the inner code of a SCCC was recursive. For this reason we attempt to make the inner code of a TE system appear recursive so that its performance can be further improved.

One such way to make the inner code of a TE system appear recursive is by the use of a precoder. It was shown in [18] that the performance of a TE system is tremendously improved by the use of a precoder. This improved performance is due to the inner code, e.g. the serially concatenated precoder and ISI channel, being recursive in nature which hence results in an interleaving gain.

A number of precoder schemes have been presented in the literature. In this chapter, we investigate the impact that precoders have on the channel capacity and introduce the concept of trellis code capacity. Four precoders are used in a TE system and we investigate the effect that the precoders' weight has on the convergence of TE systems for long block lengths. Furthermore, the EXIT chart is used to analyse the four precoded TE systems. A hybrid nonprecoded/precoded scheme at the transmitter is then proposed and the trellis code capacities are investigated using the EXIT chart.

The system model for a TE system using a precoder scheme is shown in section 4.2. In section 4.3 four precoders are described and the trellis code capacities of four precoded channels are presented. A review of the current literature is given in section 4.4 where a precoder was used in a TE system. Simulation results of four precoded TE systems and a

nonprecoded TE system are presented in section 4.5. In section 4.6 precoded TE systems are analysed using the EXIT chart. The K-S test is used in section 4.7. to investigate whether the PDFs of the a priori equalizer LLRs are Gaussian distributed. The design of a hybrid equalization scheme is proposed in section 4.8. Lastly, in section 4.9, a comparison between the EXIT chart method and the Arnold-Loeliger method to compute the trellis code capacities is presented.

4.2 System model of a precoded TE system

This section presents the system model of a precoder in a TE system. This system is based on the system model presented in [88] but here training symbols are employed. Fig. 4.1 shows the system model of a TE system using a precoder.

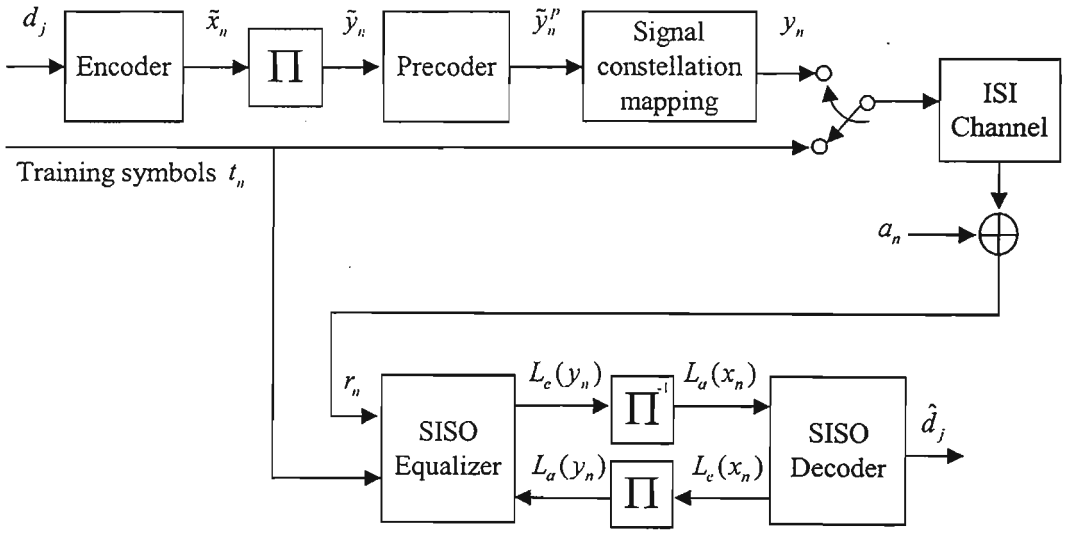

Fig. 4.1: Block diagram of a precoded TE system

The transmitter is similar to the TE system shown in Fig. 2.1, but here a precoder is included before the signal constellation mapping. This dissertation only deals with precoders that are recursive CCs of rate $R_{p'}=1$. The precoded bits $\tilde{y}_n^{p'}$ are mapped to a signal constellation to form y_n. The symbols y_n are then, together with a block of N_t training symbols t_n, transmitted over an ISI channel. The inner code is composed of the concatenation of the precoder and the ISI channel which we denote as the super-channel.

The receiver structure is similar to the nonprecoded TE system shown in Fig. 2.1. However, the SISO equalizer, in a precoded TE system, computes the extrinsic LLRs $L_e(y_n)$ based on the trellis of the super-channel.

4.3 Trellis code capacities of precoded channels

In this section we define four precoders to be used in a TE system. The concept of the trellis code capacity is introduced and evaluated for four precoded channels. A comparison between the trellis code capacity C_T and the $C_{i.i.d.}$ is then made.

We seek to investigate four precoders with different weights in their feedback connections. Table 4.1 shows the name of the four precoders with their respective octal representation.

Table 4.1: Octal representation of four precoders

Name	Octal representation
Precoder 1	(1/1)
Precoder 2	(1/3)
Precoder 3	(1/7)
Precoder 4	(1/15)

It was explained in [89] that a precoder introduces a form of coding before modulation and hence the inner code is a type of TCM. Therefore the transmitted symbols y_n^p are no longer i.i.d. due to the absence of an interleaver between the precoder and the ISI channel. For this reason the i.i.d. channel capacity is no longer applicable for a precoded channel. Since the interleaved coded bits $\tilde{y}_n$ are i.i.d., the trellis code capacity of the super-channel can be computed. In [90] the concept of trellis code capacity was introduced and was defined as the information rate between the super-channel input sequence $\tilde{y}_n$ and the super-channel output sequence r_n when the super-channel input sequence was i.i.d. and uniformly distributed. We denote the trellis code capacity of the super-channel comprising of precoder 1, 2, 3 and 4 as $C_{T,1}$, $C_{T,2}$, $C_{T,3}$ and $C_{T,4}$ respectively.

A comparison between C_T and $C_{i.i.d.}$, for the Proakis C channel, has not been made in the literature according to the knowledge of the author. We therefore seek to investigate this aspect. In Fig. 4.2 the trellis code capacities of the four precoded channels are compared with the i.i.d. channel capacity. The Arnold-Loeliger method is used to compute the trellis code capacities and the i.i.d. channel capacity.

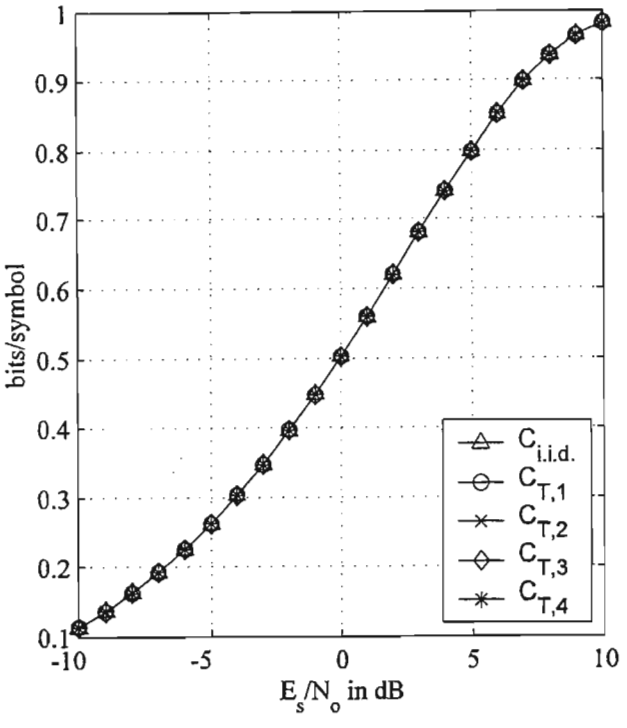

Fig. 4.2: Comparison between the trellis code capacities and the i.i.d. channel capacity

We denote the MAP equalization of the super-channel when precoder 1, 2, 3 and 4 are used as MEPs 1, 2, 3 and 4 respectively. Fig. 4.2 shows that the trellis code capacities are very close to the i.i.d. channel capacity. It was noted in [91] that the areas underneath the transfer functions of the MAP equalizer and the MEP on the EXIT chart are the same. It was shown in section 3.7 that the area the underneath the transfer function of the MAP equalizer evaluates to the i.i.d. channel capacity. Therefore we can assume that the area underneath the transfer function of the MEP would yield the trellis code capacity. This assumption is later shown to be correct in section 4.9. Therefore the results obtained for the trellis code capacities in Fig. 4.2 are justified.

In [90], it was discovered that the i.i.d. channel capacity was less than the trellis code capacity of particular trellis codes. However, in Fig. 4.2 the trellis code capacities are very close to the i.i.d. channel capacity. A mathematical proof to determine the conditions under which the trellis code capacity is the same as that of the i.i.d. channel capacity is still an open problem.

4.4 Current literature

It was shown in [92] that the use of precoders in magnetic recording channels results in a degraded performance at low SNRs but an improved performance for high SNRs. The low complexity precoded TE systems, using the M-MAP and M-SOVA equalizers, were proposed in [93]. Simulation results showed that these precoded TE systems do significantly outperform a nonprecoded system without any increase in the complexity.

In [94], the performance of a precoded partial response channel in conjunction with high rate tail-biting CCs was presented. It was shown that the use of a precoder was important in a TE system and that the use of precoder 1, given in Table 4.1, provided the best performance amongst the precoders considered.

The effect of precoders' weight on the performance of TE systems was investigated in [18], for small block lengths. The observations made from the simulation results reveal that there exists a trade-off between the performance at the turbo cliff and error floor region. Simulation results showed that the use of weight-two and multiweight precoders are suited for TE systems which require an error floor at low SNRs and high SNRs respectively.

In the literature there has been no work that deals with the performance of a precoded TE system for large block lengths and how the weight of a precoder influences the convergence. In the next section we investigate these aspects in precoded TE systems, using large block lengths.

4.5 Simulation results

In this section the BER results of precoded TE systems are shown. These results compare the

performance of precoded TE systems with that of a nonprecoded TE system. The MAP equalizer is used for the equalization of the super-channel when a precoder is used. Since the number of states in the trellis of the ISI channel and the super-channel remain the same, the computational complexity of the MAP equalizer is the same for both a nonprecoded and precoded channel.

The simulation parameters that were given in section 2.6 are used for the precoded TE system. We refer to the performance of TE systems employing the MEPs or the MAP equalizer, briefly by the name of the respective SISO equalizer. Fig. 4.3 shows the BER performance of the four MEPs and the MAP equalizer in a TE system. Note that the legend of the MAP equalizer represents the performance of the nonprecoded TE system. The iterations to achieve convergence are defined as the number of iterations used such that a BER performance of below 10^{-5} is achieved. For clarity, the number of iterations in order to achieve convergence for the MEPs is not shown in Fig. 4.3.

Simulation results, in Fig. 4.3 for the initial equalization and decoding process, show the performance of the MAP equalizer is much improved compared with the performance of MEPs 1, 3 and 4. However, the performance of MEP 2 is superior to that of the MAP equalizer for SNRs > 3 dB. It is thus thought that the use of some precoders do have a superior performance compared with the no precoder case during the initial iterative decoding process at high SNRs.

It can also be seen in Fig. 4.3, for 4 and 14 iterations, that the MAP equalizer has a lower BER performance compared with the MEPs at low SNRs. However, the MEPs have a superior performance compared with the MAP equalizer at high SNRs. This is due to an interleaving gain being observed in a precoded TE system. Another observation made from 4 and 14 iterations is that the slope of the turbo cliff region of the MEPs is relatively steep compared with that of the MAP equalizer. This confirms the comments given in [95] which stated that a recursive inner code does not exhibit an error shoulder after decoding convergence.

It is clear from the BER performance of the MEPs that the weights of the precoders do have an effect on their respective performances. MEPs 1, 2, 3 and 4 are arranged in descending order of performance for 4 iterations, 14 iterations and iterations to achieve convergence. However, at 4 iterations we observe a crossover point between MEPs 1 and 2 at a SNR of

1.6 dB. This suggests that the MEPs have different rates of convergence during the iterations.

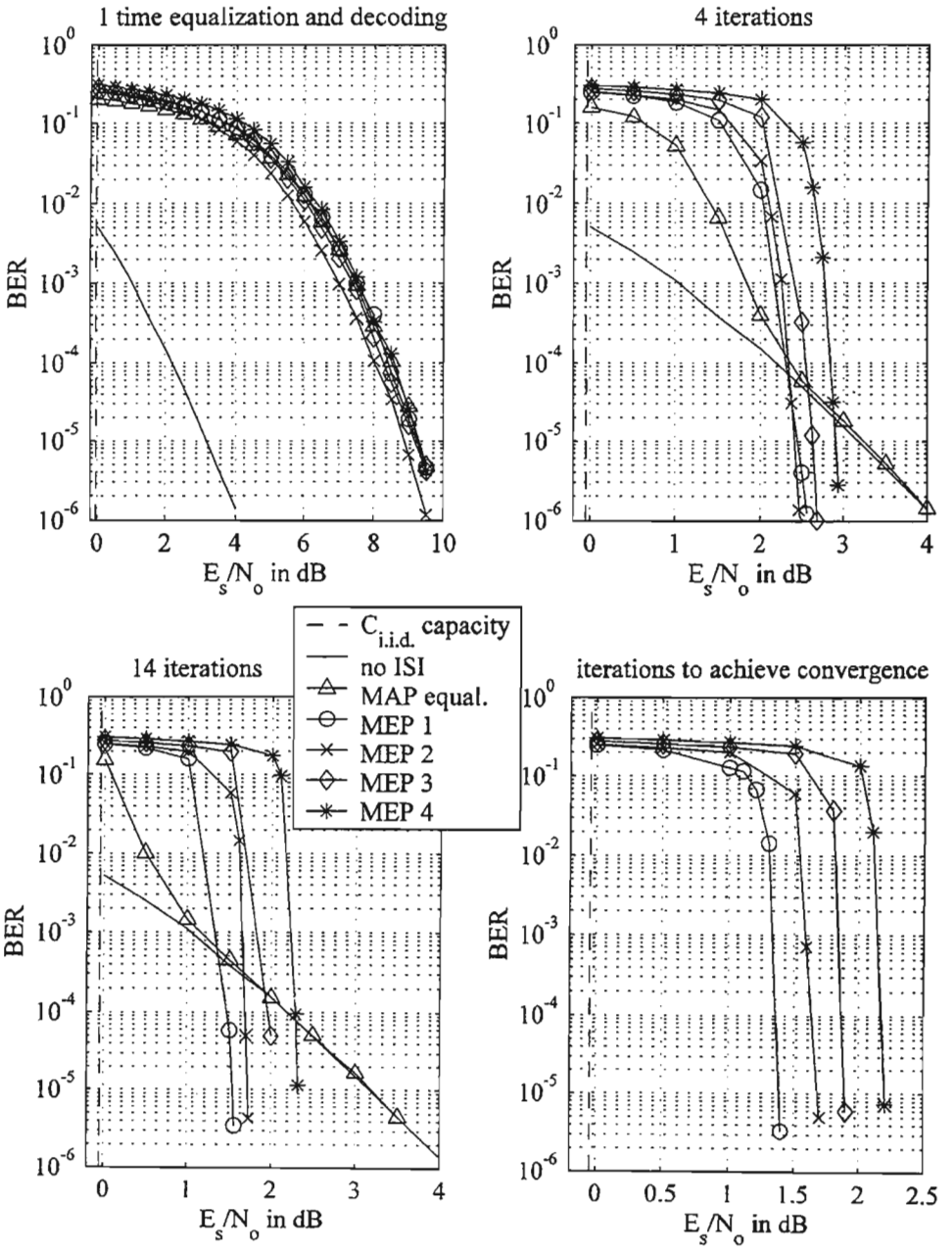

Fig. 4.3: BER performance comparison of the one time equalization and decoding, 4, 14 iterations and iterations to achieve convergence

In Fig. 4.3, the number of iterations in order to achieve convergence for MEPs 1, 2, 3 and 4 are 34, 15, 34 and 66 respectively. The simulation results obtained for more than 14 iterations show that the MEPs converge at a much lower SNR compared with the MAP equalizer. This is due to the interleaving gain observed for precoded TE systems. The SNRs at which MEPs 1, 2, 3 and 4 achieve convergence are 1.4 dB, 1.7 dB, 1.9 dB and 2.2 dB respectively. It is thus intuitive to conclude that a TE system using low weight precoders converge at a lower SNR compared with a TE system using high weight precoders.

It was shown in Fig. 4.2 that the i.i.d. channel capacity was identical to the trellis code capacities of the precoded channels. For this reason the i.i.d. channel capacity is shown in Fig. 4.3 to assess how closely the MEPs do approach this bound. It is observed from Fig. 4.3 that MEP 1 converges 1.4043 dB away from the i.i.d. channel capacity (or trellis code capacity), after 34 iterations, at a BER of $3.3 \cdot 10^{-6}$.

It can be noted that even with the interleaving gain observed from the simulation results in Fig. 4.3, the best MEP is still 1.4043 dB away from the i.i.d. channel capacity. This difference is thought to be due to the relative poor performance of the outer code, ie. the MF bound. It is thought that the use of more powerful outer encoding/decoding methods would improve the MF bound and thus a precoded TE system which yields an interleaving gain, using these encoding/decoding algorithms will achieve a performance very close to the i.i.d. channel capacity.

4.6 EXIT chart analysis of precoded TE systems

Simulation results in section 4.5 showed that the use of a precoder significantly improved the performance of a TE system. For this reason we seek to analyse precoded TE systems such that conclusions can be made as to why a precoded TE system offers substantial coding gain compared with a nonprecoded TE system at high SNRs and which factors are important in the convergence of the MEPs.

Some work on the analysis of precoded TE systems has been presented in the literature. In [18] the union bound analysis technique was presented. It was shown that the union bound gave a fairly good approximation of the system performance at high SNRs. The design of precoders based on the union bound was considered in [96]. Convergence prediction

methods to analyse a precoded TE system were shown in [88, 94, 97] using the fidelity, mutual information and SNR measure respectively.

It was observed in the literature that two main factors affect the convergence of the MEP. The first factor was that the MEPs had a loss of information compared with the MAP equalizer during the initial equalization phase [88, 94, 97]. Furthermore, an analysis proof was presented in [88] which showed that all MEPs for the 2-tap ISI channel had a loss of information. In [97], it was shown that different MEPs have different losses of information.

Another factor that affects the convergence of a precoded TE system is the slope of the MEP's transfer function in the convergence prediction diagrams. It was observed in [94, 97] that different MEPs have different slopes in their respective transfer functions.

In [88], a method that used a mixture of precoding and no precoding was presented to improve the convergence of a TE system. An optimization method to determine the ratio of precoded blocks to nonprecoded blocks was also presented.

To the extent of the author's knowledge, no literature has considered the use of the EXIT chart to analyse a precoded TE system for large block lengths. In this section the analysis of precoded TE systems is presented using the EXIT chart.

The EXIT chart is used as the analysis tool due to the reasons given in section 3.1. In this section, the EXIT chart is used to analyse TE systems employing MEPs 1, 2, 3 and 4. The characteristics of the MEPs are considered over a range of SNRs, for zero input mutual information, and with varying input mutual information, at a particular SNR. The system trajectories of the four precoded TE systems are also presented. The K-S test is used to investigate the validity of the EXIT chart analysis.

The computation of the transfer functions and system trajectories, using the HM and TAAM, was found to be very similar for the MAP equalizer in section 3.3.2. However, it was outlined in section 3.2, that the complexity of the TAAM is much lower than the HM. For this reason we choose to use the TAAM in this section for the computation of the output mutual information. Unless otherwise stated, the parameters given in section 2.6 and section 3.3 are used for the analysis.

4.6.1 Zero input mutual information

In this section the MAP equalizer, MEPs 1, 2, 3 and 4 are analysed, during the initial equalization stage, in order to compare their respective characteristics. Fig. 4.4 shows the output mutual information of the four MEPs and the MAP equalizer over varying SNRs.

It was shown in the literature that the use of precoders results in a loss of information during the initial equalization phase. This is also observed from the results shown in Fig. 4.4 for MEPs 1, 3 and 4. However, we do note that MEP 2 does have an improved performance compared with the MAP equalizer for SNRs > 3 dB. This explains why the performance of MEP 2, shown in Fig. 4.3 in section 4.5, is superior to the performance of the MAP equalizer for SNRs > 3 dB. For this reason we can conclude that the performance of the MEP, in particular ISI channels, can be superior to that of the MAP equalizer during the first equalization stage at high SNRs.

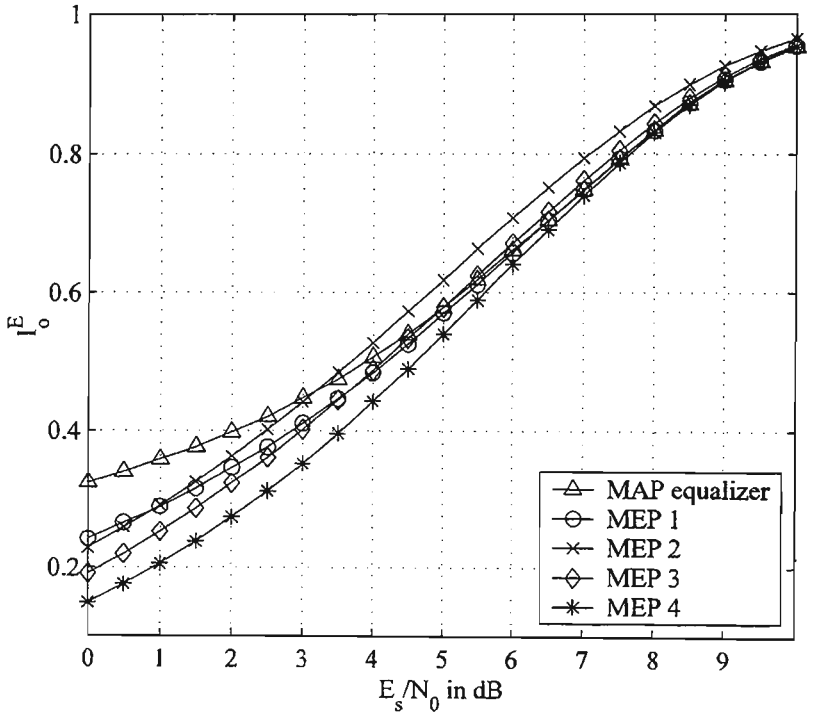

Fig. 4.4: Plot of output mutual information as a function of SNR for MEPs 1, 2, 3, 4 and the MAP equalizer

It was also observed in the literature that different MEPs results in different losses of information during the initial equalization. This characteristic can also be noted in Fig. 4.4 which shows that the MEP relating to a low weight precoder has a greater loss of information compared with the MEP relating to a high weight precoder. Furthermore, this loss of information is shown to be more significant at low SNRs. This explains why the performance of the MAP equalizer, shown in Fig. 4.3 in section 4.5 after the initial equalization and decoding stage, is slightly improved with respect to the MEPs for low SNRs and why the performance of MEPs 1, 3 and 4 and the MAP equalizer are indistinguishable at high SNRs.

4.6.2 Varying input mutual information

In this section the transfer functions of the four MEPs are presented and compared with the transfer function of the MAP equalizer. In Fig. 4.5 a comparison is shown between the transfer function of the MAP equalizer and the transfer functions of the MEPs at 2.2 dB.

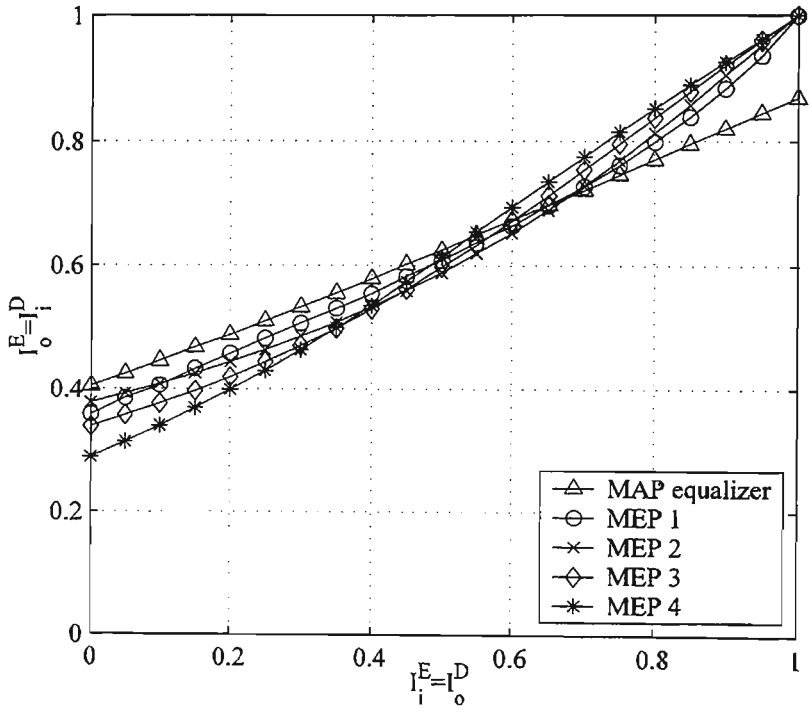

Fig. 4.5: Transfer functions of the MEPs and the MAP equalizer at $E_s / N_o = 2.2$ dB

Fig. 4.5 shows that the MEPs do approach $I_o^E = 1$ when $I_i^E = 1$. This characteristic is important for iterative decoding processes so that an error shoulder does not exist after decoding convergence [95]. This explains the excellent performance of a precoded TE system in section 4.5 and why a precoded TE system has a sharp turbo cliff region in contrast to a nonprecoded TE system which has an error shoulder after decoding convergence.

It can also be seen from Fig. 4.5 that the slope of the MEPs are higher than that of the MAP equalizer for high I_i^E values. Further, at high I_i^E values, the slopes for MEPs 1, 2, 3 and 4 are arranged in descending order. From the simulation results in Fig. 4.3, MEPs 1, 2, 3 and 4 were shown to converge in ascending order of SNRs. However, it can be seen from Fig. 4.4 that MEP 1 has a loss of information relative to MEP 2 at a SNR of 1.4 dB. Based on these above observations, we can conclude that the convergence of precoded TE systems is influenced more by the slope of the MEP's transfer functions than the loss of information during the initial equalization stage.

Another interesting observation from Fig. 4.5 is that MEPs 1 and 2 possess a higher output mutual information compared with MEPs 3 and 4 at low I_i^E values. However, for high I_i^E, MEPs 3 and 4 have a higher output mutual information compared with MEPs 1 and 2. This implies that the MAP equalization of a super-channel using low weight precoders are more suited for the early iterations while the MAP equalization of a precoded channel using a high weight precoder performs better during the future iterations.

4.6.3 Convergence thresholds and system trajectories

In this section the EXIT chart is used to determine the convergence threshold and the predicted convergence of precoded TE systems. A comparison is then made between the: convergence threshold, predicted convergence and actual convergence. The system trajectories of the four precoded TE systems are also shown at the predicted convergences.

Figs. 4.6 - 4.9 show the EXIT chart analysis of the precoded TE systems utilizing MEPs 1, 2, 3 and 4.

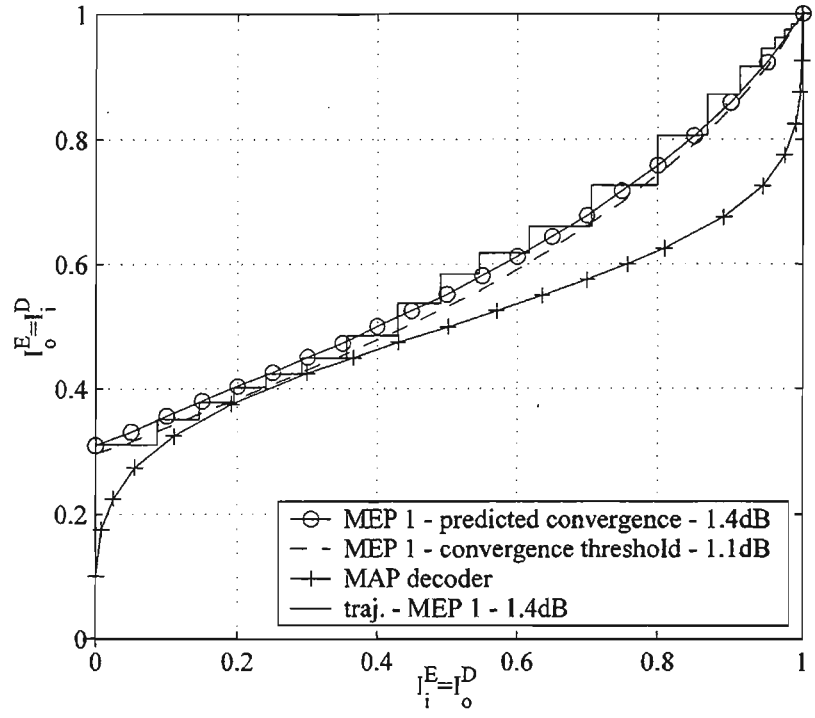

Fig. 4.6: EXIT chart of MEP 1

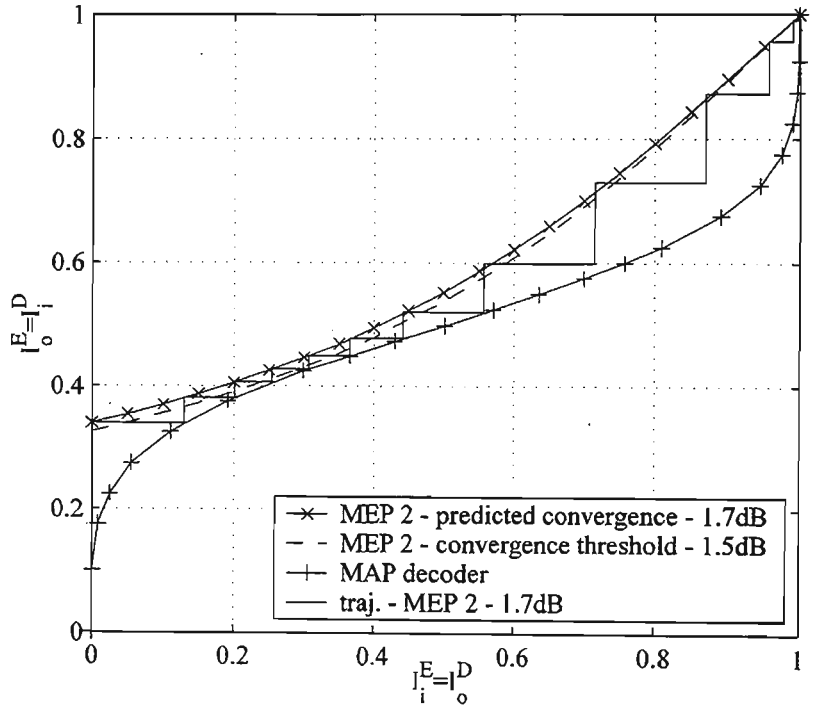

Fig. 4.7: EXIT chart of MEP 2

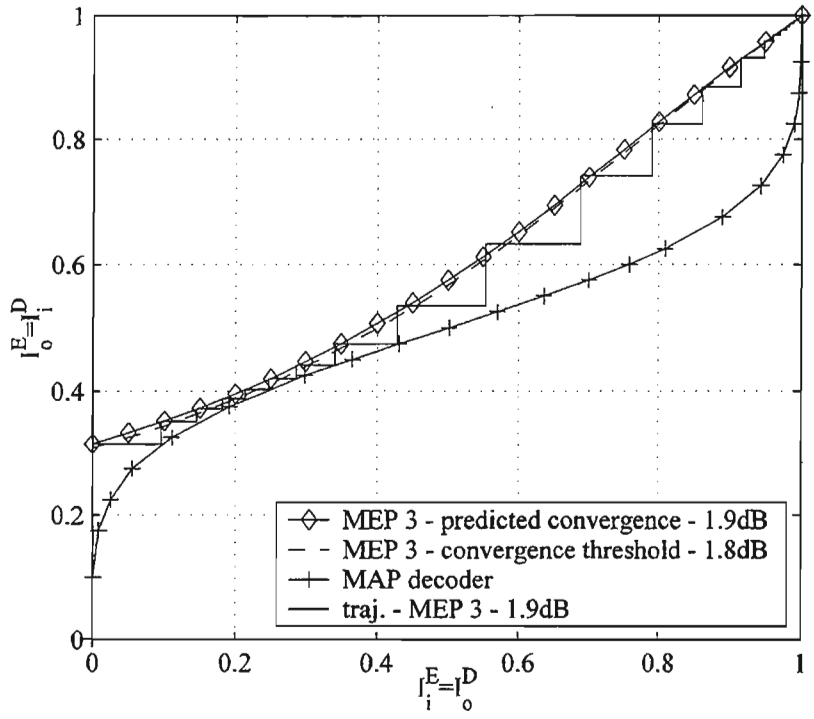

Fig. 4.8: EXIT chart of MEP 3

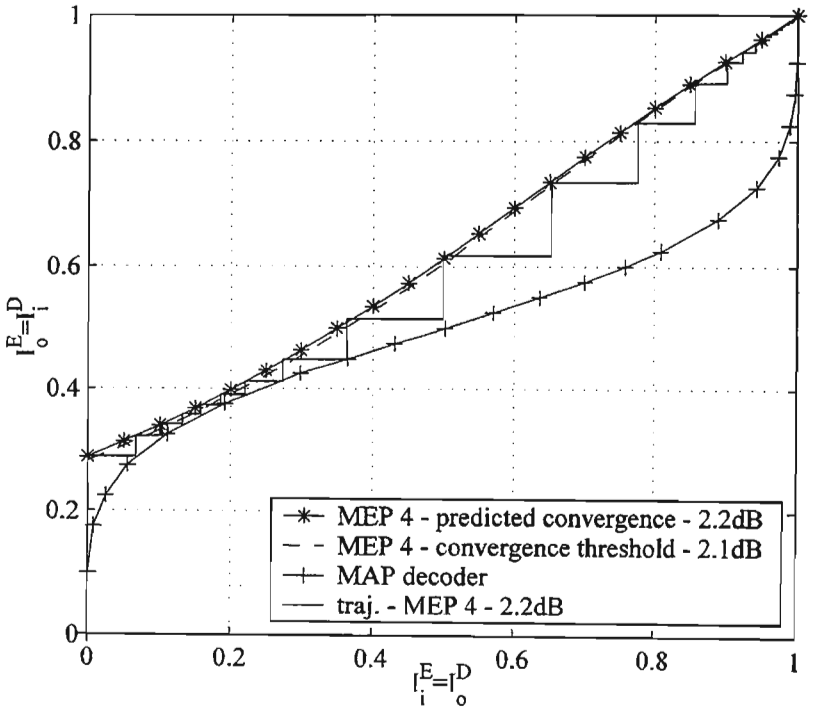

Fig. 4.9: EXIT chart of MEP 4

A summary of the following properties relating to the MEPs are given in Table 4.1: convergence thresholds, predicted convergences and actual convergences. The convergence threshold is defined as the lowest SNR at which the two transfer functions $I_o^E = \Upsilon_e(I_i^E, \text{SNR})$ and $I_i^D = \Upsilon_d^{-1}(I_o^D)$ do not intersect. The predicted convergence is defined as the minimum SNR for which the system trajectory reaches $I_o^E = 1$, while the actual convergence of MEPs 1, 2, 3 and 4 are obtained from Fig. 4.3, in section 4.5, after 34, 15, 34 and 66 iterations respectively.

Table 4.2: Convergence thresholds, predicted and actual convergences for the MEPs

Equalizer type	**Convergence threshold**	**Predicted convergence**	**Actual convergence**
MEP 1	1.1 dB	1.4 dB	1.4 dB
MEP 2	1.5 dB	1.7 dB	1.7 dB
MEP 3	1.8 dB	1.9 dB	1.9 dB
MEP 4	2.1 dB	2.2 dB	2.2 dB

The difference between the convergence thresholds and predicted convergences in Table 4.2 is due to the bottleneck region [84] between the transfer functions of the equalizer and decoder being too small and hence the system trajectories are prohibited to reach $I_o^E = 1$. The results shown in Table 4.2 reveal that the predicted convergence and the actual convergence are the same. Therefore the predicted convergence is an accurate estimate of the actual convergence.

The convergence thresholds obtained for MEPs 1, 2, 3 and 4 are noted to be in ascending order of magnitudes. This explains why the performance of the MEPs relating to a low weight precoder, shown in Fig. 4.3 in section 4.5, has a coding gain with respect to the MEPs corresponding to high weight precoders.

The system trajectories shown in Figs. 4.6 - 4.9 approach the bounds of the transfer function on the EXIT chart only during the early iterations. The Gaussian assumption made on the PDFs of the a priori equalizer and decoder LLRs during the iterations, similar to the hybrid MAP/MMSE LE-EF (I), MMSE LE-EF (I) and (II) in section 3.3.2, is thought to be the

source of the inaccuracies incurred when the transfer functions are obtained for the EXIT chart.

A summary is given in Table 4.3 for the number of iterations that the system trajectories reach the bounds of the transfer functions on the EXIT chart and the number of iterations for the system trajectories to obtain a value of $I_o^E = 1$ at the MEPs' predicted/actual convergence.

Table 4.3: Summary of the important characteristics of the system trajectory for the MEPs

Equalizer type	**Number of iterations for the system trajectory to reach the bounds of the transfer functions**	**Number of iterations for the system trajectory to reach (1,1) on the EXIT chart**
MEP 1	6	21
MEP 2	6	13
MEP 3	7	25
MEP 4	7	47

The number of iterations to achieve convergence for the MEPs in section 4.5 differs from the number of iterations for the system trajectory to reach $I_o^E = 1$ shown in Table 4.3 due to the requirement of having at least 100 bit errors in the BER results.

4.7 The K-S test

The PDFs of the a priori equalizer LLRs are investigated in this section due to the system trajectories of the precoded TE systems not following the bounds of the transfer functions on the EXIT chart. The K-S test is presented to compare the predicted CDFs to the real CDFs for the precoded TE systems during the iterative equalization and decoding process.

The method and parameters of the K-S test given in section 3.4 are used in this section. Fig. 4.10 shows the D values from the K-S test performed on the conditional CDFs of the a

priori equalizer LLRs during the iterations for the precoded TE systems.

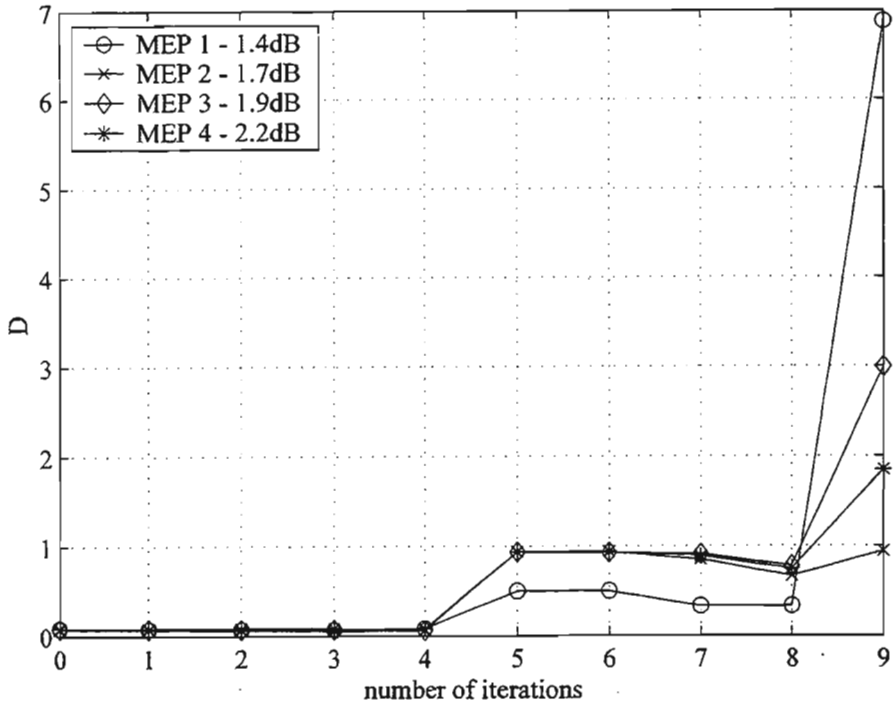

Fig. 4.10: K-S test performed on the conditional CDFs of the a priori equalizer LLRs

The D value obtained in the K-S test in Fig. 4.10 for the MEPs remains relatively low and constant during the early iterations. However, an increase in the D value is observed after the fifth iteration. Therefore the PDFs of the equalizers' a priori information are not Gaussian distributed during the fifth iteration when the MEPs are used in a TE system. Further, the number of iterations for the system trajectories to reach the bounds of the transfer functions, shown in Table 4.2, is reasonably close to the number of iterations when the D value increases. This explains why the MEP's system trajectories do not reach the bounds of the transfer functions in Figs. 4.6 – 4.9.

4.8 Design of the hybrid MAP/MEP equalizer

It was observed in section 4.6.2 that the transfer functions of the MEPs and the transfer function of the MAP equalizer had different characteristics. This suggests the use of a hybrid

equalization scheme would be optimal in a TE system. In this section the design of the hybrid MAP/MEP receiver is proposed in order to further improve the convergence of a TE system. Fig. 4.11 shows the transfer functions of the MEPs and the transfer function of the MAP equalizer and the MAP decoder at 0.8 dB.

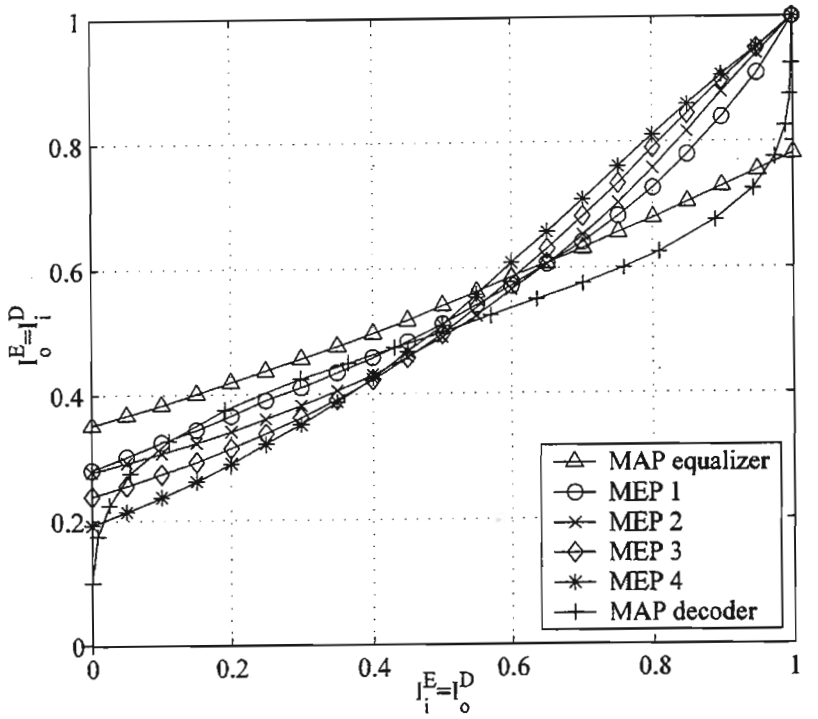

Fig. 4.11: Transfer functions of the MEPs, MAP equalizer and the MAP decoder at $E_s / N_o = 0.8$ dB

It can be seen from Fig. 4.11 that the transfer functions of the MEPs intersect with the transfer function of the MAP decoder. However, the transfer function of the MAP equalizer and the MAP decoder do not intersect at low I_i^E values. This implies that a hybrid equalization scheme can be realised as follows: use the MAP equalizer during the early iterations and then switch to the MEP that has the highest I_o^E for the future iterations. Such a hybrid equalizer in a TE system would further improve the performance of a TE system.

The disadvantage of such a hybrid equalizer is that parallel channels are required in order to obtain the received inputs from both a nonprecoded and precoded channel. A criterion to determine when to switch between the MAP equalizer and the MEPs would also be needed.

4.9 C_T computation using the EXIT chart

It was shown in section 3.6 that the area underneath the transfer function of the MAP equalizer provides a very close estimate to the actual i.i.d. channel capacity. Extending this idea, we use the EXIT chart method to compute the trellis code capacities of precoded channels in this section.

Figs. 4.12 – 4.15 show the trellis code capacities of four precoded channels using two different methods. Similar to the result observed from section 3.7, at low SNRs the EXIT chart method slightly overestimates the trellis code capacities. However, the EXIT chart method slightly underestimates the C_T values at high SNRs. This shows that the EXIT chart method is also an accurate method to compute the trellis code capacity.

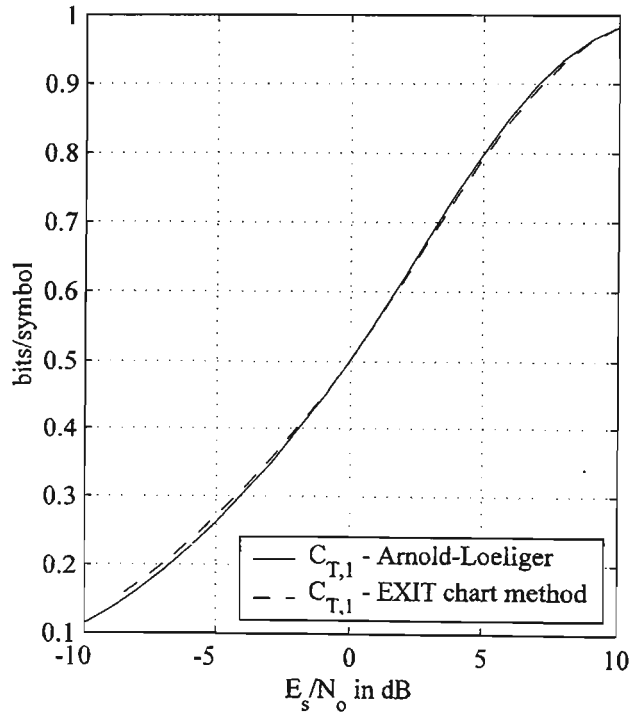

Fig. 4.12: Comparison of the Arnold-Loeliger and EXIT chart methods to compute $C_{T,1}$

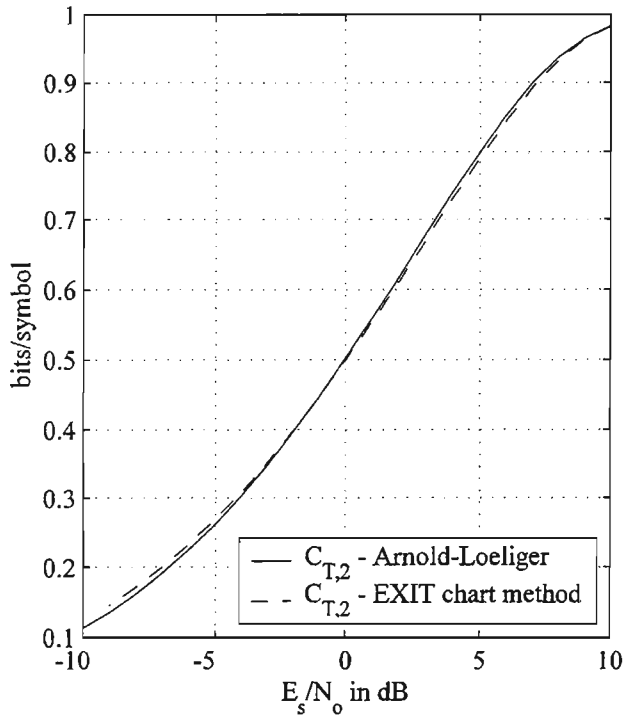

Fig. 4.13: Comparison of the Arnold-Loeliger and EXIT chart methods to compute $C_{T,2}$

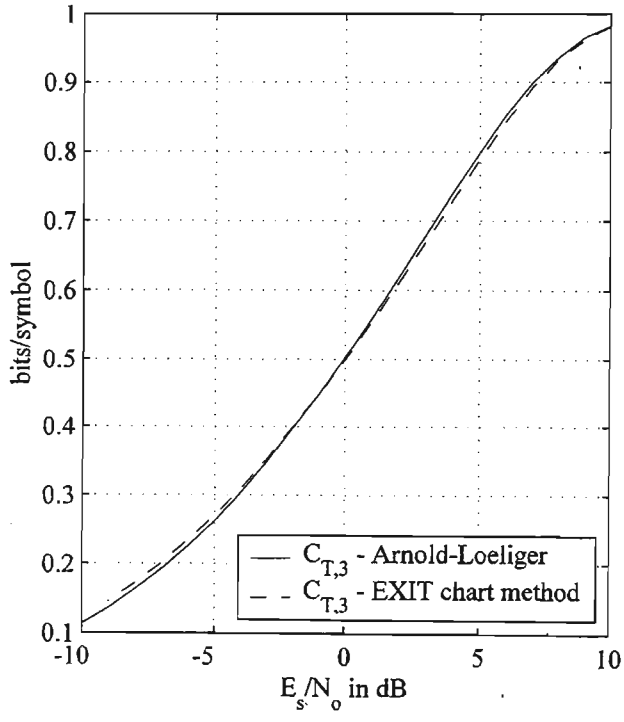

Fig. 4.14: Comparison of the Arnold-Loeliger and EXIT chart methods to compute $C_{T,3}$

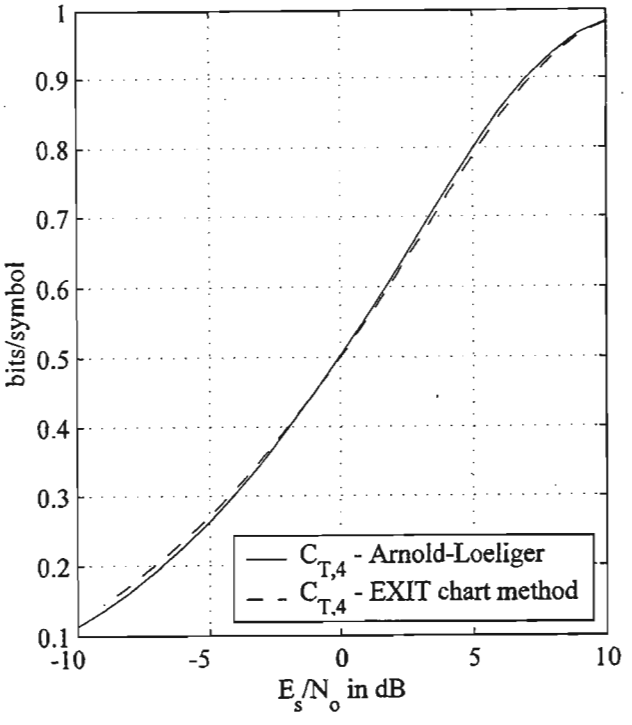

Fig. 4.15: Comparison of the Arnold-Loeliger and EXIT chart methods to compute $C_{T,4}$

4.10 Summary

In this chapter, we considered the use of four precoders in a TE system. The concept of trellis code capacity was introduced and was applied to four precoded channels. It was shown that the trellis code capacities of the four precoded channels are very close to the i.i.d. channel capacity. This demonstrated that the use of these four precoders did not change the maximum achievable rate of an ISI channel.

The performances of the four precoded TE systems were then presented. It was shown that precoded TE systems result in an interleaving gain and hence perform better than nonprecoded TE systems. Furthermore, it was noted that, during the initial equalization and decoding stage, a TE system employing MEP 2 does perform better than a TE system using the MAP equalizer. Interesting observations were revealed as to how the precoders' weight impacts the convergence of TE systems. We found that TE systems utilizing the MEPs corresponding to low weight precoders converged at a lower SNR with respect to the MEPs related to high weight precoders. The precoded TE system employing MEP 1 was observed

to have the best performance and was shown to converge 1.4043 dB away from the trellis code capacity at a BER of $3.3 \cdot 10^{-6}$. We noted that the performance of precoded TE systems could be further improved if the MF bound was closer to the i.i.d. channel capacity.

A comparison of the transfer functions of the MEPs and the transfer function of the MAP equalizer, for zero input information and varying SNRs, was presented using the mutual information measure. We then found that not all MEPs acquired a loss of information during the initial equalization stage. The transfer functions of the four MEPs were presented and compared with the transfer function of the MAP equalizer on the EXIT chart. It was shown that the slopes of the transfer functions of the MEPs were greater than the slope of the transfer function of the MAP equalizer at high I_i^E values. The EXIT chart analysis of the four precoded TE systems was then presented. We observed that the MEP relating to a low weight precoder possessed a lower convergence threshold and predicted convergence compared with the MEP corresponding to a high weight precoder. We found that the slope of the MEPs' transfer function, at high I_i^E values, played a greater role in determining the convergence of precoded TE systems rather than the loss of information during the initial equalization stage.

We then assessed the legitimacy of the EXIT chart analysis using the K-S test. We found that the Gaussian assumption imposed on the PDFs of the a priori LLRs was only valid during the early iterations.

A hybrid MAP/MEP scheme was proposed such that further improvements in the performance of TE systems could be achieved. We showed that the convergence of a TE system could be further improved if this hybrid equalization scheme was realised.

Finally, we used the EXIT chart to compute the trellis code capacities. A comparison between the computation of the trellis code capacities using the Arnold-Loeliger and the EXIT chart method was then presented. We found that the EXIT chart method provided an accurate measure of the trellis code capacities.

Chapter 5

Conclusion and Future Work

In this dissertation, the three ingredients used to make up the turbo principle were discussed. The turbo principle was then applied to the equalization problem which originated into the field of TE [41].

The first part of this research investigated SISO equalization algorithms used for nonprecoded TE systems. The MMSE LE-EF (I), MMSE LE-EF (II) and the hybrid MAP/MMSE LE-EF (I) were proposed to be used in TE systems such that the performance of MMSE equalizers in TE systems could be improved. We also presented a general structure for MMSE equalizers from which instances such as the MMSE LE, MMSE DFE, MMSE LE-EF (I) and (II) could be derived. We compared the performance of the TE systems using the proposed MMSE LE-EF (I) and hybrid MAP/MMSE LE-EF (I) to TE systems employing the existing MAP equalizer, MMSE LE and MMSE DFE. It was found that the MMSE LE-EF (I) and the hybrid MAP/MMSE LE-EF (I) suffered from the error propagation problem during the early iterations. However, we observed that these equalizers did overcome the error propagation problem during the later iterations. Simulation results demonstrated that the MMSE LE-EF (I) and the hybrid MAP/MMSE LE-EF (I) performed better than the MMSE LE in a TE system. The MMSE LE-EF (I) and the hybrid MAP/MMSE LE-EF (I) were shown to be 4.0043 dB away from i.i.d. channel capacity for a BER of $1.5 \cdot 10^{-5}$. This relatively large difference was due to relative poor performance of the MF bound and not the respective SISO equalization algorithms.

The second part of this research involved the EXIT chart analysis of nonprecoded TE systems. We compared the transfer functions of the MMSE LE-EF (I) and (II) with the transfer functions of existing SISO equalization schemes. We then compared the TAAM and HM to obtain the EXIT chart for the TE systems utilizing the MAP equalizer, hybrid MAP/MMSE LE-EF (I) and the MMSE equalizers. It was discovered that TAAM method was only accurate for the MAP equalizer and the MMSE LE. This was thought to be due to

the violation of the assumptions made in the TAAM, when the other SISO equalizers were used in a TE system.

We observed that the MMSE LE-EF (I) converged faster than the MMSE LE while the MMSE LE-EF (II) had a slower rate of convergence with respect to the MMSE LE. This was due to the error propagation problem being more severe in the MMSE LE-EF (II). We observed that the error propagation problem in the hybrid MAP/MMSE LE-EF (I) was less severe compared with the MMSE LE-EF (I) and hence the hybrid MAP/MMSE LE-EF (I) possessed a faster rate of convergence with respect to the MMSE LE-EF (I). This was due to the hybrid MAP/MMSE LE-EF (I) using the optimal MAP equalizer for the initial equalization and hence providing more reliable decisions compared with the MMSE LE-EF (I). We then used the K-S test in order to assess the validity of the EXIT chart analysis during the iterations. We found the Gaussian assumption holds reasonably well for the MAP equalizer and the MMSE LE but fails for the MMSE LE-EF (I), MMSE LE-EF (II) and the hybrid MAP/MMSE LE-EF (I) after decoding in the first iteration. This was due to the error propagation problem, inherent in the MMSE LE-EF (I), MMSE LE-EF (II) and the hybrid MAP/MMSE LE-EF (I), consequentially causing incorrect MAP decoding during the first iteration. It was also shown that the EXIT chart method provided an accurate measure of the i.i.d. channel capacity. Therefore the EXIT chart has additional benefits compared with other measures for predicting the convergence of iterative decoding processes.

The final part of this research involved the performance and analysis of precoded TE systems. The concept of trellis code capacity was introduced and we computed the trellis code capacities of four precoded channels. It was shown that precoded TE systems result in an interleaving gain and hence perform better than nonprecoded TE systems. We also showed by simulations and analysis that not all MEPs had a loss of information during the initial equalization. Interesting observations were revealed as to how the precoders' weight impacts the convergence of TE systems. We found that the TE systems utilizing the MEPs corresponding to low weight precoders converged at a lower SNR with respect to the MEPs related to high weight precoders. We observed that the precoded TE system employing MEP 1 had the best performance amongst the MEPs considered and MEP 1 was observed to converge 1.4043 dB away from the trellis code capacity for a BER of $3.3 \cdot 10^{-6}$. We noted that performance of precoded TE systems could be further improved if the MF bound was closer to the i.i.d. channel capacity.

The transfer functions of four MEPs was presented and compared with the transfer function of the MAP equalizer. It was shown that the slopes of the transfer functions of the MEPs were greater than the slope of the transfer function of the MAP equalizer. The EXIT chart analysis of four precoded TE systems was then presented. We observed that the MEP relating to a low weight precoder possessed a lower convergence threshold and predicted/actual convergence in comparison with the MEP corresponding to a high weight precoder. We concluded that the slope of the MEPs' transfer function, at high I_i^E values, played a greater role in determining the convergence of precoded TE systems rather than the loss of information during the initial equalization stage.

We then assessed the legitimacy of the EXIT chart analysis using the K-S test. We found that the Gaussian assumption imposed on the PDFs of the a priori LLRs was only valid during the early iterations. A hybrid MAP/MEP scheme was proposed such that further improvements in the performance of TE systems could be achieved. Using the EXIT chart, we showed that the convergence of a TE system can be further improved if this hybrid equalization scheme was realised. We also found the EXIT chart method did provide an accurate measure of the trellis code capacities.

It is expected that TE systems should receive increasing attention by the many researchers in order to develop efficient and reliable communication systems for ISI channels. Topics of future research could involve any of the topics given in the paragraphs below.

The MMSE LE-EF (I) was shown to offer performance gains with respect to the MMSE LE. However, the MMSE LE-EF (I) does suffer from the error propagation problem. Further investigation and characterization of the error propagation effect in the MMSE LE-EF (I) would yield insightful knowledge of the MMSE LE-EF (I) receiver. We could then use this knowledge in order to overcome or mitigate the error propagation problem during the early iterations.

Thus far no analytic expressions exist for SISO equalization algorithms. This is due to the incorporation of a priori information in SISO equalizers. Future work should investigate how different patterns and qualities of a priori LLRs affect the performance of SISO equalizers and hence obtain reasonable assumptions on these SISO equalizers. Analytic results may then be possible for the respective SISO equalizers based on these assumptions. Thereafter,

once the MAP decoding algorithm is also fully understood, analytic results are possible for TE systems.

The use of the BAD receiver [15] in an uncoded system was shown to offer an improved performance with respect to the classical DFE. Therefore using this inventive approach of the BAD receiver, a bi-directional MMSE LE-EF (I) can be realized for a TE system in order to further improve the performance of MMSE equalizers in TE. The computational complexity of the bi-directional MMSE LE-EF (I) would only be of a quadratic order and would thus offer a lower computational complexity compared with the MAP equalizer if the length of the time varying FIR filters in the bi-directional MMSE LE-EF (I) is not much greater than the length of the CIR.

The major disadvantage of the EXIT chart is that it is not accurate after the early iterations for a TE system. Therefore other distributions should be investigated to model the PDFs of the a priori information during the later iterations. Another disadvantage is that the EXIT chart is obtained through simulations. A leading researcher in the field of channel coding has expressed an urgent need to obtain analytic results for the EXIT chart [98]. However, before analytic results are obtained for the EXIT chart, the complex MAP decoding algorithm is required to be fully analyzed. Thus future work should focus on ingenious ideas of analyzing the MAP decoding algorithm.

The derivation of performance criterion for the hybrid MAP/MEP receiver, in order to switch between the MAP equalizer and the MEPs, is another source of future work. It is thought that this task would be simpler once analytic results for the MAP equalizer and the MEPs are obtained. Similar to the idea developed in [38], the mean and variance of the mathematical expression for the extrinsic information can be used to derive this performance criterion for the hybrid MAP/MEP.

It was shown in [72] that the performance of irregular LDPC codes in TE systems closely approached the i.i.d. channel capacity. However, this TE system did not consider the use of a precoder and hence an interleaving gain was not achieved. It is thought that the use of a precoder would improve the speed of convergence. For this reason precoded TE systems with powerful outer codes such as irregular LDPC codes or the irregular codes considered in [95] are sources of future research.

The MAP equalizer has been the popular choice in the literature for the equalization of precoded channels. However, SISO MMSE equalizers have not been considered for the equalization of precoded channels. Future research work should thus investigate the feasibility of SISO MMSE equalizers in precoded TE systems.

It was also discussed that precoding is a type of TCM. However, it is well known that TCM is an instant of multilevel codes. The choice of component codes for multilevel codes is very important and directly affects its performance. Therefore future research work could involve using the EXIT chart to design optimized multilevel codes for TE systems.

Lastly, in this dissertation we focused on TE systems that use long block lengths. However, long block lengths can only be used for delay insensitive services such as email, as well as on slow fading channels. The design of capacity approaching TE systems for short block lengths requires serious attention such that high quality delay services like streaming voice and video can be realized in future communication systems.

Bibliography

[1] C. Shannon, "A mathematical theory of communications," *Bell System Technical Journal*, vol. 27, pp. 379-423, 623-656, Oct. 1948.

[2] J. Proakis, *Digital Communications*, 3rd ed. Singapore: McGraw-Hill, 1995.

[3] G. Forney, "Maximum-likelihood sequence estimation of digital sequences in the presence of intersymbol interference," *IEEE Trans. on Inform. Theory*, vol. 18, pp. 363-378, May 1972.

[4] G. Forney, "The Viterbi Algorithm," *Proc. of the IEEE*, vol. 61, pp. 268-278, Mar. 1973.

[5] J. Hayes, T. Cover, and J. Riera, "Optimal sequence detection and optimal symbol-by-symbol detection: Similar algorithms," *IEEE Trans. on Comm.*, vol. COM-30, pp. 152-157, Jan. 1982.

[6] M.V. Eyuboglu and S. Qureshi, "Reduced-state sequence estimation with set-partitioning and decision-feedback," *IEEE Trans. on Comm.*, vol. 36, pp. 13-20, Jan. 1988.

[7] G. Kechriotis, E. Zervas, and E. Manolakos, "Using recurrent neural networks for adaptive communication channel equalization," *IEEE Trans. on Neural Networks*, vol. 5, pp. 267-278, Mar. 1994.

[8] S. Chen, G. Gibson, C. Cowan, and P. Grant, "Reconstruction of binary signals using an adaptive radial basis-function equalizer," *Signal Processing*, vol. 22, pp. 77-93, 1991.

[9] R. Lucky, "Automatic equalization for digital communications," *Bell System Technical Journal*, vol. 44, pp. 547-588, Apr. 1965.

[10] M. Austin, "Decision feedback equalization for digital communication over dispersive channels," *MIT Research Laboratory of Electronics Technical Report 437*, Aug. 1967.

[11] N. Beaulieu, "Bounds on recovery times on decision feedback equalizers," *IEEE Trans. on Comm.*, vol. 42, pp. 2786-2794, Oct. 1994.

[12] R. Kennedy, B. Anderson, and R. Bitmead, "Channels leading to rapid error recovery for decision feedback equalizers," *IEEE Trans. on Comm.*, vol. 37, pp. 1126-1135, Nov. 1989.

[13] K. Dogancay and R. Kennedy, "Blind detection of equalization errors in communication systems," *IEEE Trans. on Inform. Theory*, vol. 43, pp. 469-482, Mar. 1997.

[14] J. Balakrishnan, "Mitigation of error propagation in decision feedback equalization," M.Sc Thesis, Cornell University, Ithaca, NY, U.S.A., Aug. 1999.

[15] C. McGahey, A. Singer, and U. Madhow, "BAD: A bi-directional arbitrated decision feedback equalizer," in *Proc. Conf. on Inform. Sciences and Sys., Princeton, U.S.A.*, vol. 2, Mar. 2000.

[16] M. Tomlinson, "New automatic equalizers employing modulo arithmetic," *Electronic Letters*, vol. 7, pp. 138-139, Mar. 1971.

[17] H. Harashima and H. Miyakawa, "Matched-transmission technique for channels with intersymbol interference," *IEEE Trans. on Comm.*, vol. 29, pp. 774-780, Aug. 1972.

[18] I. Lee, "The effect of a precoder on serially concatenated coding systems with an ISI channel," *IEEE Trans. on Comm.*, vol. 49, pp. 1168-1175, Jul. 2001.

[19] T. Richardson, M. Shokrollahi, and R. Urbanke, "Design of capacity-approaching irregular low-density parity check codes," *IEEE Trans. on Inform. Theory*, vol. 47, pp. 619-637, Feb. 2001.

[20] R. Bose and D. Ray-Chaudhuri, "On a class of error correcting binary group codes," *Inf. Control*, vol. 3, pp. 68-79, Mar. 1960.

[21] I. Reed and G. Solomon, "Polynomials codes over certain finite fields," *SIAM Journal on Applied Mathematics*, vol. 8, pp. 300-304, 1960.

[22] V. Ponnampalam and B. Vucetic, "Soft Decision Decoding of Reed-Solomon Codes," *IEEE Trans. on Comm.*, vol. 50, pp. 1758-1768, Nov. 2002.

[23] P. Elias, "Coding for noisy channels," *IRE Conv. Record*, vol. 4, pp. 33-47, 1955.

[24] L.R. Bahl, J. Cocke, F. Jelinek, and R. Raviv, "Optimal decoding of linear codes for minimizing symbol error rate," *IEEE Trans. on Inform. Theory*, vol. 20, pp. 284-287, Mar. 1974.

[25] S. Benedetto, D. Divsalar, G. Montorsi, and F. Pollara, "A soft-input soft-output maximum a posteriori (MAP) module to decode parallel and serial concatenated codes," *TDA Progress Report*, pp. 42-127, Nov. 1996.

[26] F. R. Kschischang, B. J. Frey, and H. Loeliger, "Factor graphs and the sum-product algorithm," *IEEE Trans. on Inform. Theory*, vol. 47, pp. 498-519, Feb. 2001.

[27] P. Robertson, E. Villebrun, and P. Hoeher, "A comparison of optimal and sub-optimal MAP decoding algorithms operating in the log domain," in *Proc. Int. Conf. on Comm., Seattle, U.S.A.*, pp. 1009-1013, Jun. 1995.

[28] J. Hagenauer and P. Hoeher, "A Viterbi algorithm with soft-decision outputs and its application," in *Proc. of the IEEE Global Telecomm. Conf., Dallas, U.S.A.*, pp. 1680-1686, Nov. 1989.

[29] D. Forney, "Concatenated codes," Cambridge MA: MIT Press, 1966.

[30] J. Hagenauer and P. Hoeher, "Concatenated Viterbi-decoding," *Fourth Joint Swedish-Soviet International Workshop on Inform. Theory*, pp. 29-33, Aug. 1989.

[31] C. Berrou and A. Glavieux, "Near optimum error correcting coding and decoding: turbo codes," *IEEE Trans. on Comm.*, vol. 44, pp. 1261-1271, Oct. 1996.

[32] C. Berrou, A. Glavieux, and P. Thitimajshima, "Near Shannon limit error-correcting coding and decoding," in *Proc. of IEEE Intern. Conf. on Comm., Geneva, Switzerland*, pp. 1064-1070, May 1993.

[33] J. Woodard and L. Hanzo, "Comparative study of turbo decoding techniques: an overview," *IEEE Trans. on Vehic. Tech.*, vol. 49, pp. 2208-2232, Nov. 2000.

[34] B. Vucetic and J. Yuan, *Turbo codes: Principles and applications*: Kluwer Academics Publishers, 2000.

[35] S. Benedetto, D. Divsalar, G. Montorsi, and F. Pollara, "Serial concatenation of interleaved codes: performance analysis, design and iterative decoding," *IEEE Trans. on Inform. Theory*, vol. 44, pp. 909-926, May 1998.

[36] S. Benedetto, D. Divsalar, G. Montorsi, and F. Pollara, "Bandwidth efficient parallel concatenated coding schemes," *Electronic Letters*, vol. 31, pp. 2067-2069, Nov. 1995.

[37] X. Wang and H. Poor, "Iterative (turbo) soft interference cancellation and decoding for coded CDMA," *IEEE Trans. on Comm.*, vol. 47, pp. 1046-1061, Jul. 1999.

[38] M. Tüchler, R. Koetter, and A. Singer, "Turbo equalization: principles and new results," *IEEE Trans. on Comm.*, vol. 50, pp. 754-767, May 2002.

[39] J. Porter and J. Thweatt, "Microwave propagation characteristics in the MMDS frequency band," in *Proc. IEEE Int. Conf. on Comm., New Orleans, U.S.A.*, pp. 1578-1582, Jun. 2000.

[40] Cambridge Broadband, "Single carrier and OFDM modulation: Their suitability for broadband fixed wireless access systems," http://www.cambridgebroadband.com/media_publications/sc_and_ofdm.pdf, Apr. 2001.

[41] C. Douillard, M. Jézéquel, C. Berrou, A. Picart, P. Didier, and A. Glavieux, "Iterative correction of intersymbol interference: Turbo equalization," *European Trans. on Telecomm.*, vol. 6, pp. 507-511, Sep./Oct. 1995.

[42] M. Tüchler, A. Singer, and R. Koetter, "Minimum mean squared error equalization using A-priori information," *IEEE Trans. on Signal Processing*, vol. 50, pp. 673-683, Mar. 2002.

[43] A. Berthet, R. Visoz, and P. Tortelier, "Sub-optimal turbo-detection for coded 8-PSK over ISI channels with application to EDGE advanced mobile system," in *Proc. of Personal, Indoor and Mobile Radio Comm., London*, vol. 1, pp. 151-157, Sep. 2000.

[44] G. Bauch, H. Khorram, and J. Hagenauer, "Iterative equalization and decoding in mobile communications systems," in *Proc. of the 2nd European Personal Mobile Comm. Conf.*, pp. 307-312, Sept./Oct. 1997.

[45] R. Otnes and M. Tüchler, "Soft iterative channel estimation for turbo equalization: comparison of channel estimation algorithms," in *Proc. Int. Conf. on Comm. Sys., Singapore*, vol. 1, pp. 72-76, Nov. 2002.

[46] W. Hirt, "Capacity and information rates of discrete-time channels with memory," ETH-Diss. no. 8671, ETH Zurich, 1988.

[47] S. Shamai and R. Laroia, "The intersymbol interference channel: Lower bounds on capacity and channel precoding loss," *IEEE Trans. on Inform. Theory*, vol. 42, pp. 1388-1404, Sep. 1996.

[48] P. Vontobel and D. Arnold, "An upper bound on the capacity of channels with memory and constrainted input," *presented at the IEEE Information Theory Workshop, Cairns, Australia*, pp. 147-149, Sep. 2001.

[49] A. Kavcic, "On the capacity of markov sources over noisy channels," in *Proc. IEEE Global Comm. Conf., San Antonio, U.S.A.*, vol. 5, pp. 2997-3001, Nov. 2001.

[50] D. Arnold and H. Loeliger, "On the information rate of binary-input channels with memory," in *Proc. IEEE Int. Conf. on Comm., Helsinki, Finland*, pp. 2692-2695, Jun. 2001.

[51] H. Pfister, J. Soriaga, and P. Siegel, "On the achievable information rates for finite-state ISI channels," in *Proc. IEEE Globecom, San Antonio, U.S.A.*, pp. 2992-2996, Nov. 2001.

[52] V. Sharma and S. Singh, "Entropy and channel capacity in the regenerative setup with applications to markov channels," in *Proc. IEEE Intern. Symp. on Inform. Theory, Washington, U.S.A.*, pp. 283, Jun. 2001.

[53] T. Cover and J. Thomas, *Elements of Information Theory*: John Wiley & Sons, 1991.

[54] B. Leroux, "Maximum-likelihood estimation for hidden markov models," *Stochastic Processes and their Applications*, vol. 40, pp. 127-143, 1992.

[55] W.E. Ryan, "A turbo tutorial," *Unpublished paper.*

[56] G. Bauch and V. Franz, "A comparison of soft-in/soft-out algorithms for 'turbo detection'," in *Proc. on the Intern. Conf. on Telecomm.*, pp. 259-263, Jun. 1998.

[57] E. Tungsrisaguan and R. Rajatheva, "Turbo equalization with sequential sequence estimation over multipath fading channels," *IEEE Comm. Letters*, vol. 6, pp. 93-95, Mar. 2002.

[58] S. Vishwanath, M. Mansour, and A. Bahai, "Complexity based design for iterative joint equalization and decoding," in *Proc. IEEE Vehic. Tech. Conf., Birmingham, U.S.A.*, pp. 1699-1638, May 2002.

[59] M. Tüchler and J. Hagenauer, "Turbo equalization using frequency domain equalizers," in *Proc. of the Allerton Conference, Monticello, U.S.A.*, pp. 1234-1243, Oct. 2000.

[60] M. Tüchler and J. Hagenauer, "Linear time and frequency domain turbo equalization," in *Proc. of the 53rd IEEE Vehic. Techn. Conf., Rhodes, Greece*, vol. 2, pp. 1449-1453, May 2001.

[61] A. Glavieux, C. Laot, and J. Labat, "Turbo equalization over a frequency selective channel," in *Proc. of the Intern. Symp. on Turbo codes, Brest, France*, pp. 96-102, Sept. 1997.

[62] H. Omori, T. Asai, and T. Matsumoto, "A matched filter approximation for SC/MMSE iterative equalizers," *IEEE Comm. Letters*, vol. 5, pp. 310-312, Jul. 2001.

[63] S. Ariyavisitakul and Y. Li, "Joint coding and decision feedback equalization for broadband wireless channels," *IEEE Journal on Sel. Areas in Comm.*, vol. 16, pp. 1670-1678, Dec. 1998.

[64] X. Yu, "Iterative turbo decoder with decision feedback equalization for signals transmitted over multipath channels," in *Proc. of the 53rd IEEE Vehicular Techn. Conf., Rhodes, Greece*, pp. 1634-1638, May 2001.

[65] R. R. Lopes and J. R. Barry, "Exploiting error-control coding in blind channel estimation," in *Proc. IEEE Global Comm. Conf., San Antonio, U.S.A.*, vol. 2, pp. 1317-1321, Nov. 2001.

[66] M. Yee, T. Liew, and L. Hanzo, "Turbo equalization of convolutional coded and concatenated space time trellis coded systems using radial basis function aided equalizers," in *Proc. 54th IEEE VTS Vehic. Tech. Conf., VTC 2001 Fall, Atlantic City, U.S.A.*, vol. 2, pp. 1935-1945, Oct. 2001.

[67] M. Tüchler, "Iterative equalization using priors," Masters thesis, University of Illinois at Urbana-Champaign, U.S.A., 2000.

[68] D. Raphaeli and Y. Zarai, "Combined turbo equalization and turbo decoding," in *Proc. of the IEEE Global Telecomm. Conf., Phoenix, U.S.A.*, vol. 2, pp. 639-643, Nov. 1997.

[69] M. Tüchler, "Convergence prediction for iterative decoding of threefold concatenated systems," in *Proc. Globecom 2002, Taipei, Taiwan*, vol. 2, pp. 1358-1362, Nov. 2002.

[70] B. Yeap, T. Liew, and J. Hámorský, "Comparative study of turbo equalization schemes using convolutional, convolutional turbo, and block-turbo codes," *IEEE Trans. on Wireless Comm.*, vol. 1, pp. 266-273, Apr. 2002.

[71] A. Kavcic, X. Ma, and M. Mitzenmacher, "Binary intersymbol interference channels: gallager codes, density evolution and code performance bounds," *submitted to the IEEE Trans. on Inform. Theory*, Feb. 2001.

[72] N. Varnica and A. Kavcic, "Optimized LDPC codes for partial response channels," in *Proc. IEEE Intern. Symp. on Inform. Theory, Lausanne, Switzerland*, pp. 197, Jun./Jul. 2002.

[73] K.R. Narayanan and X. Wang, "LDPC code design for MMSE turbo equalization," in *Proc. IEEE Intern. Symp. on Inform. Theory, Lausanne, Switzerland*, pp. 415, Jun./Jul. 2002.

[74] X. Li, W. Song, and H. Luo, "Joint turbo equalization and turbo TCM for mobile communication systems," in *Proc. 12th IEEE International Symposium on Personal, Indoor and Mobile Radio Communications, San Diego, U.S.A.*, pp. 184-188, Sep./Oct. 2001.

[75] S. ten Brink, "Exploiting the chain rule of mutual information for the design of iterative decoding schemes," in *Proc. 39th Ann. Allerton Conf. on Commun., Control, and Computing, Monticello, U.S.A.*, Oct. 2001.

[76] S. Chung, J. Forney, T. Richardson, and R. Urbanke, "On the design of low-density-parity-check codes within 0.0045dB of the Shannon limit," *IEEE Comm. Letters*, vol. 5, pp. 58-60, Feb. 2001.

[77] S. Benedetto and G. Montorsi, "Unveiling turbo codes: some results on parallel concatenated coding schemes," *IEEE Trans. on Inform. Theory*, vol. 42, pp. 409-428, Mar. 1996.

[78] S. Benedetto, E. Biglieri, and V. Castellani, *Digital Transmission Theory*: Prentice-Hall, New York, U.S.A., 1987.

[79] T. Richardson and R. Urbanke, "The capacity of low density parity check codes under message passing decoding," *IEEE Trans. on Inform. Theory*, vol. 47, pp. 599-618, Feb. 2001.

[80] D. Divsalar, S. Dolinar, and F. Pollara, "Iterative turbo decoder analysis based on density evolution," *IEEE Journal on Sel. Areas in Comm.*, vol. 19, pp. 891-907, May 2001.

[81] J. Lee and R. Blahut, "Analysis of the extrinsic values in the finite length turbo decoding," in *Proc. Conf. on Inform. Sciences and Sys., Princeton, U.S.A.*, Mar. 2002.

[82] M. Tüchler, S. ten Brink, and J. Hagenauer, "Measures for tracing convergence of iterative decoding algorithms," in *Proc. 4th IEEE/ITG Conf. on Source and Channel Coding, Berlin, Germany*, pp. 53-60, Jan. 2002.

[83] S. ten Brink, "Convergence of iterative decoding," *Electronic Letters*, vol. 35, pp. 806-808, May 1999.

[84] S. ten Brink, "Convergence behaviour of iteratively decoded parallel concatenated codes," *IEEE Trans. on Comm.*, vol. 4, pp. 1727-1737, Oct. 2001.

[85] S. ten Brink, "Rate one-half code for approaching the Shannon limit by 0.1dB," *Electronic Letters*, vol. 36, pp. 1293-1294, Jul. 2000.

[86] M. Tüchler and J. Hagenauer, "EXIT chart of irregular codes," in *Proc. Conf. on Inform. Sciences and Sys., Princeton, U.S.A.*, Mar. 2002.

[87] W. Daniel, *Applied non parametric statistics*: Houghton Mifflin Company, 1978.

[88] N. Doan and K. Narayanan, "Some new results on the design of codes for inter-symbol interference channels based on convergence of turbo equalization," in *Proc.*

IEEE Intern. Symp. on Inform. Theory, Lausanne, Switzerland, pp. 1873-1877, Jun./Jul. 2002.

[89] W. Ryan, "Concatenated codes for class IV partial response channels," *IEEE Trans. on Comm.*, vol. 47, pp. 445-454, Mar. 2001.

[90] A. Kavcic, X. Ma, M. Mitzenmacher, and N. Varnica, "Capacity approaching signal constellations for channels with memory," in *Proc. of the Allerton Conference, Allerton, U.S.A.*, pp. 311-320, Oct. 2001.

[91] M. Tüchler and R. Otnes, "EXIT chart analysis applied to adaptive turbo equalization," in *Proc. Nordic Signal Processing Symp., on board Hurtigruten, Norway*, Oct. 2002.

[92] T. Souvignier, M. Öberg, P. Siegel, R. Swanson, and J. Wolf, "Turbo decoding for partial response channels," *IEEE Trans. on Comm.*, vol. 48, pp. 1297-1308, Aug. 2000.

[93] K. Narayanan, U. Dasgupta, and B. Lu, "Low complexity turbo equalization with binary precoding," in *Proc. Intern. Conf. of Comm., New Orleans, U.S.A.*, vol. 1, pp. 1-5, Jun. 2000.

[94] M. Tüchler, C. Weiß, E. Eleftheriou, A. Dholakia, and J. Hagenauer, "Application of high-rate tail-biting codes to generalized partial response channels," in *Proc. IEEE Globecom, San Antonio, U.S.A.*, vol. 5, pp. 2966-2971, Nov. 2001.

[95] M. Tüchler, "Design of serially concatenated systems for short or long block lengths," *submitted to IEEE Trans. on Comm.*, Jul. 2002.

[96] W. Ryan, "Design considerations for concatenating convolutional codes with partial response channels," in *Proc. Allerton Conf. Comm., Control and Computing, Urbana-Champaign, U.S.A.*, pp. 1324-1333, Sep. 1999.

[97] K. Narayanan, "Effect of precoding on the convergence of turbo equalization for partial response channels," *IEEE Journal on Sel. Areas in Comm.*, vol. 19, pp. 686-698, Apr. 2001.

[98] J. Hagenauer, "Mutual Information and EXIT Charts: A Primer," in *Proc. 12th Joint Conference on Comm. and Coding, Saas Fee, Switzerland*, Mar. 2002.